

**BUCKLING AND DYNAMIC
CHARACTERISTICS OF
CENOSPHERE/EPOXY SYNTACTIC
FOAM COMPOSITES AND SANDWICHES
UNDER MECHANICAL AND THERMAL
LOADS**

Thesis

Submitted in partial fulfillment of the requirements for the degree of

DOCTOR OF PHILOSOPHY

by

SUNIL SHANKAR WADDAR



DEPARTMENT OF MECHANICAL ENGINEERING
NATIONAL INSTITUTE OF TECHNOLOGY KARNATAKA,
SURATHKAL, MANGALORE – 575025

MAY, 2019

DECLARATION

I hereby *declare* that the Research Thesis entitled “**BUCKLING AND DYNAMIC CHARACTERISTICS OF CENOSPHERE/EPOXY SYNTACTIC FOAM COMPOSITES AND SANDWICHES UNDER MECHANICAL AND THERMAL LOADS**” which is being submitted to the **National Institute of Technology Karnataka, Surathkal** in partial fulfillment of the requirements for the award of the Degree of **Doctor of Philosophy** in **Department of Mechanical Engineering** is a *bonafide report of the research work carried out by me*. The material contained in this Research Thesis has not been submitted to any University or Institution for the award of any degree.

Register Number : **158038ME15F25**

Name of the Research Scholar : **SUNIL SHANKAR WADDAR**

Signature of the Research Scholar :

Department of Mechanical Engineering

Place : **NITK, Surathkal**

Date :

C E R T I F I C A T E

This is to *certify* that the Research Thesis entitled “**BUCKLING AND DYNAMIC CHARACTERISTICS OF CENOSPHERE/EPOXY SYNTACTIC FOAM COMPOSITES AND SANDWICHES UNDER MECHANICAL AND THERMAL LOADS**” submitted by **Mr. SUNIL SHANKAR WADDAR (Register Number: 158038ME15F25)** as the record of the research work carried out by him, is *accepted as the Research Thesis submission* in partial fulfillment of the requirements for the award of degree of **Doctor of Philosophy**.

Research Guides

Dr. Jeyaraj Pitchaimani

Associate Professor

Department of Mechanical Engineering

Dr. Mrityunjay Doddamani

Assistant Professor

Department of Mechanical Engineering

Chairman – DRPC

Date:

ACKNOWLEDGEMENT

I would like to extend my sincere gratitude to Dr. Jeyaraj Pitchaimani, Associate Professor Mechanical Engineering Department for their invaluable constructive guidance and encouragement extended throughout my study. I would also like to extend my gratitude to Dr. Mrityunjay Doddamani, Assistant Professor, Mechanical Engineering, Department for the constant encouragement and support extended throughout this research work. Sincere gratitude is expressed to Prof. Nikhil Gupta, USA and Prof. Ever J. Barbero, USA for their encouragement and help extended.

I would like to thank Research Progress Assessment Committee Members Dr. Subhaschandra Kattimani, and Dr. Arun Kumar Thalla for their valuable inputs. Useful discussions and suggestions are deeply appreciated.

I would like to thank former head of department Prof. Narendranath S., and Prof. Shrikantha S Rao, Head of Mechanical Engineering Department and all the faculty members at Mechanical Engineering Department for their support throughout this research work.

Constant encouragement of my family to pursue higher studies has made it possible for me to reach at this stage. I wish to thank all my family members for love, help and encouragement provided. I express my sincere thanks to Dr. M. Rajesh, Dr. Bharat Kumar, Dr. Nivish George, Dr. Vinod Bhagat, Dr. Arun Kumar, Dr. Jayavardhana M. L., Dr. Kiran Shahapurkar, Dr. Mahantayya Mahtapati, Dr. Hargovind Soni, Mr. Ashrith H. S., Mr. Praveen J., Mr. Balu Patil and our research team for their help and kind cooperation extended throughout this research work. Special note of thanks to all my friends and well-wishers for their constant help, encouragement and understanding.

ABSTRACT

Polymer matrix composites provide lower weight structures and result in improved efficiency and performance in many transportation engineering applications. Thermosetting polymers reinforced with suitable hollow particle constituents, higher specific properties can be achieved. Development of syntactic foams with cenospheres serves dual purpose of beneficial utilization of industrial waste fly ash and reduction in the component cost in addition to weight reduction. In the present study, LAPOX L-12 epoxy resin is used as the matrix material and fly ash cenospheres in as received and silane modified conditions are used as filler material. Manual stirring method is employed for developing cenosphere/epoxy syntactic foams with as received and surface treated cenospheres in 20, 40 and 60 volume %. Sandwich composites are also prepared using sisal fiber woven fabric reinforced in epoxy as facings and syntactic foam as core. With increasing cenosphere content, density of untreated and silane treated foams decreases in general. Influence of cenosphere surface treatment and volume fraction of cenospheres in epoxy matrix on buckling and dynamic characteristics are experimentally investigated in this work.

Buckling and free vibration behavior of cenosphere/epoxy syntactic foams under mechanical and thermal loadings are investigated experimentally in this work. Buckling load is obtained from the load-deflection curve based on the Double Tangent Method (DTM) and Modified Budiansky Criteria (MBC). Further, the influence of axial compression load on the natural frequencies associated with the first three transverse bending modes is analyzed. Finally, the buckling loads predicted using DTM and MBC are compared with the buckling load calculated based on the vibration correlation technique (VCT). It is observed that the buckling loads predicted through the three different methods are in close agreement. Experimental results revealed that the buckling load and natural frequency of syntactic foams increase with cenosphere volume fraction. It is observed that natural frequencies reduce with increase in axial compression load for all the modes. However, rapid increase in the fundamental frequency is observed when the compressive load is near and beyond the critical

buckling load. It is observed that silane modified cenosphere embedded in epoxy matrix registered superior performance (rise in critical buckling load and natural frequencies to the tune of 23.75 and 11.46% respectively) as compared to untreated ones. Experimental results are compared with the analytical solutions that are derived based on Euler-Bernoulli hypothesis and results are found to be in good agreement. Finally, property map of buckling load as a function of density is presented by extracting values from the available literature.

Experimental investigation on deflection behavior of fly ash cenosphere/epoxy syntactic foam under thermal environment (three different heating conditions) is investigated. Three different heating cases (*increase-decrease*, *decrease* and *decrease-increase*) are considered. Influence of fly ash cenosphere volume fraction and nature of temperature variation on deflection behavior of syntactic foam beam is discussed elaborately. The temperature rise on the test specimens are measured using K-type thermocouples and lateral deflections are measured using Linear variable differential transducer (LVDT). The data is collected with the help of in-built LabVIEW program to plot temperature deflection curve. Results reveal that the syntactic foam beam experience snap-through buckling under thermal environment and is reflected by two bifurcation points in temperature-deflection plot also. It is observed that the time duration for which the syntactic foam beam stays in the first buckled position increases with increase in cenosphere content. Thermal environment induces compressive stresses in the samples causing such snap-through buckling. However, such phenomenon is not observed when the syntactic foam beams are exposed to mechanical compressive loads. Temperature variation across the beam length strongly influences snap-through buckling in syntactic foams in addition to volume fraction of filler content.

An experimental study on buckling and dynamic response of cenosphere reinforced epoxy composite (syntactic foam) core sandwich beam with sisal fabric/epoxy composite facings under compressive load is presented. Influence of cenosphere loading and surface modification on critical buckling load and natural frequencies of the sandwich beam under compressive load is presented. The critical buckling load is

obtained from the experimental load-deflection data while natural frequencies are obtained by performing experimental modal analysis. Results reveal that natural frequencies and critical buckling load increase significantly with fly ash cenosphere content. It is also observed that surface modified cenospheres enhance natural frequencies and critical buckling load of the sandwich beam under compressive load. Vibration frequencies reduce with increase in compressive load. Fundamental frequency increases exponentially in post-buckling regime. Experimentally obtained load-deflection curve and natural frequencies are compared with finite element analysis wherein results are found to be in good agreement.

Buckling behaviour of sandwich composites made of syntactic foam core and sisal fabric/epoxy composite facings subjected to non-uniform heating is investigated. The critical buckling and snap-initiation temperatures are found from the temperature-deflection plots. It is observed that, the critical buckling temperature increase with the filler content in the core material and surface treatment show slightly higher buckling temperature. The sandwich beams undergo snap-through buckling at higher temperatures due to developed viscoelastic forces. Due to increase in stiffness of the beam with filler content the deflection of the beam found to be less. The sandwich beams showed higher buckling temperatures than the neat syntactic foam samples.

Keywords: *Syntactic foam; Epoxy; Fly ash cenosphere; Natural fiber; Surface treatment; Buckling; Free vibration; Thermal environment.*

CONTENTS

Declaration	
Certificate	
Acknowledgement	
Abstract	
CONTENTS.....	i
LIST OF FIGURES	v
LIST OF TABLES	viii
ABBREVIATIONS	ix
NOMENCLATURE	xi
1 INTRODUCTION.....	1
1.1 Composite materials.....	1
1.2 Syntactic foam composites.....	3
1.3 Processing of syntactic foams	5
1.4 Role of interface and its modification.....	6
1.5 Sandwich structured composites	9
1.5.1 Core materials	11
1.5.2 Facing materials	11
1.6 Natural fiber composites	12
1.7 Literature survey	13
1.7.1 Buckling under mechanical load.....	13
1.7.2 Buckling and free vibration under axial compression	15
1.7.3 Vibration correlation technique (VCT).....	17
1.7.4 Temperature dependent properties of syntactic foams	17
1.7.5 Buckling under thermal load.....	18

1.7.6	Snap-through buckling behavior.....	19
1.7.7	Buckling and free vibration studies of sandwich composites.....	20
1.7.8	Thermal buckling of sandwich composites.....	23
1.8	Closure	24
1.9	Motivation.....	25
1.10	Objectives of the work	25
1.11	Outline of the thesis.....	26
2	MATERIALS AND METHODS	27
2.1	Constituents.....	27
2.1.1	Matrix.....	27
2.1.2	Fly ash cenospheres	28
2.1.3	Sisal woven fabric.....	29
2.2	Surface treatment of cenospheres.....	29
2.3	FTIR spectroscopy and particle size analysis	30
2.4	Syntactic foam fabrication	30
2.5	Sandwich preparation.....	31
2.6	Density test.....	32
2.7	Buckling at room temperature under mechanical loading	33
2.8	Free vibration under axial compressive load.....	33
2.9	Coefficient of thermal expansion (CTE).....	35
2.10	Buckling under non-uniform thermal load.....	35
2.11	Dynamic mechanical analysis (DMA)	38
2.12	Scanning electron microscopy (SEM).....	39
3	BUCKLING AND FREE VIBRATION BEHAVIOUR OF SYNTACTIC FOAMS UNDER MECHANICAL LOAD	40
3.1	Introduction	40

3.2	FTIR and particle size analysis	40
3.3	Fabrication of specimens.....	42
3.4	Density of syntactic foams	44
3.5	Elastic modulus measurement from free vibration testing.....	45
3.6	Determination of Young's modulus of syntactic foams using Bardella-Genna model (Theoretical approach)	45
3.7	Theoretical formulation.....	47
3.8	Buckling test.....	50
3.9	Free vibration under axial compressive loads	52
3.10	Comparison with untreated cenosphere/epoxy syntactic foams	54
3.11	Vibration correlation technique (VCT).....	56
3.12	Conclusions	57
4	BUCKLING BEHAVIOUR OF SYNTACTIC FOAMS UNDER THERMAL LOAD	58
4.1	Introduction	58
4.2	Buckling under mechanical load	58
4.3	Coefficient of thermal expansion (CTE).....	60
4.4	Comparison of deflection behaviour under mechanical and thermal loading... ..	62
4.5	Buckling under non-uniform heating	64
4.6	Conclusions	71
5	BUCKLING AND FREE VIBRATION BEHAVIOUR OF SYNTACTIC FOAM SANDWICH COMPOSITES UNDER MECHANICAL LOAD	73
5.1	Introduction	73
5.2	Material characterization.....	73
5.3	Density of syntactic foams and their sandwich composites.....	74
5.4	Evaluation of elastic properties of skin	75

5.5	Finite element analysis	78
5.6	Buckling behaviour	80
5.7	Free vibration behaviour at no load and axial compression.....	84
5.8	Comparison of experimental and numerical buckling and free vibration results	86
5.9	Conclusions	91
6	BUCKLING BEHAVIOUR OF SANDWICH COMPOSITES UNDER THERMAL LOAD	93
6.1	Introduction	93
6.2	Buckling under non-uniform thermal load.....	93
6.3	Conclusions	99
7	SUMMARY AND CONCLUSIONS	101
7.1	Summary	101
7.2	Conclusions	102
	SCOPE OF FUTURE WORK	106
	REFERENCES	107
	LIST OF PUBLICATIONS	119
	BIO-DATA	120

LIST OF FIGURES

Figure 1.1 Schematic representation of syntactic foams (a) two phase (b) three phase (Gupta et al. 2013).	4
Figure 1.2 Illustration of syntactic foam fabrication steps (Gupta et al. 2013).	6
Figure 1.3 Reaction between Silane-69 coupling agent and fly ash (Alkadasi et al. 2004).	9
Figure 1.4 The structure of the Sandwich Composite.....	10
Figure 2.1 (a) Epoxy resin and hardener (b) Cenospheres and (c) Sisal woven fabric used in this study.....	28
Figure 2.2 Aluminium mold used to prepare syntactic foams.	31
Figure 2.3 Syntactic foam core sandwich composite preparation steps.	32
Figure 2.4 (a) Schematic representation and (b) actual experimental setup, showing buckling and free vibration tests and (c) Schematic representation of test specimen. 34	
Figure 2.5 (a) Schematic representation and (b) actual experimental buckling setup in thermal environment.	36
Figure 2.6 Schematic representation of (a) Case 1: increase-decrease (b) Case 2: decrease and (c) Case 3: decrease- increase thermal loading conditions.....	37
Figure 2.7 LabVIEW program used to perform buckling experiments under thermal load.....	38
Figure 2.8 (a) DMA machine and (b) DMA test set-up.....	39
Figure 3.1 (a) FTIR spectroscopy and (b) particle size analysis of untreated and treated cenosphere.....	41
Figure 3.2 Micrographs of (a) Untreated (b) treated cenospheres (c) wall thickness variations and in-built porosity present in cenospheres.	42
Figure 3.3 Micrographs of (a) E60 (b) E60T foams showing uniform distribution of cenospheres. (c) Lack of bonding for E60 and (d) good interfacial bonding in E60T is noted.....	43
Figure 3.4 Illustration of the estimation of P_{cr} from experimental results using (a) DTM and (b) MBC methods.....	50
Figure 3.5 A representative set of graphs showing experimental buckling behavior of neat epoxy and syntactic foams.	51
Figure 3.6 Frequency response functions for E20T sample.	52

Figure 3.7 Influence of compressive load on natural frequency of (a) E0 (b) E20 (c) E40 (d) E60 (e) E20T (f) E40T (g) E60T samples.	54
Figure 3.8 Comparison of buckling load and first natural frequency of untreated and treated cenosphere syntactic foams.....	55
Figure 3.9 Buckling load plotted against density from available studies (Rajesh 2017, Rajesh and Pitchaimani 2017).	55
Figure 3.10 P_{cr} using VCT for (a) untreated (b) treated cenosphere/epoxy syntactic foams in Mode 1.	56
Figure 3.11 Buckling load comparison between VCT and experimental approaches.	57
Figure 4.1 Deflection of neat epoxy and their syntactic foams under mechanical loads.	59
Figure 4.2 Test in-progress for representative foam sample (a) pre (b) during and (c) post loading conditions.	60
Figure 4.3 Heat flow mechanism in (a) neat epoxy and (b) syntactic foam (red arrows indicate conduction and blue arrows indicate convection mode of heat transfer).	61
Figure 4.4 Behavior of E20 syntactic foams under (a) mechanical and (b) thermal load.....	62
Figure 4.5 Estimation of buckling temperature from the temperature-deflection plot for representative E20 sample.....	63
Figure 4.6 Influence of cenosphere loading on (a) Case 1: Increase-decrease (b) Case 2: Decrease and (c) Case 3: Decrease-increase heating conditions.	65
Figure 4.7 Influence of temperature variation on (a) E0 (b) E20 (c) E40 (d) E60 (e) E20T (f) E40T (g) E60T samples.	67
Figure 4.8 Progressive images of syntactic foam beam deflecting under increase-decrease heating condition.....	69
Figure 4.9 Representative foam sample (a) pre-buckling (b) post thermal buckling.	69
Figure 4.10 Influence of cenosphere volume fraction on storage modulus (a) untreated (b) treated and loss modulus of (c) untreated (d) treated syntactic foams.	70
Figure 5.1 (a) Schematic representation of sandwich and (b) prepared sandwich composite.	74
Figure 5.2 SEM images of sandwich composites indicating (a) top and (b) bottom facing thickness and bonding interfaces.	74
Figure 5.3 Sisal yarn tensile test in-progress.	76

Figure 5.4 Macrostructural geometry of the fabric (Barbero 2018).	77
Figure 5.5 Flow chart showing steps of numerical analysis.	78
Figure 5.6 Representative set of compressive load-deflection behavior for sandwich beams with syntactic foam core.	81
Figure 5.7 Representative images of syntactic foam sandwich beams (a) before and (b) during buckling test.	82
Figure 5.8 Representative micrographs of SE40 sample (a) lower skin (b) upper skin showing no delamination.	83
Figure 5.9 Effect of axial compressive load on natural frequencies of (a) 1 st (b) 2 nd and (c) 3 rd mode.	86
Figure 5.10 (a) Sisal fibers (b) yarns (c) plain woven fabric and (d) SEM image of dry fabric.	87
Figure 5.11 Representative stress-strain response for tested yarn.	87
Figure 5.12 Comparison of load-deflection curves obtained experimentally and numerically for (a) SE40 and (b) SE40T sandwich composites.	90
Figure 6.1 (a) Determination of critical buckling temperatures from temperature-deflection curve of sandwich beam (b) deflection behaviour of syntactic foam.	95
Figure 6.2 Effect of non-uniform heating of (a) SE0 (b) SE20 (c) SE40 (d) SE60 sandwich composites.	96
Figure 6.3 Effect of filler content on (a) Increase-decrease (b) Decrease and (c) decrease-increase heating conditions.	97
Figure 6.4 Effect of surface modification on thermal buckling behaviour of representative sandwich sample under increase-decrease heating.	99
Figure 6.5 Test in progress images of the representative sample under decrease-increase heating condition.	99

LIST OF TABLES

Table 2.1 Properties of epoxy resin and hardener*	27
Table 2.2 Physical, chemical and sieve analysis details of cenospheres*	29
Table 3.1 Density, void content and weight saving potential of syntactic foams.....	44
Table 3.2 Comparison of Young's modulus values obtained from frequency data and Bardella-Genna model for pure epoxy and syntactic foams.....	47
Table 3.3 Experimental and theoretical critical buckling load for pure epoxy and syntactic foams.....	51
Table 4.1 CTE of neat epoxy and their syntactic foams.....	61
Table 4.2 Buckling temperatures (above ambient) for neat epoxy and syntactic foams at various non-uniform heating conditions.....	68
Table 5.1 Density and void content of cenosphere/epoxy syntactic foam sandwich composites.....	75
Table 5.2 Critical buckling loads for sandwich composites.....	81
Table 5.3 Comparison of buckling loads of cenosphere/epoxy syntactic foams and their sandwiches.....	83
Table 5.4 Experimental natural frequencies of sandwich beams at no load condition.....	84
Table 5.5 Properties of sisal fibres.....	88
Table 5.6 Properties of Epoxy matrix.....	88
Table 5.7 Lamina intrinsic properties and reinforcement geometry.....	89
Table 5.8 Comparison of sisal fabric/epoxy laminate properties obtained from CADEC and experimental.....	89
Table 5.9 Comparison of experimental and numerically obtained buckling loads of sandwich composites.....	91
Table 5.10 Comparison of natural frequency values obtained through experimental and numerical approaches.....	92
Table 6.1 Thermal buckling temperatures of the sandwich composites subjected to non-uniform thermal loads.....	98

ABBREVIATIONS

APTS	: Amino Propyl Tri Ethoxy Silane
ASTM	: American Society for Testing and Materials
BGM	: Bardella-Genna Model
CADEC	: Computer Aided Design Environment for Composites
CMC	: Ceramic Matrix Composite
CNT	: Carbon Nanotube
CTE	: Coefficient of Thermal Expansion
DAQ	: Data Acquisition System
DGEBA	: Diglycidyl Ether of Bisphenol A
DMA	: Dynamic Mechanical Analysis
DTM	: Double Tangent Method
EDS	: Energy Dispersive Spectroscopy
FFT	: Fast Fourier Transform
FTIR	: Fourier Transform Infrared Spectroscopy
GFRP	: Glass Fiber Reinforced Polymer
GMB	: Glass Microballoon
HDPE	: High Density Polyethylene
IR	: Infrared
LVDT	: Linear Variable Differential Transducer
MBC	: Modified Budiansky Criteria
MMC	: Metal Matrix Composite
PEEK	: Polyether-Ether-Ketone
PMC	: Polymer Matrix Composite
PPS	: Polyphenylene Sulfide
PVC	: Poly Vinyl Chloride
SEM	: Scanning Electron Microscope
SF	: Syntactic Foam

TC : Thermal Conductivity
VCT : Vibration Correlation Technique
XRD : X-Ray Diffraction

NOMENCLATURE

ω	Angular natural frequency	rad/s
K	Bulk modulus	MPa
K_m	Bulk modulus of matrix	MPa
P	Compressive load	N
β	Constant	----
P_{cr}	Critical buckling load	N
A	Cross sectional area	mm ²
$\rho_{ceramic}$	Density of cenosphere wall material	kg/m ³
ρ^{exp}	Experimental density of composite	kg/m ³
h_f	Fill thickness	mm
a_f	Fill width	mm
ρ_f	Filler density	kg/m ³
v_f	Filler volume fraction	%
n_g	Harness of yarns	----
T_{cr1}	Initial critical buckling temperature	°C
G_{12}	In-plane shear modulus	MPa
G_{23}	Inter laminar shear modulus	MPa
n_i	Interlacing of yarns	----
h	Lamina thickness	mm
L	Length of the beam	mm
E_x	Longitudinal Young's modulus	MPa
ϑ_{12}	Longitudinal Poisson's ratios	----
ρ_m	Matrix density	kg/m ³
v_m	Matrix volume fraction	%
I	Moment of inertia	mm ⁴
f	Natural frequency	Hz
f_n	Natural frequency at no load	Hz
N_f	Number of yarns per unit width in fill direction	----
N_w	Number of yarns per unit width in warp direction	----

η	Radius ratio	----
G	Shear modulus	MPa
G_f	Shear modulus of fibers	MPa
G_m	Shear modulus of matrix	MPa
n_s	Shift of yarns	----
T_{cr_2}	Snap-initiation temperature	°C
ρ^{th}	Theoretical density of composite	kg/m ³
E_y	Transverse Young's modulus	MPa
ν_{23}	Transverse Poisson's ratios	----
ϕ_v	Void content	%
h_w	Warp thickness	mm
a_w	Warp width	mm
E	Young's modulus	MPa

1 INTRODUCTION

1.1 Composite materials

A formal definition of composite materials given by ASM Handbook (ASTM D3878-18) is “macroscopic combination of two or more distinct materials, having a recognizable interface between them”. Increasing performance demands for modern technology applications make it necessary to look for new materials. More down-to-earth, however, is the fact that our society has become more energy conscious. This has led to an increasing demand for lightweight yet strong and stiff structures in all walks of life (Chawla 2012). Composite materials are widely used to enhance the properties of materials to sustain higher service loads. Composite materials can strengthen the properties like strength, stiffness, corrosion and wear resistance, weight reduction, fatigue life, temperature dependent behaviour and thermal properties. Composite materials are widely used in aerospace, marine and automobile sector due to their lightweight and high strength. Almost all modes of transportation and sports equipment also use considerable number of composites. These materials provide unique combination of properties, which cannot be obtained from any of the constituent material used individually.

Composites are classified based on two phases namely matrix and reinforcement. Matrix phase is a continuous phase and reinforcement is a discontinuous or dispersed phase. Interface between matrix phase and the reinforcement is a third phase of composite. Based on the matrix material, composites can be classified as Metal matrix composite (MMC), Ceramic matrix composite (CMC) and Polymer matrix composite (PMC). PMC's are becoming promising materials for variety of structural and automotive applications since they possess favourable combinations of mechanical properties (Barbero 2018). PMC's are extensively used because of their relative ease of processing, low density, desirable electrical/thermal properties and excellent chemical/corrosion resistance. Hence, these find applications ranging from specialized functions in aerospace and electronics engineering to day-to-day consumer industries like construction and transport.

PMC's consist of thermoplastic or thermosetting resin reinforced by filler (fiber, particle, etc.). These materials can be molded into a variety of shapes and sizes. Owing to lower density of the constituents the polymer composites often show excellent specific properties. In particular, polymer matrix has low strength and stiffness comparable with metal and ceramic. This implies that there is a considerable benefit to be gained by reinforcing polymers with the reinforcements, to have special properties. Secondly, the processing of PMC's need not involve high pressures and temperatures. Problems associated with the degradation of the reinforcement during manufacture are less significant for PMC's than for composites with other matrices. Also, the equipment required for PMC's are simpler. For these reasons PMC's developed rapidly and soon become accepted for structural applications.

Today glass fibre reinforced polymers (GFRP) are still by far the most used composite material in terms of volume with the exception of concrete. There are two types of polymers namely thermoset and thermoplastics. Thermosetting polymers are insoluble and infusible after cure as the chains are rigidly joined with strong covalent bonds. Typical examples of thermosets include epoxies, polyesters, phenolics and polyamides. While thermoplastics are formable at high temperatures and pressure since the bonds are weak and are of Van-der-Waal type. Typical examples of thermoplastics include polyethylene, polystyrene, polyether-ether-ketone (PEEK) and polyphenylene sulfide (PPS). To see the advantages in using composite materials, a comparison between their properties and those of newer class of composites should be done in terms of specific values (per unit of weight). When it comes to weight saving without sacrificing structural performance, composites and in particular syntactic foam (SF) composites are without doubt far superior to other traditional composites. In the present scenario, SF is a special class of structural composite which has become very popular due to high specific strength and bending stiffness. Low density of these materials makes them especially suitable for use in aeronautical, space, marine and sports applications (Gupta et al. 1999).

1.2 Syntactic foam composites

Lightweight materials are of great interest in several structural engineering applications. In transportation engineering applications, the structural weight reduction directly translates into fuel saving and increased payload capacity. Porous materials can provide significant weight saving potential but their applications are limited by their low strength and modulus. In this context, a unique class of composite material, called syntactic foam, is rapidly gaining attention wherein porosity is incorporated in matrix resin to reduce the structural weight without compromising on mechanical properties (Gupta et al. 2014).

Syntactic foams (SF's) are composite materials prepared by dispersing hollow particles in matrix. The term was originally coined by the Bakelite Company of New York in 1955, for their lightweight composites made of hollow phenolic microspheres bonded to a matrix of phenolic, epoxy, or polyester. These foams are low-density materials. Foams are classified as open cell and closed cell foams. Due to the cellular materials, open cell foam always has limitations due to lower compressive strength and modulus (Gupta et al. 2004). In order to overcome these prevailing issues, a class of closed cell foam known as syntactic foams were introduced by dispersing rigid hollow particles in matrix material (Puterman et al. 1980). These composites are found to possess high specific strength and low thermal conductivity (Gupta et al. 2005). These materials were developed in the 1960s as buoyancy aid materials, for deep sea applications. Currently they are used in aircraft, spacecraft and ship structures (Gupta et al. 2002). One of the major advantages of syntactic foams is ability to be designed and fabricated according to the physical and mechanical property requirements of the application. Microspheres can be considered versatile fillers compared to any other fillers because these materials can develop a variety of products and process improvements including low density, improved dimensional stability, increased impact strength, smoother surface finish, greater thermal insulation, easier machinability, faster cycle times, as well as cost savings (van Belle 2002). Microspheres are made from rigid shell materials such as polymeric (i.e., thermoplastic or thermoset resin), ceramic, carbon, metal and glass (Wouterson et al. 2005) to obtain excellent properties. On the other hand, the matrix material binds the

microspheres and gives the composite its shape and further determines the quality of its surface finish. Depending upon the service conditions the matrix can be chosen from a wide range of thermosetting and thermoplastic resins. Similarly, microspheres of glass, polymer, ceramic or metal can be chosen (Gupta et al. 2005, Gupta et al. 2004) based on the requirements.

SF's are usually a two-phase structure, namely matrix and microballoons. These foams are classified as closed pore foams, due to the existence of porosity within the microballoons. However, during fabrication of syntactic foams, air or voids can be entrapped within the matrix. The presence of air or voids within the matrix is termed as open cell porosity and thus making syntactic foams a three-phase structure. Two-phase syntactic foam consists of hollow spheres dispersed in a matrix resin either in loose or close-packed structures whereas a three-phase syntactic foam consists of hollow spheres dispersed in a matrix resin containing gaseous voids. Usually, conventional syntactic foams are in two-phase systems. It has high density and superior mechanical properties compared to the conventional blown foams, particularly in compression. The lowest practical densities for two-phase syntactic foams containing glass microspheres are limited and lie in the range of 500–600 kg/m³ (Narkis et al. 1980). Schematic representation of different phases present in syntactic foam microstructure is shown in Figure 1.1.

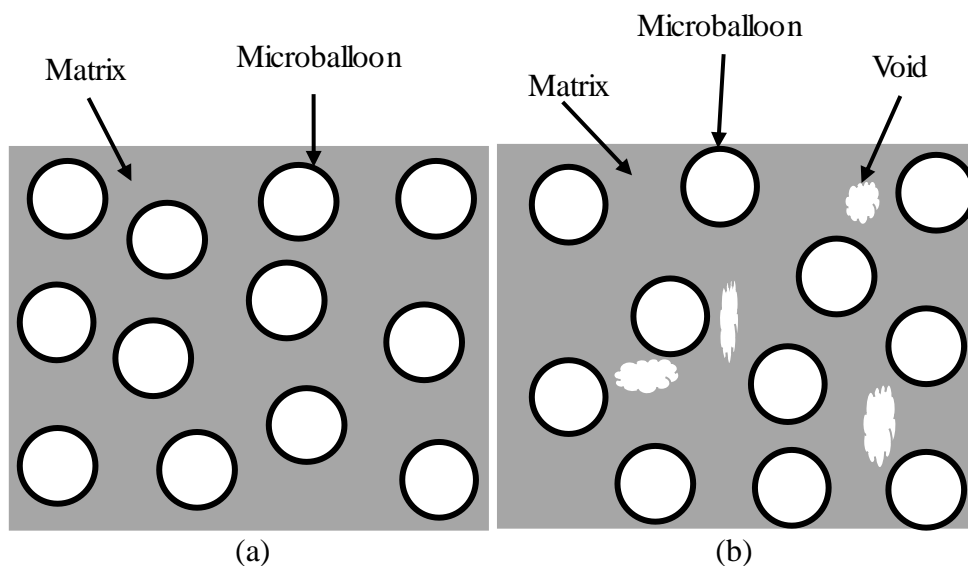


Figure 1.1 Schematic representation of syntactic foams (a) two phase (b) three phase (Gupta et al. 2013).

As seen in Figure 1.1, there are two constituents in SF namely, hollow particles (cenospheres) and matrix. For stresses to efficiently get transferred from matrix to filler, interfacial bonding between them plays a very vital role. Surface modification of the constituents might improve the performance of the SF's. When two or more constituents are blended together, often times they are not compatible with each other. Thus, the resulting blend has insufficient properties for most end uses. Functional additives can improve this compatibility. Compatibilizers are often used as additives to improve the compatibility of immiscible polymers and thus improve the morphology and resulting properties of the blend. Similarly, it is often challenging to disperse fillers effectively in the polymer matrix of a composite. The general principle of compatibilization is to reduce interfacial energy between the constituents in order to increase adhesion. Generally, adding compatibilizer also results in finer dispersion, as well as more regular and stable morphologies. Compatibilizer addition (typically at 5 - 7 wt. %) increases mechanical performance and surface properties. If a polymer (or blend) contains reinforcing fillers (such as inorganic fibers), an additive that can compatibilize the polymers in a blend may also act as a "coupling agent" enhancing interfacial strength and thus increase the stiffness (modulus), strength and impact toughness of the composite (Wu et al. 2007).

1.3 Processing of syntactic foams

Every material system has unique physical, mechanical and processing characteristics. A suitable manufacturing method must be chosen to transform the material to its final form. Processes used for the fabrication of parts prepared from composite materials have evolved in the later twentieth century from skilled labour operations to sophisticated microprocessor systems having automatically controlled equipment. Hand lay-up techniques or spray-up in open molds are used by early pioneers to form the final system by combining raw materials and cured at ambient temperature. Advantages of PMC's have steered these synthetic materials to enter almost every other market worldwide, from consumer products, automotive and marine to primary structural elements of aircraft and bridges. Such extensive growth in product applications commanded corresponding growth in materials technology, design approaches, and fabrication processes. In case of fabricating syntactic foam

composites, processing route must be carefully designed to effectively reinforce hollow particles into the resin. It is necessary to avoid particle breakage and unintentional effect of higher matrix porosity by steadying gas bubbles in polymer matrix. The processing methods need to be efficient enough in helping wetting of reinforcement by the matrix resin, breaking clusters without damaging reinforcement and attaining uniform distribution of reinforcement in the resin material. Figure 1.2 presents commonly used fabrication method for thermoset based syntactic foams. In this method, a two-step mixing process is used. Reinforcement (Cenospheres) is added to the neat resin and thoroughly mixed until the slurry of consistent viscosity is obtained in first step. In the second step, the hardener or catalyst is added to the resin and stirred slowly. The mixture is cast into the molds and cured as per the resin.

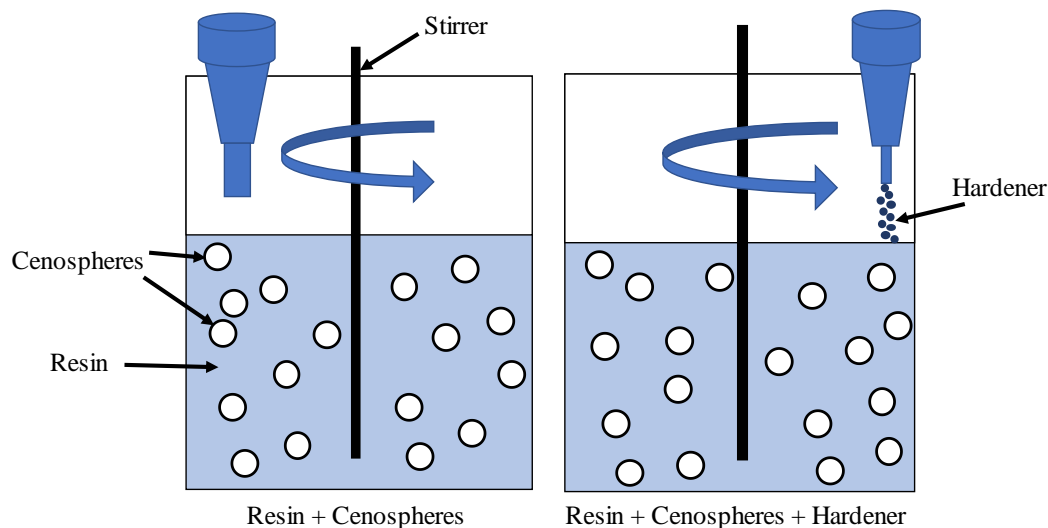


Figure 1.2 Illustration of syntactic foam fabrication steps (Gupta et al. 2013).

1.4 Role of interface and its modification

Interfacial bonding between reinforcement and matrix plays a very vital role in transferring load from matrix to cenospheres. Surface modification of the constituents might improve the performance of these SF's owing to better compatibility. Improvement in the morphology and resulting properties of the composite can be attained by using additives in the form of compatibilizer. Interfacial energy between the constituents reduces due to compatibilization resulting in increased adhesion. Generally, adding compatibilizer results in finer dispersion, alongside more regular

and stable morphologies resulting in higher stiffness, strength and impact toughness of the resultant composites.

A key region that influences mechanical properties of the composite is the matrix/reinforcement interface (Guru et al. 2015). A series of phenomena takes place at such interfaces. The structure of interface and the stresses developed during different stages of processing and services have a bearing on the fracture and failure of the composite. Hence, it is essential to consider the interfaces in detail and examine their effect on the composite properties, so as to alter the properties to suit ones need in the end product. Good interfacial bonding is essential to have effective load transfer from matrix to the filler. The interfacial characteristics can be improved in different ways; chemical treatment is one such effective method. Reinforcing materials such as fly ash cenospheres contain oxides like Al_2O_3 , SiO_2 and Fe_2O_3 which form links to hydroxyl groups during their contact with moisture and convert into water molecule (Rugele et al. 2017). The presence of water, additionally, reduces the wettability of the reinforcement as it lowers the surface energy. Coatings that function as coupling agents are expected to raise the effective surface energy of the reinforcement. The coupling agents are primarily aimed at creating a bridge between the oxide groups on the surface of filler and molecules of the matrix (Plueddemann 2016).

General formula of silane coupling agents is R-Si-X_3 , wherein this multifunctional molecule reacts with filler surface on one side and polymer phase on the other. In these 'X' group represent hydrolysable and thereby hydrolysis silane to corresponding silanol (R-OH) in the presence of aqueous solution. These silanol molecules and water molecules compete with each other to form hydrogen bonds with the hydroxyl groups that are strongly bonded to the reinforcement surface (Hull and Clyne 1996). Once the reinforcement is dried, the free water is taken away and condensation takes place both at silanol/surface junction and between the adjacent silanol particles. The resultant is a polysiloxane (X-R-Si (OH)_3) coating bonded to the filler/reinforcing surface offering an array of 'R' functional groups to the environment. These open functional groups involve in curing reaction with the polymer matrix and establish a bond (Hull and Clyne 1996). Besides improving the bonding and the mechanical

properties, the coupling enhances the electrical, thermal and magnetic properties due to increased effective contact at the interface. Another important feature is the increased resistance to environmental effects. The bonding also serves to reduce the effect of hostile environments at the reinforcement causing degradation and thus retains useful mechanical properties of the composite in spite of its exposure to such environments.

Silane treatments help in better wetting, wherein dirt or greasy/oily layers envelope the fillers the effectiveness of the medium to wet reinforcements/fillers reduces (Farinha et al. 2000). Their presence also affects the properties including mechanical behaviour. The mechanical property of polymer-cenosphere composite is lower attributed to poor interfacial interactions between the hydrophilic surface of cenospheres and hydrophobic polymer (Guhanathan et al. 2001). However, surface treated cenosphere is found to improve the interfacial interactions (Thongsang and Sombatsompop 2006).

A mechanism of interaction between Silane-69 (Bis (3-triethoxy silyl) propyl tetrasulfide) coupling agent and fly ash (Alkadasi et al. 2004), is shown in Figure 1.3. Effect of surface treated fly ash on the mechanical properties of high density polyethylene (HDPE) as compared to conventional calcium carbonate filler reveal increase in tensile strength on addition of fly ash (Atikler et al. 2006). However, higher increase is noticed when modified fly ash is used with 30% filler content. The decrease in elongation at break is higher for ash filled composites when compared to calcium carbonate ones. The decrease in property is higher in case of treated fly ash. Mechanical behavior of mica/epoxy composites is investigated to study the effect of silane and zirconate coupling agents (Bajaj et al. 1992). Tensile modulus and flexural strength are improved by the surface treatment. Properties of silica filled styrene-butadiene rubber composites are enhanced through plasma surface modification of silica (Kulkarni and Kishore 2002). Scanning electron microscopy revealed improved filler dispersion post plasma and silane treatment. Mathew et al. (2004) reported that the fly ash filled epoxy composite presented better strength in compression post exposure to aqueous media but the surface treated fly ash fillers in epoxy exhibited

reduction in compression strength. Ramakrishna et al. (2006) concluded that the toughened epoxy/fly ash composites revealed improved compressive and impact strength. However, the tensile strength decreased while modulus increased with increase in fly ash content (Srivastava and Shembekar 1990). Surface modifications are crucial and influence mechanical behaviour to a greater extent (Shahapurkar et al. 2018b).

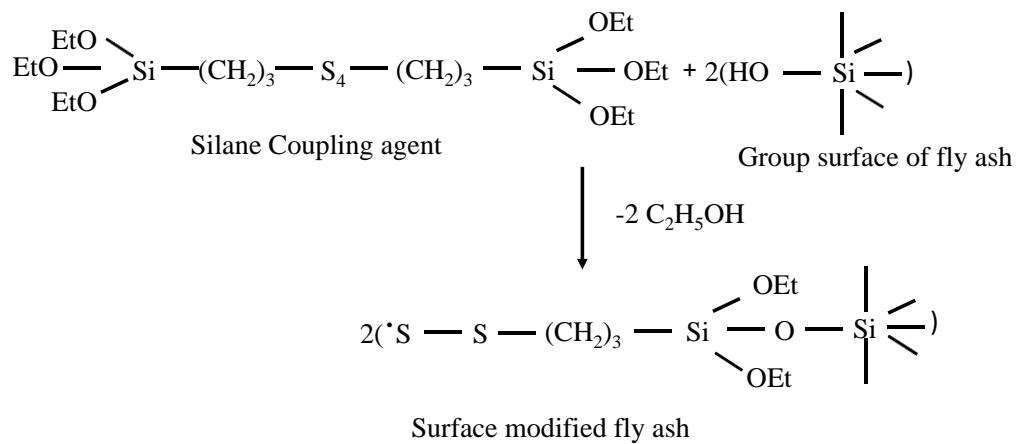


Figure 1.3 Reaction between Silane-69 coupling agent and fly ash (Alkadasi et al. 2004).

1.5 Sandwich structured composites

Sandwich structured composites are a special class of composite materials which have become very popular due to higher specific strength and bending stiffness. Low density of these materials makes them especially suitable for use in aerospace, automotive and marine structural engineering applications. Concept of sandwich structured composite materials can be traced back to as early as 1849 AD (Noor et al. 1996) but potential of this construction was realized only during the second world war. Developments in aviation posed requirement of lightweight, high strength and highly damage tolerant materials. Sandwich structured composites, fulfilling these requirements became the first choice for many applications including structural components. Now their structural applications spread even to the ground transport and marine vessels.

Sandwich composites comprise of two thin but stiff face sheets/facings/skins attached on either side of a lightweight, thick slab known as core. Many variations of this definition are available but the key factor in making this type of materials remains the lightweight core, which reduces the overall density of the material and stiff skins provide strength. The typical structure of sandwich composite is presented in Figure 1.4.

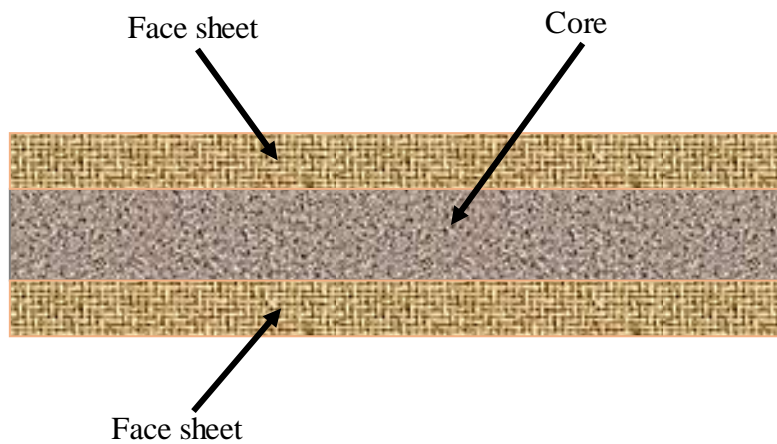


Figure 1.4 The structure of the Sandwich Composite.

Bonding between facings and core prevents the interfacial failure under the applied load enhancing the flexural rigidity of sandwich composites. There is no general rule about the relationship between the thickness of skin and core. It depends on the application and required properties. Major advantage of sandwich structured composites is the possibility of tailoring properties by choosing appropriate constituting materials and their volume fractions.

Sandwich composites basically consists of two components, facing and core as shown in Figure 1.4. If an adhesive is used to bind facings with the core, the adhesive layer can also be considered as an additional component in the structure. The thickness of the adhesive layer is generally neglected because it is much smaller than the thickness of skins or the core. The properties of sandwich composites depend upon properties of the core and skins, their relative thickness and the bonding characteristics between them.

1.5.1 Core materials

As per requirement for the application of the structured component many types of materials can be used as cores in sandwich panels. The choice of appropriate structure for core provides additional parameter to design a sandwich composite as per given specifications or service conditions. Low density solid materials such as open and close cell structured foams, balsa wood and polymeric foams seems to have higher specific compressive strength than the expanded high density cellular (Honeycomb, web core) and corrugated materials (Truss and corrugated sheets). Use of hollow particles, known as cenospheres, has increased considerably in recent years in the production of core materials of low density and high damage tolerance. Density values of syntactic foams can be tailored over a wide range by changing the material or density of cenospheres. Syntactic foams are known for their high specific compressive strength, low moisture absorption and excellent damping properties. They are used as core materials in sandwich composites for weight sensitive structural applications. Syntactic foams are multi-functional composite materials due to their broad range of mechanical properties coupled with vibration damping characteristics, fire performance and ability to be fabricated in functionally graded configurations (Gupta et al. 2014).

1.5.2 Facing materials

A wide variety of materials are available to use as facing material. Sheets of metals like aluminium, titanium and steel and fiber reinforced plastics are some of the common examples of facing materials. In case of fiber reinforced facings, the material properties can be controlled directionally in order to tailor the properties of the sandwich composite. Fiber reinforced polymers are used widely as facings due to their low density and high specific strength. Another advantage offered by the use of polymer composites in facings is that the same polymer can be used to make the skin and the core. Cross-linking of polymer between core and facings would provide adhesion strength level equal to the strength of the polymer. This provides possibility of making the facings an integral part of the structure eliminating the requirement of the adhesive. When an adhesive is used to bond the facing and the core together,

selection of adhesives becomes very important as they should be compatible with both the facing and the core materials. The adhesion must have desired strength level and should remain unaffected by the working environment. In case of metallic components, welding or brazing is used as a means of binding the core and facings together. Use of adhesives is also possible but is limited to such cases where one or more of the components cannot withstand heat. Choice of facings is important from the point of view of the work environment as this part of the structure which comes in direct contact with the environment. Corrosion, heat transfer characteristics, thermal expansion characteristics, moisture absorption and other properties of the whole sandwich composite can be controlled by proper choice of facing material. In most of the cases facing layer of a sandwich composite is made of same material. However, it can be of different type of material depending upon specific requirements. Mechanical properties of a sandwich composites can be tailored in terms of materials, thickness, fiber orientation, fiber volume fraction or in any other possible form.

1.6 Natural fiber composites

In recent years, plant and animal fibres are utilized to produce fiber reinforced composite for mechanical, civil, aerospace, automotive part due to their low density, good acoustic behaviour, lower pollutant emission and availability of resource (Mittal et al. 2016). Because of their easier availability, natural fibers have become good alternative material compared to synthetic and man-made fiber. The natural fibres are reinforced in polymer matrix with short and random orientations. Recently, some researchers demonstrated that reinforcement of natural fibre in fabric form will increase the mechanical properties of the composite significantly (Van Vuure et al. 2000).

Textile composites find applications in primary and secondary load bearing structures. Woven fabric composites are a type of textile composites wherein two or more yarn systems are interlaced at an angle. These composites have better properties in fabric plane and higher resistance under impact loading than the unidirectional composites. Due to interlacing of yarns higher out of plane strength can be achieved. This can take up the secondary loads due to load path eccentricities and local buckling. Handling of

woven fabric is easier as compared to continuous/short fiber form. Therefore, fabrication of woven fabric composites is less laborious forms, reduced manufacturing errors. These advantages are attained at the cost in-plane stiffness and strength properties due to the undulation of yarns (Naik and Shembekar 1992).

Sisal fiber is one of the most widely used natural fiber and can be cultivated easily. It is hard fiber extracted from the leaves of the sisal plant. The botanical name of sisal is “*Agave Sisalana*”. A sisal plant produces about 200-250 leaves and each leaf contains 1000-200 fiber bundles which is composed of 87.25% water, 8% dry matter, 4% fiber and 0.75% cuticle (Mukherjee and Satyanarayana 1984). Apart from ropes, general cordage and twines, sisal is also used in low-cost and specialty paper, buffing cloth, dartboards, geotextiles, filters, carpets, mattresses, handicrafts, and wire rope cores. Sisal has been utilized as an environmentally friendly strengthening agent to replace asbestos and fibreglass in composite materials in various uses including the automobile industry (Ku et al. 2011).

1.7 Literature survey

Exhaustive amount of research work has been carried out on characterisation of mechanical properties of syntactic foams and their sandwich composites. As demonstrated by various researchers through their theoretical and experimental investigations, the influence of particle size (Gupta et al. 2004), volume fraction (Bharath Kumar et al. 2016, Garcia et al. 2018, Shahapurkar et al. 2018a), reinforcements (Colloca et al. 2013) and functional grading of microballoons (Gupta et al. 2008) are seen to be used effectively to tailor the mechanical properties of these foams.

1.7.1 Buckling under mechanical load

Slender structural members subjected to in-plane compressive loads experiences lateral deflection beyond a threshold limit known as buckling loads. Buckling load is well below the load which causes yielding failure. Buckling instabilities of thick and thin elastic beams subjected with axial stresses is investigated by Matsunaga (1996) and the results are compared with Timoshenko beam theory with good agreement.

Tuttle et al. (1999) investigated buckling of flat laminated panel subjected to biaxial loading, and found that the buckling load increase with the load ratio. Byklum et al. (2004) presented computational model for global and post buckling analysis of the stiffened panels. They compared results obtained by the proposed model and with non-linear finite element method with good correspondence having high calculation efficiency. Esfahani et al. (2010) investigated the effect of delamination position on buckling load and buckling mode shape of carbon fibre and glass fibre reinforced polymer composites and found that the experimental results are in good agreement with the numerical results with higher buckling resistance compared with non-hybrid composites. Tariq et al. (2011) analysed tensile and buckling of polyester reinforced by natural jute fiber at different volume fractions. They found that the tensile stress and critical buckling load increases with increase in volume fraction.

Shams et al. (2013) investigated non-linear buckling of a spherical shell embedded in an elastic medium under uniaxial compressive load. Numerical investigations revealed that failure of syntactic foam is not governed by the microballoon shell buckling, but rather is governed by shearing of the particle as syntactic foams are fabricated with thin walled particles to obtain weight saving advantage. Sudhir Sastry et al. (2015) analysed pre-and postbuckling behavior of woven fabric carbon fiber/epoxy and E-glass/epoxy thin wall stiffened composite panels. They compared the variations of buckling stresses and loads obtained from numerical model with experimental results and found results were in good agreement. Li and Qiao (2015) reported buckling and postbuckling behavior of shear deformable anisotropic glass fibre reinforced epoxy laminated composite beams with initial imperfection subjected to axial compression. Their results revealed that the geometric, physical properties and boundary conditions have significant effects on postbuckling behaviour of anisotropic laminated composite beams. Abramovich et al. (2015) presented buckling and post buckling behavior of curved laminated composite panels and shells under axial compression. They observed large scatter between the results calculated from numerical and experimental analysis. Luu and Lee (2016) investigated the effects of geometric parameters on the buckling and post buckling of elliptical curved beams. They found that the symmetric snap-through mode governs the buckling of clamped–

clamped elliptical curved beams. Yang et al. (2017) investigated buckling and postbuckling of functional graded multilayer graphene platelet reinforced composite beams resting on elastic foundation based on shear deformation theory. Their results show that buckling and postbuckling resistance of polymer composite beams increased with addition of graphene platelet nanofillers.

1.7.2 Buckling and free vibration under axial compression

Any repetitive motion is called vibration or oscillation. The phenomenon of vibration involves an alternating interchange of potential energy to kinetic energy and kinetic energy to potential energy. Hence, any vibrating system must have a component that stores potential energy (spring or elastic element) and component that stores kinetic energy (mass or inertia element). The initial excitation to a vibrating system can be in form of initial displacement and/or initial velocity of the mass element(s). This amounts in imparting potential and/or kinetic energy to the system. The initial excitation sets the system into oscillatory motion, which is called free vibration. When a structure is subjected to any pre-stress caused by a static load its dynamic behavior will be different from that of the stress-free condition. It is important to analyse free vibration characteristics of a structure subjected to axial compression for its better design as the axial compressive load alters the structural stiffness significantly.

Although significant amount of work has been done on mechanical characterization of syntactic foam composites, studies on their free vibration behavior is very limited. Lateral vibrations of thin walled structures are of practical interest. Amba-Rao (1967) investigated fundamental frequencies in lateral vibration mode for straight bars under compressive loads for various fractions (less than one) of the Euler load for various boundary conditions. Later, Galef (1968) presented an approximate formulation relating fundamental natural frequencies of compressed and uncompressed beam with applied compressive and Euler buckling load. Investigation of Shaker (1975) resulted in expressions for mode shape and characteristics equations for various boundary conditions. The effect of preload on natural frequencies and mode shape are represented graphically. Bokaian (1988) presented analytical solutions for variation of natural frequencies of an isotropic beam subjected to axial compression loads under

various boundary conditions and found that Galef's expression is not valid for pinned-free and free-free beams.

Matsunaga (1999) analyzed natural frequencies and buckling stresses of deep beam – columns on two parameter elastic foundations taking account of shear deformation, depth change and rotatory inertia. He found that the natural frequency reaches zero when the beam is subjected to critical buckling load. Rahmani et al. (2009) investigated free vibration frequencies of sandwich beams with functionally graded syntactic foam core based on higher order sandwich panel theory. They found that natural frequency of the sandwich beam increases with inhomogeneity of the core material. Zhu et al. (2012) investigated bending and free vibrations of thin to moderately thick single walled carbon nanotube reinforced composite plates using finite element method based on shear deformation theory. They found that the carbon nanotube volume fraction, width to thickness ratio and the boundary conditions have influence on deflections in bending mode, natural frequencies and mode shapes of the composite plate.

Recently Carpinteri et al. (2014) investigated the dependence of the fundamental frequency on the axial load in slender beams which were subjected to imposed axial end displacements. They observed that the zero frequency was never reached at the buckling load, due to the combined effects of geometric and material imperfections. Lenci and Rega (2016) analyzed free vibrations of planar elastic beams considering geometric non-linearities and linear elastic behavior of the material using asymptotic method. They observed that for slender beams, softening behavior for hinged–supported and stronger hardening for hinged–hinged boundary conditions. Rajesh and Pitchaimani (2017) investigated buckling and free vibration behavior of woven natural fabric and sandwich composites with glass fiber facings and natural fiber fabric core under axial compression. They observed that the weaving pattern of the fabric have significant influence on the buckling strength pattern and the natural frequency reduces with increase in axial compressive load in pre-buckling regime.

1.7.3 Vibration correlation technique (VCT)

Several investigators used VCT to predict the critical buckling load of structures under axial compression. Plaut and Virgin (1990) examined Singer's procedure and suggested guidelines to estimate lower and upper bounds on buckling load. Souza and Assaid (1991) presented a new technique for prediction of buckling loads of structural elements with post buckling unstable characteristics. They observed that the characteristic curves show linear relationship at lower load levels and there is sudden change in these curves when the load approaches the buckling value. Arbelo et al. (2014) used VCT for estimation of real boundary conditions and buckling load of unstiffened plates and cylindrical shells. They observed variation of natural frequencies of perfect and imperfect plate and found that the frequencies decrease with increase in compressive load. The fundamental natural frequency reached minimum value when buckling occurred and after buckling the frequency starts to increase. Abramovich et al. (2015) used VCT to predict buckling loads of stringer stiffened curved panels which are made of aluminium and laminated composites. Based on the modal tests performed on curved panels and on a shell, guidelines are formulated for the application of the VCT to thin-walled structures with stable post-buckling behavior.

1.7.4 Temperature dependent properties of syntactic foams

Existing literature on the temperature dependent properties of the syntactic foams represent coefficient of thermal expansion (CTE), thermal conductivity (TC) and dynamic mechanical analysis (DMA) (Gupta et al. 2018). Parameters such as volume fraction and wall thickness can be used to tailor these properties effectively. Labella et al. (2014) examined CTE of vinyl ester matrix/fly ash and observed 48% decrease in CTE by with increasing filler content from 30 to 60 vol.%. In comparison with neat resin, foams exhibited lower CTE values. Li et al. (2017) presented numerical investigation of TC in syntactic foams. Their results revealed that TC of foam decrease with increase in volume percentage of GMB's. Numerical investigation by Park et al. (2008) revealed that thermal conductivity ratio (ratio of thermal conductivities of microballoon shell to matrix) increases significantly with relative wall thickness of the microballoons at all volume fractions. Effect of volume fraction

and wall thickness of GMB's on thermo mechanical properties of epoxy matrix syntactic foams are studied by Lin et al. (2009). They observed that the CTE of syntactic foams is lower than the neat epoxy due to presence of ceramic particles. The filler volume fraction has a strong effect on the glass transition temperature as compared to wall thickness variations.

Temperature dependent elastic properties of syntactic foam composites have been addressed by Sankaran et al. (2006) and Gupta and Pinisetty (2013). Gu et al. (2007) investigated DMA of fly ash/epoxy syntactic foams and reported that the addition of fly ash enhanced the damping capacity. Studies also revealed that the damping mechanism is governed by matrix viscoelasticity, grain boundary sliding with the cenosphere particles and interfacial sliding friction between the constituents. Similar trend is also observed for modified epoxy and fly ash cenosphere syntactic foams Wu et al. (2007). Hu and Yu (2011) investigated thermal, DMA and tensile properties of hollow polymer particle filled in epoxy resin. As compared to neat resin these foams showed higher damping with peaks shifting to higher temperature.

1.7.5 Buckling under thermal load

Thin walled slender members are exposed to heat during their service and subjected to thermal stresses when free expansion of the structure is restricted. The thermal stresses will change stiffness of the structure which in turn alter dynamic characteristics of the structure. The temperature rise above ambient temperature which causes buckling is known as critical buckling temperature. Thin-walled structural members with in-plane restrained deflections subjected to thermal environment results in buckling mode failure. Cotterell and Parkes (1962) analysed the buckling mode shapes of circular plates that were subjected to heating at centre and at the edge. Biswas (1976) analysed the thermal buckling behaviour of orthotropic plates having different geometry and edge constraints using Galerkin's approach. Aydogdu (2007) obtained critical buckling temperature for cross ply laminated composite beams with different combinations of hinged and clamped edge constraints using Ritz method. Gupta et al. (2009) used finite element and intuitive formulations to investigate the thermal post buckling behaviour of slender and shear

flexible columns under different boundary conditions. Sharifian (2010) computed the critical buckling loads of isotropic rectangular plates having two simply supported opposite edges and the other two supported against rotation. Jeyaraj (2013) investigated the buckling and free vibration behaviour of isotropic plates subjected to arbitrarily varying temperature fields. The influence of free edge on the critical buckling temperature and corresponding modes shapes are detailed in the study. The impact of non-uniform temperature profiles on the thermal buckling behavior of anisotropic panels was investigated by Li et al. (2015).

Several researchers investigated effect of thermal load on buckling behavior of structural components having simple geometrical shapes. However, most of the studies are based on analytical (Fu et al. 2014) and numerical (Jeyaraj 2013, Li et al. 2015, Shen et al. 2017) approaches with a very less focus on experimental investigations. The influence of non-uniform temperature field on non-linear buckling behavior of isotropic beam is investigated through experimental and numerical methods by George et al. (2016). They observed that the critical buckling temperature is strongly influenced by temperature variation conditions. It was observed that the structure which is subjected to centre heating in comparison to edge heating have significant influence on the thermal buckling behaviour. Bhagat and Jeyaraj (2018) investigated buckling strength of the aluminium cylindrical panel subjected to non-uniform temperature profiles through experimental approach. Results revealed that the buckling strength significantly varied with location of heating source. These studies bring forth the role of non-uniform temperature profile on the thermal buckling behavior of the structures and needs to be looked into.

1.7.6 Snap-through buckling behavior

The snap-through buckling of curved beams, shallow arches, cylindrical panels and shells under thermal and mechanical loads has been studied analytically and numerically by several researchers (Crisfield 1981, Haftka and Mallett 1971, Lee and Kim 2013, Watts et al. 2018). However, experimental investigation on snap-through buckling is scarce. The snap-through buckling of beam structures subjected to quasi-static loading is analyzed by using elastic theory of prismatic bars by Huang and

Vahidi (1971). Chen and Hung (2011) studied the snap-through buckling of a hinged elastica subjected to a midpoint force theoretically and compared the results with experimental observations. Chandra et al. (2012) examined the performance of beam using continuum non-linear finite element formulations in conjunction with several popular implicit time stepping algorithms to assess the accuracy and stability associated with numerical simulations of snap-through events. Chandra et al. (2013) combined experimental-computational framework to analyse the snap-through buckling behaviour of clamped-clamped shallow arches subjected to harmonic distributed loadings.

Plaut (2015) investigated numerically snap-through buckling characteristics of beams and circular arches with the help of unilateral displacement control technique. Liu et al. (2015) investigated the stochastic non-linear snap-through response of a clamped composite panel subjected to the combined severe acoustic excitation and a steady thermal effect using single mode Fokker plank distribution function. Studies indicated that the stationary statistical solution of the single-mode analysis captures the features of the displacement density distribution and showed the evolution from no snap-through to a persistent stochastic response. Wang and Fancey (2015) studied bistable morphing of polymeric composite caused due to viscoelastic force induced owing to temperature changes. Dehrouyeh-Semnani et al. (2017) examined snap-through buckling behavior of microbeam made of functionally graded material when subjected to uniform thermal load using numerical method. Plaut and Virgin (2017) investigated snap-through behavior of shallow elastic arches under dynamic, unilateral displacement control, with the indenter moving at constant velocity. Keleshteri et al. (2018) investigated snap-through instability of functionally graded carbon nanotube reinforced composite plate with piezoelectric layers.

1.7.7 Buckling and free vibration studies of sandwich composites

Studies on syntactic foam sandwich composites are available in literature wherein majority of research is focused on mechanical characterisation of foams and their sandwiches. Gupta and Sankaran (1999) investigated compressive properties of glass microballoon reinforced syntactic foam core with glass-epoxy and glass-carbon-epoxy

skins. They observed delayed crack initiation for glass-carbon/epoxy hybrid skin than glass/epoxy ones. Gupta and Woldeesenbet (2005) investigated flexural properties of sandwich composites with microballoons/epoxy syntactic foam core E-glass fiber/epoxy skins. They found that the core shear strength and skin bending stress decrease with radius ratio of microballoons. Islam and Kim (2012) investigated tensile and flexural response of sandwich composites with syntactic foam core and paper skin. They observed that, syntactic foams synthesized by lower particle size exhibits higher flexural properties than the sandwich with higher particle size. Salleh et al. (2016) investigated mechanical properties of GFRP/vinyl ester skin with glass microballoon/vinyl ester syntactic foam core sandwich panels. They found that the properties are dependent on the weight fraction of the glass microballoons, void content and interfacial bonding between the constituents.

Buckling and free vibration studies of sandwich composites with syntactic foam cores are very scarce. Fleck and Sridhar (2002) carried out experimental investigations on sandwich columns made of woven glass fibre epoxy skins and PVC foams with different densities. They observed that the columns undergo different types of buckling phenomenon (Euler macrobuckling, shear microbuckling and face microbuckling) depending on the geometry of the sandwich columns. Mahfuz et al. (2005) studied buckling under in-plane compression of sandwich composites made of Klegcell foam core and S2-glass/vinyl ester face sheets. Their results revealed that buckling loads increased with density of the core material and high-density cores arrested the delamination between core and skin and core shearing phenomena during buckling. Analytical approach to evaluate the buckling load of sandwich made of glass/carbon and boron fiber laminate skin and PVC foam is established by Aiello and Ombres (2007). John et al. (2008) investigated tensile and compressive properties of glass microballoon/cyanate ester syntactic foam with carbon-cyanate ester skin and observed that the mechanical properties increase with resin content. The theoretical model predicted better global buckling behaviour of sandwich panels for lower values of skin ratio thickness to overall sandwich thickness. Jasion and Magnucki (2013) performed experimental, analytical and numerical analysis on buckling behaviour of aluminium foam core sandwich with aluminium face sheet subjected to axial

compression. Experimentally obtained critical buckling loads are found to be closer to analytical and numerical results. Mathieson and Fam (2014) investigated the effect of cross-sectional configuration and slenderness ratio on GFRP skin and polyurethane core sandwich composites. Lower slenderness ratios resulted in skin wrinkling mode of failure and length greater than critical slenderness ratios resulted in global buckling. Le Grogneq and Saoud (2015) investigated numerically elastoplastic buckling and post buckling behaviour of sandwich columns with symmetric homogenous and isotropic core/skin layers subjected to axial compression. The results obtained numerically are found to be in good agreement with the available analytical solutions. Grygorowicz et al. (2015) presented analytical and numerical buckling analysis of sandwich columns with aluminium face sheet and aluminium alloy foam core. Smyczynski and Magnucka-Blandzi (2015) analysed buckling behaviour of simply supported sandwich beam with aluminium face and foam core numerically using transverse shear deformation effect. Tang et al. (2015) investigated buckling behaviour of fixed-fixed and hinged-hinged calcium silicate face sheets sandwich panels with polyurethane foam core subjected to axial load. Buckling load values obtained through analytical, numerical (finite element method) and experimental routes matches closely.

Sokolinsky et al. (2004) investigated free vibration response of polymer foam core and steel face sheet cantilever sandwich beam analytically and experimentally. The results obtained using higher order theory are found to be in good agreement with experimental values. Wu et al. (2015) investigated buckling and free vibration response of functionally graded carbon nanotube-reinforced composite face sheets with Titanium alloy core using Timoshenko beam theory. They observed that carbon nanotube (CNT) volume fraction, slenderness ratio and end supporting conditions have significant influence on natural frequencies as well as critical buckling loads. Goncalves et al. (2017) investigated buckling and free vibration of PVC foam core sandwich with steel face sheets numerically using coupled stress finite element method. Microstructure dependent beam element predicted more accurate results than the classical Timoshenko beam model.

1.7.8 Thermal buckling of sandwich composites

Lan et al. (1993) numerically investigated three layered bimodular sandwich beam consisting of thick skins and moderately stiff cores subjected to uniform and non-uniform thermal loads. They found that the sandwich beams having lower thermal expansion coefficient undergo compression in hinged-hinged condition, whereas clamped-clamped beams show axial compressive strains in facings and its stiffness remain unaltered until buckling. Kant and Babu (2000) analysed thermal buckling analysis of skew symmetric laminates and sandwich panels with cross ply composites facings and honeycomb core. They observed that the first order shear deformation theory overestimates thermal buckling temperatures marginal than higher order shear deformation theory. Buckling of free-free plate under non-uniform thermal load is analysed numerically by Mead (2003). Shiau and Kuo (2004) investigated numerically postbuckling behaviour of graphite epoxy laminated face sheets and aluminium honeycomb core sandwich panels subjected to uniform thermal load. They observed that the buckling mode shape and temperature are influenced by fiber orientation of laminated face sheets and aspect ratio of the sandwich panel. Liu et al. (2006) investigated buckling behaviour of E-glass/vinyl ester laminate column subjected to combined axial compressive and uniform thermal load. They observed that the structure bends away from the heating source at lower temperatures and towards the heating source due to generated thermal moment. Pradeep et al. (2007) analysed vibration and thermal buckling characteristics of sandwich beam made of DYAD609 viscoelastic core and graphite/epoxy skin and plate. Considerable difference between the predicted buckling temperature and natural frequencies is observed for beam and plate elements because beam element does not consider transverse shear deformation. Yuan et al. (2014) experimentally investigated thermal buckling behaviour of sandwich panels with pyramidal truss core. They observed that experimental results are lower than the results predicated by analytical approach due to defects and imperfections induced during sandwich panel fabrication.

A finite element method is developed to analyse buckling and non-linear analysis of multi-layered sandwich plates and shells by Moita et al. (2015). The facings and core materials are modelled using classic plate theory and Reddy's third order shear

deformation theory. Bouazza et al. (2018) analytically investigated thermal buckling behaviour of jute fiber reinforced in epoxy laminate beams using higher order shear deformation theory. The results compared with other published literature found to be in good agreement.

Chao and Lin (1990) numerically investigated static and dynamic snap-through buckling of sandwich spherical caps. The dynamic buckling load are found to be much lower than the static buckling loads. Sandwich with laminated face sheets and honeycomb core where numerically investigated by Shiau and Kuo (2004). The buckling mode and critical buckling temperature are dependent on the fiber orientation and aspect ratio of the plate. Mirzaei and Kiani (2015) analytically investigated snap-through buckling of sandwich beams with functionally graded CNT face sheets and homogenous/isotropic core using Chebyshev-based polynomial Ritz method. The intensity of snap-through phenomena increases with decrease in volume fraction of CNT fibers. Sandwich beams with CNT face sheet and isotropic core subjected to thermal load is analysed analytically by Kiani (2016). Buckling behaviour of sandwich beams is influenced by CNT volume fraction, different skin and core thickness ratios. The sandwich beams with functional graded CNT's showed higher buckling temperatures compared to uniformly distribution of CNT's.

1.8 Closure

Though SF's and their sandwich composites are widely used, thrust on developing these with variety of particulate fillers is overgrowing. Interest in utilizing the advantage of low density of syntactic foams and their sandwiches in variety of applications has made it necessary to characterize these materials for buckling and dynamic characteristics and also to study various parameters governing them. Operating conditions of such syntactic foam components in service vary due to mechanical and thermal loads necessitating their investigations under varying temperature conditions. Sisal fiber reinforced composites find applications in marine and automobile industries hence usage of such natural fibers in making of sandwich composites is worthy.

1.9 Motivation

Fly ash, a waste by-product generated by combustion of coal in thermal power stations and available in abundance. The use of fly ash cenospheres as filler material in polymer composites is considered important from both economic and commercial point of view. Fly ash cenospheres are used as reinforcing filler in polymers to develop lightweight composites. Some studies have pointed to the excellent compatibility between fly ash and polymers. Other researchers have also shown the advantageous use of treated fly ash in a wide variety of polymer matrices.

Natural fibers have several advantages such as low density, inexpensive and eco-friendly compared to synthetic fibers like glass, kevlar and carbon fiber. These natural fiber reinforced polymer composite can be used as an alternative material to conventional metals and laminated composites in structural applications where the load carrying capacity of a structure is not vital. However, it is essential to analyse structural behavior of a material subjected to several loading conditions. Thin-walled structures under axial compression are subjected to buckling mode of failure. The present work is focused on investigation of buckling and free vibration characteristics of syntactic foam composites and their sandwiches under mechanical and thermal loads.

1.10 Objectives of the work

From the foregoing literature survey, it is clear that the buckling and dynamic characteristics of low-cost syntactic foams and their sandwiches are not investigated. Syntactic foam and their sandwich composites may replace conventional metals and laminated composites in several structural engineering applications. Hence, it is important to analyse buckling and dynamic behavior of structural members made out of these materials against mechanical and thermal loads for their better design.

Main objectives of the proposed work are:

- To investigate buckling characteristics of syntactic foam composites under mechanical and thermal loads.
- To investigate free vibration characteristics of syntactic foam composites under axial loads keeping buckling load as a parameter.

- To analyse the influence of fly ash cenosphere loading and its surface treatment on buckling and free vibration characteristics.
- To study buckling and free vibration characteristics of syntactic foam core sandwich composites with natural fibre fabric as face sheets under thermal and mechanical loads.
- To compare the experimental of syntactic foam composite under mechanical load with analytical results.

1.11 Outline of the thesis

The systematic study carried out with respect to above objectives is presented in the thesis. A brief skeletal structure of the thesis is.

Chapter 1. Intends to provide necessary details of the research on syntactic foam composites along with an exhaustive literature survey followed by objective and scope of the work.

Chapter 2. Focuses on the constituents used for thermosetting syntactic foam and their sandwich composites, surface treatment details, fabrication route adopted and testing methodology.

Chapter 3. Provides detailed results and discussions on material characterisation, Mechanical buckling and free vibration characteristics of syntactic foams subjected to axial compression.

Chapter 4. Behaviour of syntactic foams under non-uniform heating conditions and volume fraction of cenosphere content is presented.

Chapter 5. Presents buckling and free vibration characteristics of sandwich composites with syntactic foam core and sisal fiber woven fabric/epoxy facing subjected to axial compressive loads.

Chapter 6. Behaviour of sandwich composites with syntactic foam core and sisal fiber woven fabric/epoxy facing subjected to non-uniform heating conditions are discussed in this chapter.

Chapter 7. Presents summary, conclusions and future scope of work.

2 MATERIALS AND METHODS

2.1 Constituents

In present work, Lapox L-12 epoxy is used as matrix system to prepare syntactic foams and their sandwich composites. Lightweight syntactic foams are prepared using fly ash cenospheres in as received and silane treated form. Sisal plain woven fabric reinforced epoxy laminate is used as facing material in the syntactic foam core sandwich composite. Details about these constituents are dealt with in the sections to follow.

2.1.1 Matrix

Diglycidyl ether of bisphenol-A based epoxy resin, Lapox L-12 with a room temperature curing polyamine K-6 hardener, supplied by Atul Ltd., Gujarat, India, is used as the matrix resin and is as shown in Figure 2.1a. Lapox L-12 is a liquid, Unmodified epoxy resin of medium viscosity can be used with various hardeners for making composites. K-6 hardener is a low viscosity room temperature curing liquid hardener. The properties of epoxy resin and hardener are presented in Table 2.1.

Table 2.1 Properties of epoxy resin and hardener*.

Properties	Test method	Values	
		LAPOX L-12	K-6
Appearance	Visual	Clear, viscous liquid	Clear liquid
Color (GS)	ASTM D1544	Max 1	Max 1
Viscosity @ 25°C (m Pas)	ASTM D2196	9,000-12,000	-----
Epoxy content (Eq/kg)	ASTM D1652	5.26-5.55	-----
Specific gravity @ 25°C	ASTM D792	1.1-1.2	-----
Refractive index	-----	-----	1.494-1.50
Pot life @ 25°C (min)	ASTM D2471	-----	30-40
Recommended ratio (w/w)	-----	-----	10

*As provided by the supplier.



Figure 2.1 (a) Epoxy resin and hardener (b) Cenospheres and (c) Sisal woven fabric used in this study.

2.1.2 Fly ash cenospheres

Fly ash cenospheres of grade CIL 150 supplied by Cenosphere India Pvt. Ltd, Kolkata, West Bengal, India, is used as the filler material. Cenospheres are used in as received condition (Figure 2.1b), without any surface treatment. Table 2.2 presents the physical, chemical and sieve analysis details of fly ash cenospheres in as received condition. These cenospheres are primarily made up of silica (SiO_2), alumina (Al_2O_3), calcium oxide (CaO) and iron oxides (Fe_2O_3) as observed from Table 2.2.

Table 2.2 Physical, chemical and sieve analysis details of cenospheres*.

Physical properties		Chemical analysis		Sieve analysis	
True particle density	920 kg/m ³	SiO ₂	52-62%	+ 30 # (500µm)	Nil
Bulk density	400 – 450 kg/m ³	Al ₂ O ₃	32-36%	+ 60 # (250µm)	Nil
Hardness (MOH)	5 – 6	CaO	0.1-0.5%	+100 # (150µm)	Nil
Compressive strength	0.00176 – 0.00274 MPa	Fe ₂ O ₃	1-3%	+150 # (106µm)	0-6%
Shape	Spherical	TiO ₂	0.8-1.3%	+ 240 # (63µm)	70-95%
Packing factor	60-65%	MgO	1-2.5%	+ 240 #	0-30%
Wall thickness	5-10% of shell dia.	Na ₂ O	0.2-0.6%		
Color	Light grey – light buff	K ₂ O	1.2-3.2%		
Melting point	1200 – 1300 °C	CO ₂	70%		
pH in water	6 – 7	N ₂	30%		
Moisture	0.5% max.				
Loss on ignition	2% max.				
Sinkers	5% max.				
Oil absorption	16 – 18 g/100g				

*As provided by the supplier.

2.1.3 Sisal woven fabric

Sisal plain woven natural fibre fabric acquired from Jolly Enterprise, Kolkata, West Bengal, India is used as reinforcement in the facings of the sandwich and is as shown in (Figure 2.1c).

2.2 Surface treatment of cenospheres

Silane coating on cenospheres is carried out using 3-Amino propyl triethoxy silane (APTS), procured from M/S Sigma Aldrich, Bangalore, India. In syntactic foams, the volume fraction and size of cenospheres can alter the overall mechanical properties. Apart from the volume fraction and size, the interaction between cenospheres and epoxy also plays a major role in load transfer mechanism between the constituents (Guhanathan et al. 2001).

Mechanical properties of cenosphere reinforced polymer composites are inferior owing to poor interfacial interactions between the hydrophilic cenosphere surface and

hydrophobic polymer. Silane coupling agents are usually used as adhesion promoters between inorganic filler and organic matrix. In the present work water/ethanol mixture in the weight proportion of 20:80 is prepared and maintained at 80°C. In this 100 ml solution 50 gm of cenospheres are mixed. Solution is continuously stirred for 30 min at 80°C in a microwave reactor (Enerzi Microwave Systems, Bangalore) after adding APTS of 2 % by volume. Treated cenospheres are extracted after resultant product is filtered and washed at least three times using a mix of water/ethanol post drying in an oven. Fourier transform infrared (FTIR) spectroscopy is conducted on cenospheres to confirm the silane coating.

2.3 FTIR spectroscopy and particle size analysis

FTIR spectroscopy of cenospheres is carried out on JASCO 4200 (Japan) with automated total reflection mode using wave number in the range of 4000 to 650 cm^{-1} . X-ray diffractograms are obtained for 2Θ values using DX GE-2P, Japan having nickel filter material with scanning speed of $2^\circ/\text{min}$ and Cu $K\alpha$ ($\lambda=1.514 \text{ \AA}$) radiation. Particle size and shape analysis is carried on Sympatec (Pennington, NJ) QICPIC high speed analysis system.

A pulsed laser illuminates the particles as they pass a camera that images the particles at 175 frames/sec. For each particle imaged, the equivalent diameter is calculated as the diameter of a sphere having a projected area equal to the projection captured by the camera. Five runs of each particle type are conducted and the values presented are averaged from these runs, with weight according to the number of particles in each run. Approximately 375,000 and 550,000 particles are measured for untreated and treated particles respectively (Bharath Kumar et al. 2016).

2.4 Syntactic foam fabrication

Cenospheres (20, 40 and 60 vol.%) and epoxy resin are weighed in a predetermined quantity and stirred slowly until homogenous slurry is formed. Polymerization process is initiated by adding 10 wt.% of K6 hardener into the slurry before pouring it into the mold. Subsequently this mixture is decanted into aluminium mold (Figure 2.2). Silicone releasing agent is applied to the mold for easy confiscation of cast slabs.

The castings are allowed to cure for 24 hours at room temperature and trimmed using diamond saw to the required dimensions. Similar method is adopted to prepare syntactic foams with untreated and surface modified cenospheres. The untreated (as received) cenosphere/epoxy samples are coded as per nomenclature EXX, where letter 'E' denote neat epoxy resin, 'XX' represents cenosphere volume %. For example, E40 refers to epoxy resin filled with 40 vol.% untreated cenospheres. The surface modified cenosphere/epoxy samples are named as EXXT, where 'T' represents surface modified cenospheres. For example, E40T refers to epoxy resin filled with 40 vol.% of surface modified cenospheres. Neat resin samples are also prepared under similar processing conditions for comparison.



Figure 2.2 Aluminium mold used to prepare syntactic foams.

2.5 Sandwich preparation

Sandwich composites are prepared using hand lay-up process. Initially the skins/facings are wetted in epoxy matrix and excess epoxy from the skin is removed. The wetted skins of desired thickness are laid on the bottom plate of the mold and foam core of known thickness is placed on top of bottom skin. Later, wetted skin is placed on top of the core. The upper plate is placed on the top of upper skin and clamped firmly (Figure 2.3) to maintain overall sandwich thickness of 4 mm. Both plates are coated with silicone releasing agent for easy removal of the casted sandwich sample. The sandwich castings are allowed to cure for 24 hours at room temperature. The specimens for the testing are cut from the cast sandwich panels using diamond saw cutter. The sandwiches prepared are named by adding alphabet 'S' prior to the name to syntactic foam. For example, SE20 represent sandwich with

E20 syntactic foam core and SE20T represents sandwich composite with syntactic foam core containing 20% by volume of surface modified cenospheres.

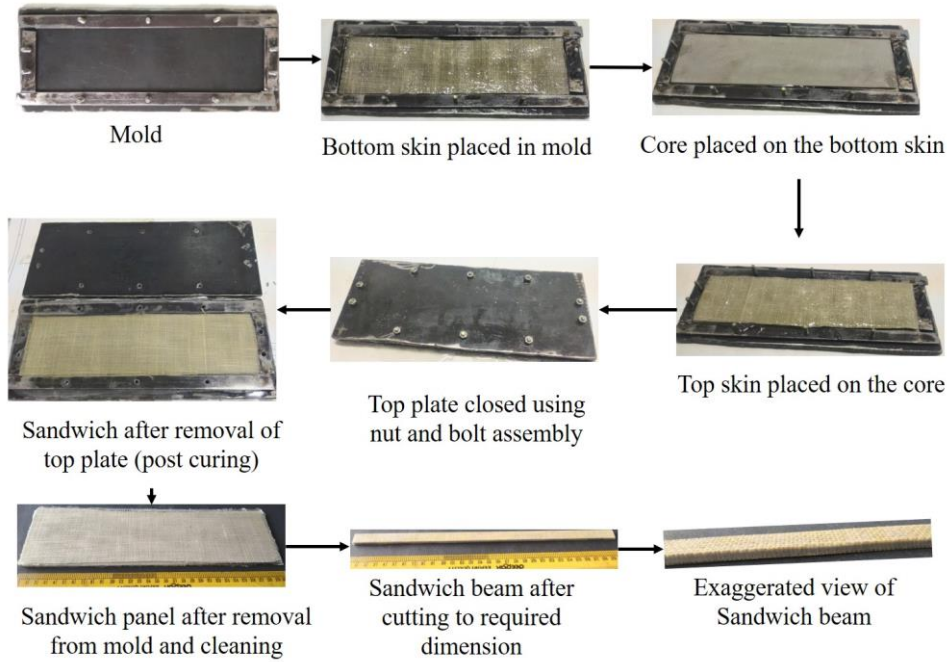


Figure 2.3 Syntactic foam core sandwich composite preparation steps.

2.6 Density test

ASTM D792-13 is employed to determine experimental densities of all the samples. For each composition of foam and sandwiches, five specimens are tested and the average values with standard deviation are presented. Theoretical densities of syntactic foams and their sandwiches are calculated using rule of mixtures and is given by,

$$\rho^{th} = \rho_m v_m + \rho_f v_f \quad (2.1)$$

where ρ and v represent density and volume fraction respectively and suffixes m and f represent matrix and filler respectively. Air entrapped during manual mixing of cenospheres in epoxy resin and while casting of sandwich composite is represented as void content. Void content (ϕ_v) is calculated by the comparative difference between the theoretical (ρ^{th}) and experimentally measured (ρ^{exp}) density (Tagliavia et al. 2010) and is given by,

$$\phi_v = \frac{\rho^{th} - \rho^{exp}}{\rho^{th}} \quad (2.2)$$

Void content estimation is crucial as it influences the mechanical properties.

2.7 Buckling at room temperature under mechanical loading

Buckling behaviour under mechanical load is carried out with the help of Universal Testing Machine (H75KS, Tinius Olsen make, UK, with load cell capacity of 50 kN). The schematic sketch of the experimental setup is shown in Figure 2.4a. Specimens are rigidly clamped at both the ends in the grippers having 210 mm of free length between them to resemble clamped-clamped condition (Figure 2.4c). Five specimens of each composition are tested and the average values are reported. Cross-head displacement rate is maintained constant at 0.2 mm/min. The least count of the data acquisition system (DAQ) used to measure deflection is 0.001 mm. For all tests, the end shortening limit is set at 0.75 mm to explore the behavioural changes, if any, in the post buckling regime.

2.8 Free vibration under axial compressive load

Experimental modal analysis is carried out to predict first three natural frequencies corresponding to first three bending modes of samples subjected to compressive load under clamped-clamped condition. Schematic representation and photograph of actual experimental setup utilised are shown in Figure 2.4a and Figure 2.4b respectively. Roving hammer method is used to excite the samples and the vibration signals are recorded by a uniaxial accelerometer. Kistler make impulse hammer (9722A2000, sensitivity of 10 mV/N) and light weight accelerometer (8778A500, sensitivity of 10 mV/g) with operating range of ± 500 g are used. Accelerometer is mounted on the specimen using bee's wax. The response signals are collected by DEWESoft software where in time domain signals are converted into frequency domain using Fast Fourier Transform (FFT) algorithm to report natural frequency and mode shapes. The experimental modal analysis is carried out at every increment load of 50 N. The application of compressive load is paused for 2 minutes to perform modal analysis.

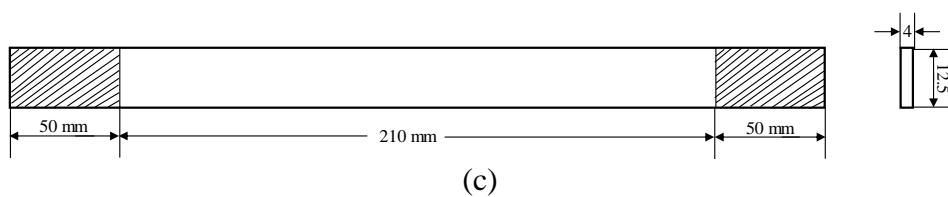
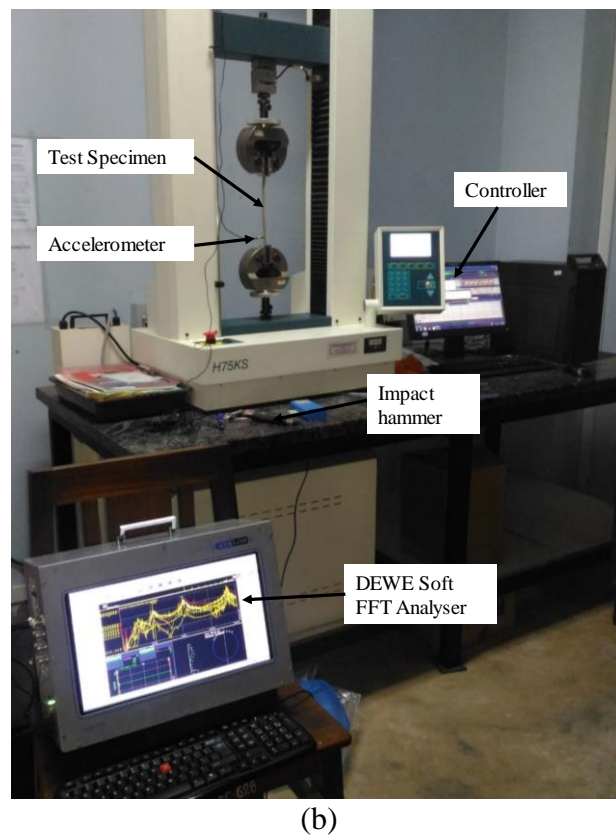
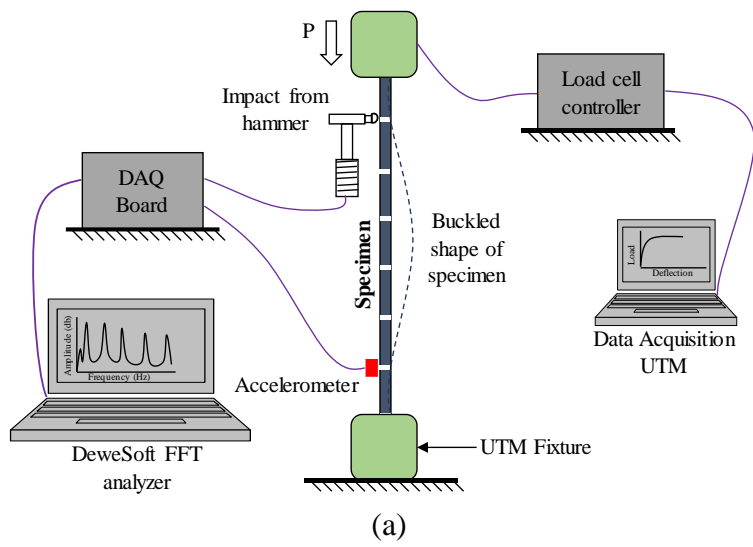


Figure 2.4 (a) Schematic representation and (b) actual experimental setup, showing buckling and free vibration tests and (c) Schematic representation of test specimen.

2.9 Coefficient of thermal expansion (CTE)

The coefficient of thermal expansion of syntactic foams are measured as per (ASTM D696-13) and the results are utilised to analyse the influence of filler loading in syntactic foams when they are exposed to thermal environment. Test temperature is varied from 20 to 90°C and the corresponding expansion is measured along linear direction using Dilatometer (CIPET, Chennai, India). Five specimens of dimension 50×12.7×3.2 mm of each composition are tested and the average values are reported.

2.10 Buckling under non-uniform thermal load

Figure 2.5 shows schematic representation and photograph of actual thermal buckling test setup which is developed in house. Infrared (IR) heaters (1000W/230V single tube short wave IR lamps) are used to heat the syntactic foams and their sandwich beams by keeping them at a distance of 30 mm from the lateral surface of the beam. The IR heaters are mounted at different locations along the length of the beam to obtain different non-uniform temperature profiles as shown in Figure 2.6. Test specimens are rigidly clamped at both the ends in a mild steel frame, having 310 mm of free length between them to resemble clamped-clamped boundary condition. Further, samples are exposed to thermal load through the radiation heat transfer mode of IR heating source. Linear Variable Differential Transducer (LVDT) of Honeywell MVL7 LVDT make with a stroke length of ±1 inch having operating temperature range of -50°C to +125°C is used to measure lateral deflection of beam. Temperature at different locations along the beam length is measured using K-type thermocouples having sensitivity of 41 μV/°C and is recorded in personal computer through the DAQ. A relay unit is used to control ON/OFF state of the IR heater based on the thermocouple output using LabVIEW program (Figure 2.7) which in turn plots temperature-deflection curves.

Peak temperature value associated with a particular heating case is measured and fed into the LabVIEW through NI9211 DAQ. Similarly, maximum transverse deflection of the beam is measured using a LVDT and noted through NI9215 DAQ. Temperature on the specimen is increased using IR heater. The entire experimentation is computer controlled using LabVIEW user interface. The temperature and deflection data are

stored using shift registers into an array to graph the temperature-deflection plots. The maximum desired temperature up to which the specimens needs to be heated is given as a user input to LabVIEW based on the preliminary experiments conducted for estimating critical buckling temperatures. These recorded temperature values are used as maximum temperature to be attained in the experiments. This procedure is repeated for all the samples prepared. Among all the recorded temperature values for all the syntactic foams and their sandwiches including neat epoxy samples, maximum temperature is noted and is set for IR heater (desired temperature). A comparison is made between the desired and thermocouple temperature. Based on the binary output obtained from the comparison, a case structure is used to switch the NI9481 DAQ which decides ON/OFF state of the IR heater. With the help of statistics palette, the rms value of the LVDT data obtained from the NI9215 DAQ is extracted before forming the array of temperature-deflection data to be used to plot the curves. All data points are merged into a Microsoft excel file using write command.

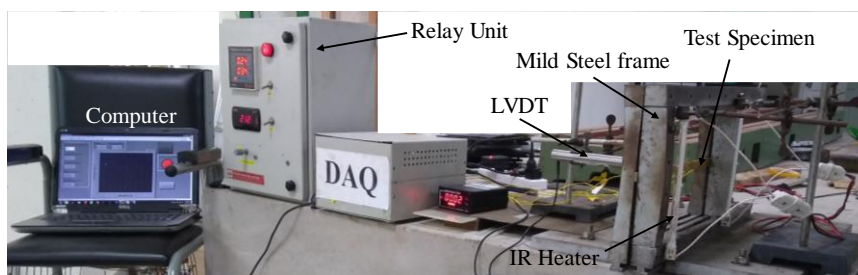
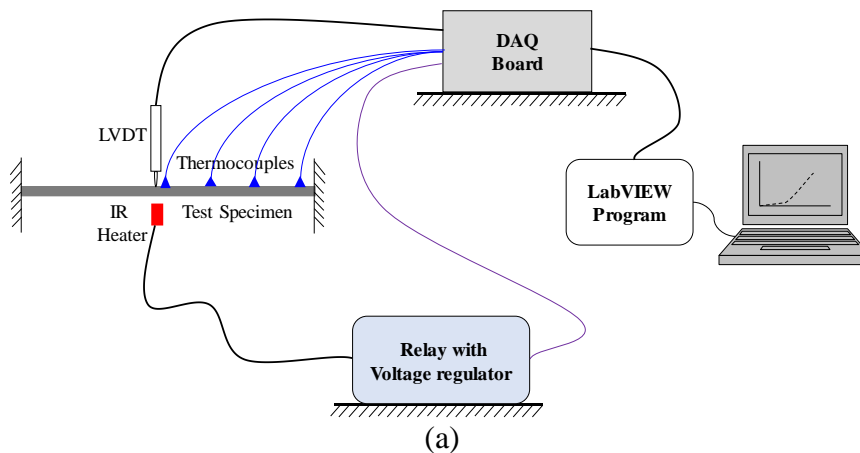


Figure 2.5 (a) Schematic representation and (b) actual experimental buckling setup in thermal environment.

Three different types of temperature conditions (Case 1, Case 2 and Case 3) are considered by keeping the IR heaters in different locations as shown in Figure 2.6. *Increase-decrease* heating (Case 1) is carried out by placing IR heater at beam centre as shown in Figure 2.6a. In this case the maximum temperature load is at the midpoint of the beam. Figure 2.6b represents Case 2 (*decrease* heating) wherein IR heater is located at left end of the beam subjecting it to the higher temperature at one end and the lower temperature at the other end. In case 3 of *decrease-increase* condition, IR heaters are placed at either beam ends and thereby maximum temperature load is applied at the both ends of the beam as presented in Figure 2.6c. These three cases represent broad spectrum of non-uniform thermal loading which may resemble practical in-service conditions.

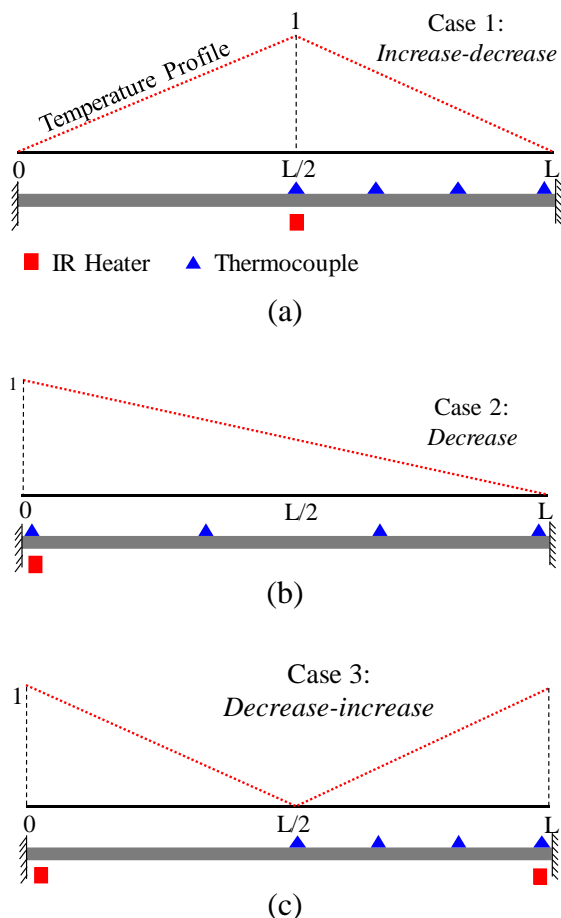


Figure 2.6 Schematic representation of (a) Case 1: *increase-decrease* (b) Case 2: *decrease* and (c) Case 3: *decrease-increase* thermal loading conditions.

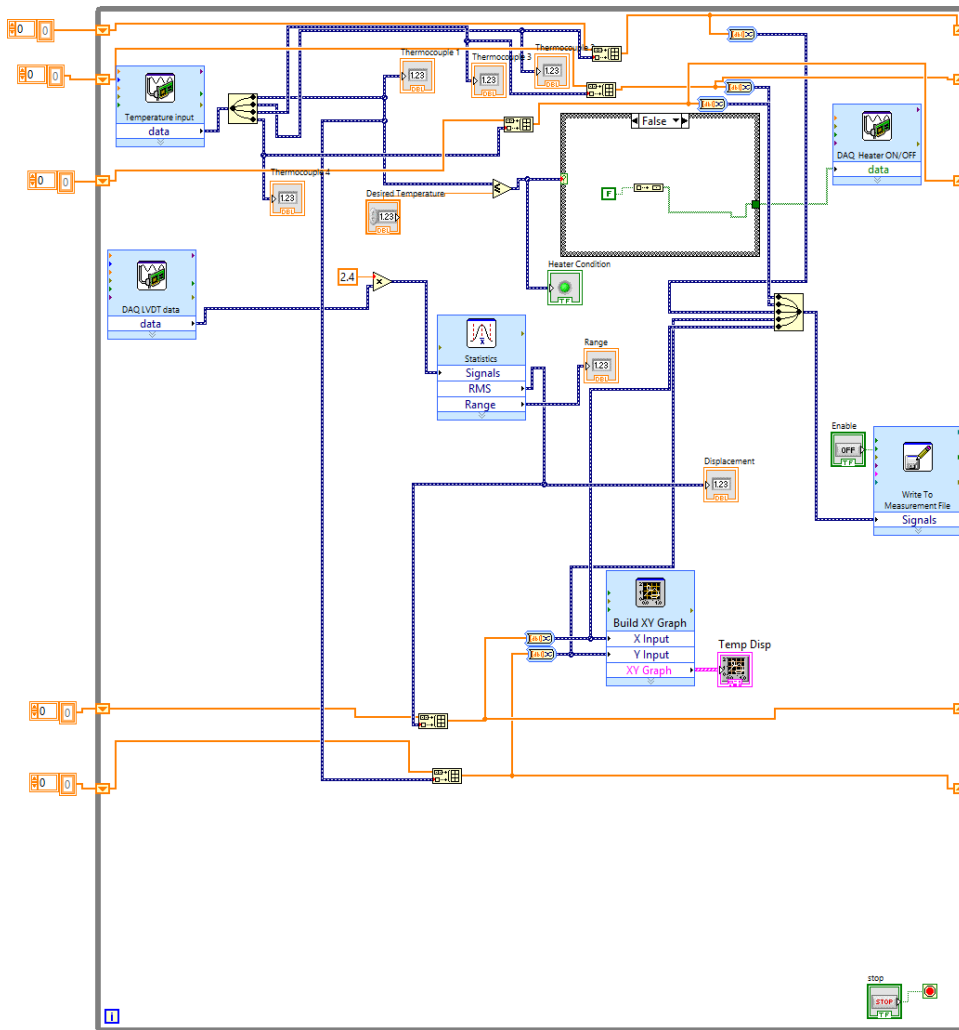
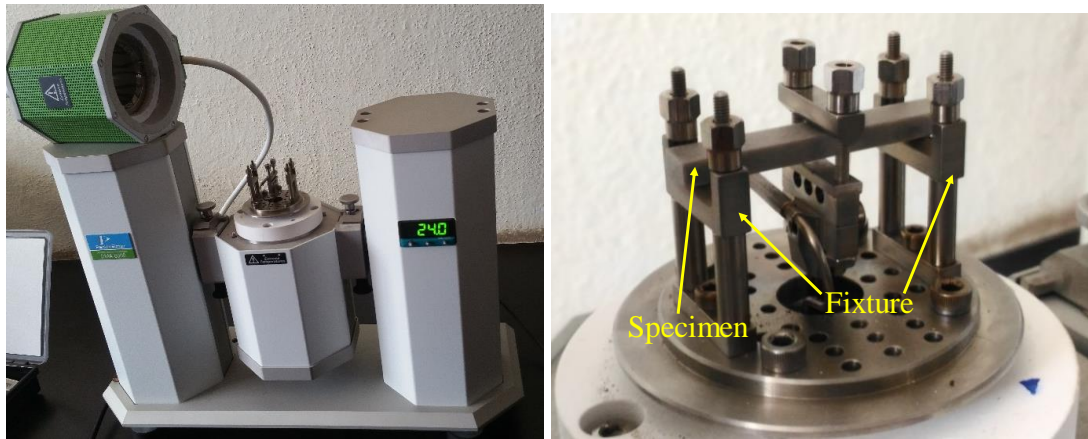


Figure 2.7 LabVIEW program used to perform buckling experiments under thermal load.

2.11 Dynamic mechanical analysis (DMA)

Temperature dependent properties of the neat epoxy and their syntactic foams are analysed using DMA 8000 (Perkin Elmer) within the temperature range of 27-180°C with incremental temperature of 5°C in dual cantilever mode (Figure 2.8) replicating clamped-clamped boundary condition. Understanding viscoelastic behaviour of the samples is important from temperature-deflection perspective in order to analyse buckling phenomena under thermal environment.



(a) (b)
Figure 2.8 (a) DMA machine and (b) DMA test set-up.

2.12 Scanning electron microscopy (SEM)

Scanning electron microscope (JSM 6380LA, JEOL, Japan) is used for micro structural analysis. All the samples are sputter coated using JFC-1600 auto fine coater (JEOL, Japan).

3 BUCKLING AND FREE VIBRATION BEHAVIOUR OF SYNTACTIC FOAMS UNDER MECHANICAL LOAD

3.1 Introduction

This chapter deals with experimental investigations of buckling and free vibration response of cenosphere/epoxy syntactic foams. These low-cost lightweight materials have potential to replace conventional materials in various applications such as automobiles, marine and aerospace. Experimental buckling loads are estimated using Double Tangent Method (DTM), Modified Budiansky Criteria (MBC) and compared with analytical formulations based on Euler-Bernoulli beam theory. Finally, fundamental frequency is estimated for first three transverse free vibration modes with varying axial load and compared with analytical results. Buckling and vibration investigations of syntactic foams are very crucial from the point of view of structural stability and hence presented herewith.

3.2 FTIR and particle size analysis

Fourier transform infrared (FTIR) spectroscopy results for silane treated and untreated cenospheres are presented in Figure 3.1a. The spectrum confirms the presence of silane layer on as received cenospheres. The characteristics peak of 3-aminopropyl tri ethoxy silane has a band lying in around 2900 cm^{-1} representing an absorbing peak of C-H bond, which belongs to CH_3 . In Figure 3.1a, the peak absorbed for fly ash cenospheres with surface modification is seen at 2929 cm^{-1} . This peak is absent in the spectrum for untreated fly ash cenospheres suggesting peak of 3-aminopropyl tri ethoxy silane (Gu et al. 2009). Figure 3.1b shows particle size analysis, the X50 weighted average median of untreated cenosphere and treated cenospheres is 48.24 and $55.08\text{ }\mu\text{m}$ respectively. It can be observed from Figure 3.1b that the peak for treated cenosphere shift towards right hand side and is broader indicating increase in particle size compared to untreated cenospheres. Density of untreated and treated cenospheres is found to be 920 (Table 2.2) and 1000 kg/m^3 (Garcia et al. 2018, Shahapurkar et al. 2018a, Shahapurkar et al. 2018b) respectively. Surface modification results in 8.69% rise in density which is still lower than the epoxy resin indicating possible avenues of weight reduction. X-ray diffraction patterns of untreated and treated cenospheres show main peaks at 2Θ value of 26.6 and 26.04 and

other numerous peaks pertaining mainly of metal oxides, predominantly SiO_2 and $3\text{Al}_2\text{O}_3$ respectively (Shahapurkar et al. 2018b).

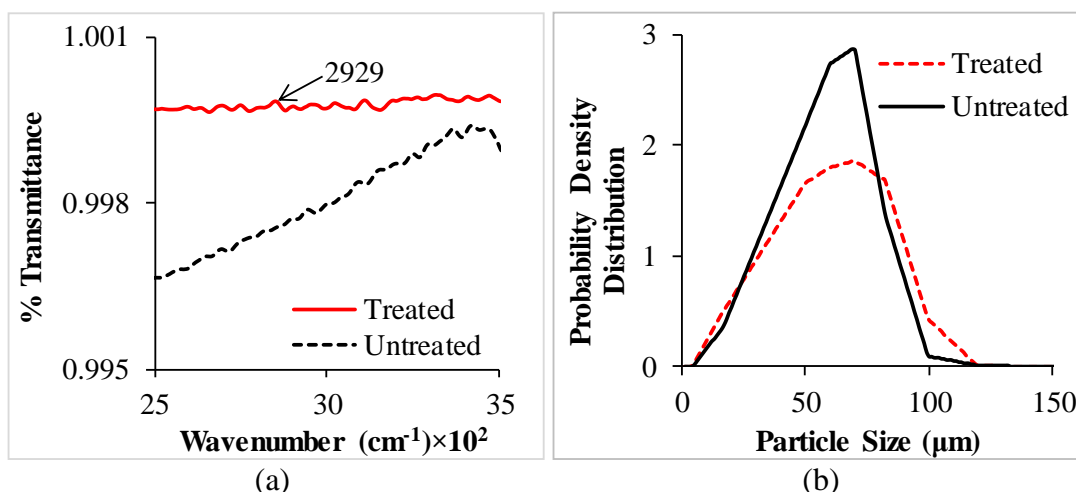


Figure 3.1 (a) FTIR spectroscopy and (b) particle size analysis of untreated and treated cenosphere.

Micrograph of as received and silane treated cenospheres are presented in Figure 3.2a and Figure 3.2b respectively. Cenospheres contain surface defects as seen from these micrographs. The coating layer is not visibly identifiable in the micrographs (Figure 3.2b) due to its small thickness, despite, FTIR results (Figure 3.1a) confirm presence of silane on the cenospheres. Sphericity variations and presence of numerous defects on cenospheres leads to non-uniform surface morphology.

Higher magnification of one such broken cenosphere (Figure 3.2c) depicts wall thickness variations and in-built porosity within the shell. Deviation between experimental and empirical and/or mathematical models is due to such variations. Sphericity range of 0.6-0.85 is observed for these fly ash cenosphere particles (Bharath Kumar et al. 2016). Surface defects as observed from Figure 3.2 and leads to deviation from '1', a perfectly spherical particle.

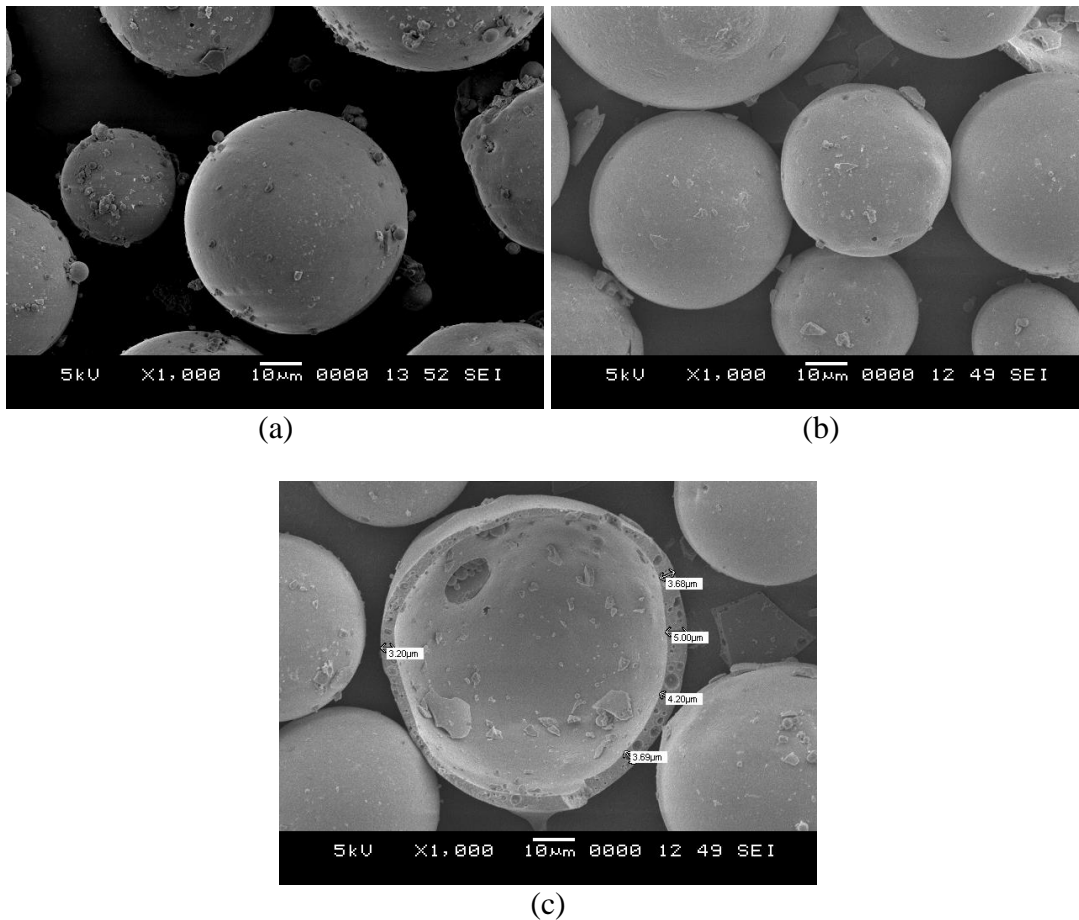


Figure 3.2 Micrographs of (a) Untreated (b) treated cenospheres (c) wall thickness variations and in-built porosity present in cenospheres.

3.3 Fabrication of specimens

Sound quality of the developed syntactic foams during processing depends upon minimum particle failure, lower cluster formation and uniform dispersion of cenospheres in the matrix resin. In the present work manual stirring approach is adopted to fabricate cenosphere/epoxy syntactic foams. Figure 3.3a and Figure 3.3b presents low magnification micrographs of as cast cenosphere/epoxy foams. Untreated and treated cenospheres are uniformly distributed in the epoxy resin as seen from these micrographs demonstrating the feasibility of the methodology adopted in the present work to prepare the foam samples. As anticipated from Figure 3.3b clusters are not seen to be formed in the E60T foam. Clusters are expected to be broken effectively due to shear forces induced owing to stirring of the cenospheres/epoxy slurry as mentioned earlier.

Interfacial adhesion between the epoxy resin and the as received cenospheres is seen to be poor as seen in Figure 3.3c. Silane treatment of cenospheres show good adhesion between the constituents (Figure 3.3d). Improvement in the interfacial bonding is expected to improve load transfer from the matrix to the particle and further improve properties of syntactic foams. Interfacial bonding strength between the constituents governs tensile and flexural properties as cracks in interfacial region forms under these conditions (Bharath Kumar et al. 2016). However, mechanical properties are less sensitive to interfacial adhesion in compression (Aureli et al. 2010, Tagliavia et al. 2010). Further, comparison of mechanical properties with non-uniform coating layer becomes quite challenging (Tagliavia et al. 2010) and is beyond the scope of the present work. Quantification of void content and cenosphere survival is crucial as it affects quality and mechanical behaviour of the samples.

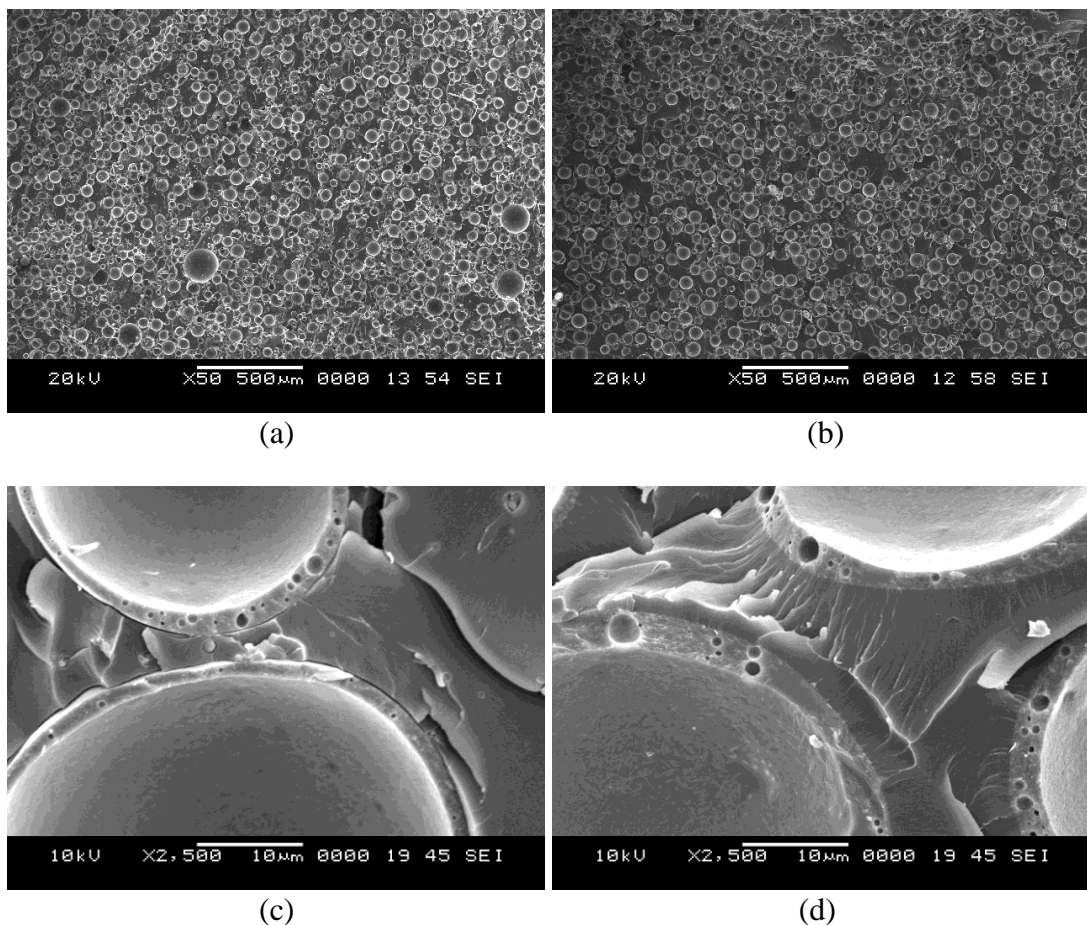


Figure 3.3 Micrographs of (a) E60 (b) E60T foams showing uniform distribution of cenospheres. (c) Lack of bonding for E60 and (d) good interfacial bonding in E60T is noted.

3.4 Density of syntactic foams

Density and void content results are presented in Table 3.1. Equation 2.1 is used to estimate theoretical density which is noted to be higher as compared to experimental value (Table 3.1). Mechanical mixing of cenospheres in the epoxy resin causes air entrapment in matrix resulting in lower experimental density values as compared to the theoretical ones. Few entrapped air pockets as seen from Figure 3.3a and Figure 3.3b are also observed in the representative samples, which are a typical feature of syntactic foams. These air pockets are referred as voids and are undesirable from mechanical properties perspective. Equation 2.2 is used to compute void content present in all the samples and average values of five replicates across each foam configuration are presented in Table 3.1. Void content increases with increase in filler loading and is observed to be lower than 5.58%. Such a low value signifies good quality of prepared samples. Density of all the foams decrease (5.67-15.81%) with increasing cenosphere content due to higher amount of hollow particles in the matrix resin. Density of foams with treated cenospheres registered higher density values for all compositions prepared. This can be attributed to silane coating on as received cenospheres increases the effective mean diameter, thereby increasing their density. Standard deviations vary in a narrow range confirming consistency in syntactic foam processing. Furthermore, Table 3.1 also reports weight saving potential by comparing foam densities with neat resin. Highest weight saving potential of 15.81% is observed for E60 and 14.61% for E60T sample as compared with neat resin. Exploiting these lightweight syntactic foams for automobile, aerospace and marine applications owing to higher specific mechanical properties in particular under buckling scenario are worth investigating.

Table 3.1 Density, void content and weight saving potential of syntactic foams.

Sample Coding	Theoretical Density (kg/m ³)	Measured Density (kg/m ³)	Matrix void content (%)	% weight reduction w.r.t E0
E0	1189.54	1189.54 ± 0.04	----	----
E20	1135.63	1113.01 ± 3.56	1.99	6.43
E40	1081.72	1057.74 ± 6.48	2.22	11.08
E60	1027.82	1001.49 ± 9.54	2.56	15.81
E20T	1151.63	1122.05 ± 3.69	2.57	5.67
E40T	1113.72	1062.10 ± 3.70	4.63	10.71
E60T	1075.82	1015.75 ± 3.71	5.58	14.61

3.5 Elastic modulus measurement from free vibration testing

Young's modulus is calculated based on the fundamental natural frequency obtained from the free vibration tests and using the analytical equation given in Thomson et al. (2008) as,

$$\omega_j = \beta_j^2 \sqrt{\frac{EI}{\rho^{exp} AL^4}} \quad (3.1)$$

$$E = \left(\frac{\omega_j}{\beta_j^2}\right)^2 \left(\frac{\rho^{exp} AL^4}{I}\right) \quad (3.2)$$

where ω_j is the angular natural frequency ($\omega = 2\pi f$), where f is natural frequency obtained from free vibration test, E is the Young's modulus and I is the moment of inertia. β is a constant (4.73, 7.8532 and 10.995 for first, second and third mode, respectively, for clamped-clamped boundary condition). ρ^{exp} is experimental density of syntactic foams and A is the cross-sectional area.

3.6 Determination of Young's modulus of syntactic foams using Bardella-Genna model (Theoretical approach)

The Bardella-Genna model (BGM) (Bardella and Genna 2001) is utilized to estimate the syntactic foam modulus through a theoretical approach, which is used to compare with experimental values. This model correlates predicted modulus with the microstructural parameters such as radius ratio and wall thickness. A homogenization scheme is used in this model to predict the bulk and shear moduli (Bardella and Genna 2001).

$$K = K_m \frac{\delta(1+v_f) + \kappa(1+v_f)\gamma}{\delta(1-v_f) + \kappa(\gamma+v_f)} \quad (3.3)$$

where $\gamma = \frac{4G_m}{3K_m}$, $\delta = \frac{4G_i}{3K_m}(1 - \eta^3)$, $\kappa = \frac{4G_i}{3K_i} + \eta^3$, η is radius ratio, K and G are bulk and shear moduli; subscripts 'm' and 'i' represents matrix and inclusions

respectively, and v_f designates volume fraction of filler. The full expression for the shear modulus is lengthy and can be found in Bardella and Genna (2001).

The radius ratio (η) is defined as ratio of internal radius to outer radius of cenospheres. Radius ratio increases with decrease in wall thickness and is used in the model to define the geometry of particle in conjunction with the particle radius (Bardella and Genna 2001). As observed from Figure 3.2c sphericity variations, porosity within the cenospheres shells and variations in wall thickness make it difficult to predict the radius ratio. Hence, the effective radius ratio is calculated based on true particle density (ρ_f) and measured density of cenosphere wall material ($\rho_{ceramic}$) (Labella et al. 2014) as,

$$\eta = \left(1 - \frac{\rho_f}{\rho_{ceramic}}\right)^{\frac{1}{3}} \quad (3.4)$$

Considering the major constituents of cenospheres, SiO_2 and Al_2O_3 , whose densities are 2650 and 3950 kg/m^3 , respectively (Labella et al. 2014) using weighted composition, the density of cenosphere wall material is found to be 3065 kg/m^3 ($\rho_{ceramic}$). ρ_f is taken as 920 kg/m^3 (Table 2.2). Radius ratio of cenospheres is found to be 0.8878 ~ 0.9. In the next step, curve fitting method is used to obtain the cenosphere modulus (keeping $\eta \approx 0.9$) that provides predictions close to the experimental values. Thereby, Young's modulus of cenospheres is found to be 73 GPa, which is used to calculate the syntactic foams modulus in the next steps. The Poisson's ratio of cenospheres is assumed to be 0.2 (Labella et al. 2014). The modulus of the matrix is obtained from the free vibration test as 3917.81 MPa (Table 3.2). The Poisson's ratio of epoxy resin is 0.35 (Shams and Porfiri 2013). Finally, the elastic modulus of foam is given by,

$$E = \frac{9KG}{3K+G} \quad (3.5)$$

Similarly, the elastic properties of treated cenosphere/epoxy syntactic foams are found using the properties of treated cenospheres as Young's modulus as 74 GPa and radius ratio as 0.85. The reduction in radius ratio of cenosphere is attributed to increase in mean particle diameter as evident from particle size analysis (Figure 3.1b). Table 3.2 represents Young's modulus obtained using Equation 3.2 and Bardella-Genna model (Equation 3.5). The modulus values increase in the range of 15.91 to 55.69 % and 29.88 to 89.45% for untreated and treated cenosphere/epoxy syntactic foams respectively for increase in filler content from 20 to 60%. Deviations in theoretical results from experimental results are attributed to defects present in the cenosphere shells.

Table 3.2 Comparison of Young's modulus values obtained from frequency data and Bardella-Genna model for pure epoxy and syntactic foams.

Sample Coding	Young's Modulus (MPa)		% Difference
	From vibration test (Equation 3.2)	Bardella-Genna Model	
E0	3917.81±105.79	3917.81	----
E20	4448.54±80.07	4541.20	-2.08
E40	5380.43±96.84	5258.30	2.27
E60	5848.68±70.18	6100.40	-4.30
E20T	5088.47±160.89	4898.40	3.74
E40T	6397.46±128.92	6137.50	4.06
E60T	7422.55±75.73	7712.00	-3.89

3.7 Theoretical formulation

Fly ash cenospheres are spherical in shape. Thereby, cenosphere/epoxy composite foam can be modelled as an isotropic material. Further, syntactic foam is assumed to behave as linearly elastic. Neglecting shear deformation and rotary inertia effects, beam differential equation of motion subjected to axial compression is given by (Bokaian 1988),

$$EI \left(\frac{\partial^4 y(x)}{\partial x^4} \right) + P \left(\frac{\partial^2 y(x)}{\partial x^2} \right) - \rho A \left(\frac{\partial^2 y}{\partial t^2} \right) = 0 \quad (3.6)$$

where $y = y(x, t)$ is transverse displacement, E is the Elastic modulus, I is moment of inertia, is the cross-sectional area, and ρ is the density of material.

If, $y(x, t) = Y(x)\cos\omega t$ for the normal mode oscillation of the beam, then Equation 3.6 becomes,

$$EI \left(\frac{\partial^4 Y(x)}{\partial x^4} \right) + P \left(\frac{\partial^2 Y(x)}{\partial x^2} \right) - \rho A \omega^2 Y(x) = 0 \quad (3.7)$$

where ω is the circular natural frequency and $Y(x)$ is the modal displacement. Considering dimensionless beam co-ordinate $\zeta = \frac{x}{l}$ ($0 \leq \zeta \leq l$), solution to Equation 3.7 can be written as,

$$Y(x) = Y(l\zeta) = C_1 \sinh Q\zeta + C_2 \cosh Q\zeta + C_3 \sin R\zeta + C_4 \cos R\zeta \quad (3.8)$$

where C_1, C_2, C_3 and C_4 are constant coefficients, Q and R are defined as,

$$Q = l \times \sqrt{\left\{ -\left(\frac{P}{2EI}\right) + \sqrt{\left[\left(\frac{P}{2EI}\right)^2 + \left(\frac{\rho A}{EI}\right)\omega^2\right]} \right\}}$$

$$R = l \times \sqrt{\left\{ \left(\frac{P}{2EI}\right) + \sqrt{\left[\left(\frac{P}{2EI}\right)^2 + \left(\frac{\rho A}{EI}\right)\omega^2\right]} \right\}}$$

$$Q = l \times \sqrt{\left\{ -(U) + \sqrt{[(U)^2 + \Omega^2]} \right\}}$$

$$R = l \times \sqrt{\left\{ (U) + \sqrt{[(U)^2 + \Omega^2]} \right\}}$$

where, $U = \frac{Pl^2}{2EI}$ is the relative axial force, $\Omega = \frac{\omega l^2}{\alpha}$ is the relative natural frequency,

$\alpha = \sqrt{\frac{EI}{\rho A}}$ is the constant parameter. Differentiating Equation 3.8 we get,

$$\frac{dY}{dx} = QC_1 \cosh Q\zeta + QC_2 \sinh Q\zeta + RC_3 \cos R\zeta - RC_4 \sin R\zeta \quad (3.9)$$

The boundary conditions for clamped-clamped case are

$$Y(x) = 0; \frac{dY(0)}{dx} = 0; Y(l) = 0; \frac{dY(l)}{dx} = 0 \quad (3.10)$$

Substituting the boundary conditions (Equation 3.10) in Equation 3.8 and Equation 3.9, results in non-trivial solution. For the non-trivial solution taking detriment of coefficient as zero we get,

$$\begin{vmatrix} 0 & 1 & 0 & 1 \\ Q & 0 & R & 0 \\ \sinh Q & \cosh Q & \sin R & \cos R \\ Q \cosh Q & Q \sinh Q & R \cos R & -R \sin R \end{vmatrix} = 0$$

$$(Q^2 - R^2) \sin R \sinh Q + 2QR(1 - \cos R \cosh Q) = 0 \quad (3.11)$$

Substituting Q and R in terms of U and Ω in Equation 3.11,

$$\begin{aligned} \Omega - U \sin \sqrt{(U + \sqrt{U^2 + \Omega^2})} \sinh \sqrt{(-U + \sqrt{U^2 + \Omega^2})} - \\ \Omega \cos \sqrt{(U + \sqrt{U^2 + \Omega^2})} \cosh \sqrt{(-U + \sqrt{U^2 + \Omega^2})} = 0 \end{aligned} \quad (3.12)$$

Equation 3.12 is the characteristics equation for variation of natural frequency as a function of compressive load. This equation is solved numerically with MATLAB code to obtain the frequency-compressive load plot.

3.8 Buckling test

Schematic diagram of the experimental setup used to perform buckling test is presented in Figure 2.4a. Critical buckling load (P_{cr}) is determined graphically (Figure 3.4) from the experimentally acquired load-deflection data using DTM and MBC techniques (Shariyat 2007, Tuttle et al. 1999). DTM is a two tangents method wherein tangents are drawn in the pre- and post-buckling regimes. The intersection point of two tangents determines P_{cr} as seen in Figure 3.4a. In MBC, the load value corresponding to the bisector at the intersection points of both the tangents determines P_{cr} (Figure 3.4b). Results from both these methods are reported for comparative studies due to the lack of available literature on buckling of syntactic foams.

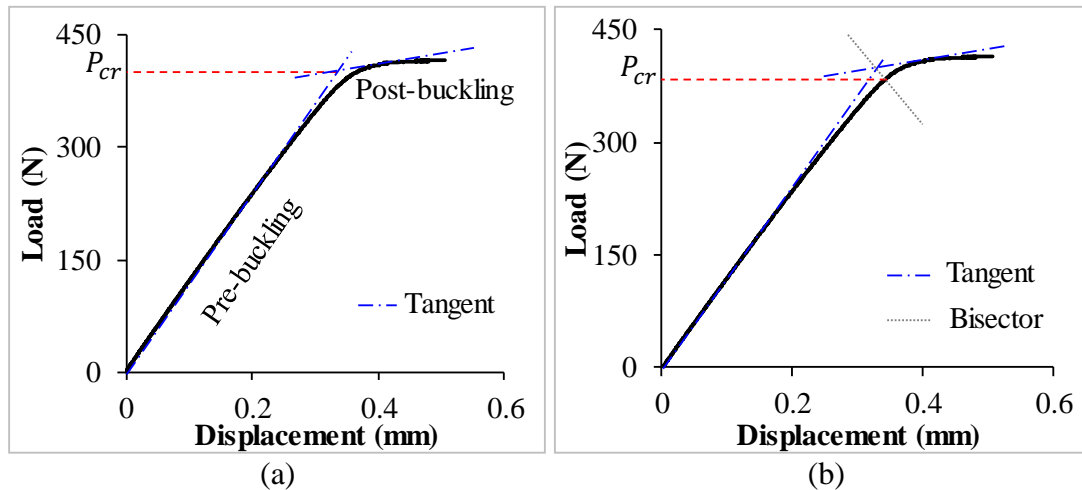


Figure 3.4 Illustration of the estimation of P_{cr} from experimental results using (a) DTM and (b) MBC methods.

For all the tested samples, the maximum deflection under axial compressive load is observed to appear in middle of sample lengthwise (Figure 2.4a). Buckling load (P_{cr}) shows increasing trend as a function of filler content (Figure 3.5 and Table 3.3). Higher loading of the untreated and silane treated cenospheres in matrix enhances modulus and hence overall stiffness of the syntactic foams. Further, it also depends on relative difference between constituents moduli. Cenosphere modulus is almost 19 times higher than that of epoxy matrix resulting in higher P_{cr} for syntactic foams. P_{cr} for neat epoxy is 237.67 N. The increase in buckling load is in the range of 20.99-62.97% and 21.56-63.55% using DTM and MBC approaches, respectively, with increasing filler volume fraction for untreated cenosphere/epoxy syntactic foams with

respect to neat resin specimens. Rise in buckling load is in the range of 32.75-101.67 % and 32.28-103.02% with increasing filler volume using DTM and MBC approaches compared to their respective values of E0 for treated cenosphere/epoxy syntactic foams. Theoretical critical buckling load for clamped-clamped beam calculated based on Euler Bernoulli assumption (Thomson et al. 2008) is, $P_{cr} = \frac{4\pi^2 EI}{L^2}$ where E is Young's modulus obtained from Bardella-Genna model (Table 3.2), I is moment of inertia, L is unclamped length of the beam. Table 3.3 shows a comparison between the experimental and theoretical buckling loads, which are found to be in good agreement for all the specimens. Deviation from the expected values might be due to particle-to-particle interactions resulting in cenosphere breakage during material fabrication. Such models can guide the development of syntactic foams as per the requirements of an application.

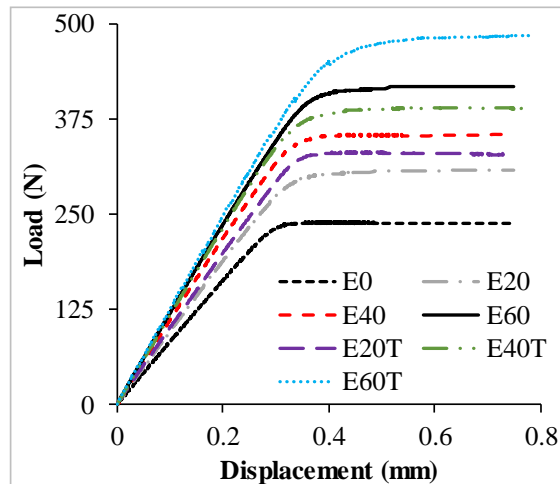


Figure 3.5 A representative set of graphs showing experimental buckling behavior of neat epoxy and syntactic foams.

Table 3.3 Experimental and theoretical critical buckling load for pure epoxy and syntactic foams.

Sample Coding	Experimental P_{cr} (N)		Theoretical P_{cr} (N)
	DTM	MBC	
E0	237.67±11.02	231.83±12.51	233.88
E20	287.58±12.35	281.83±12.85	271.08
E40	343.45±14.29	339.33±14.36	313.89
E60	387.33±15.04	379.17±17.03	364.16
E20T	315.50±12.78	306.67±12.52	292.41
E40T	393.85±16.37	383.83±17.29	366.38
E60T	479.33±17.76	470.67±16.16	460.37

3.9 Free vibration under axial compressive loads

Experimentally obtained natural frequencies corresponding to first three bending mode shapes are compared with the analytical solution (Equation 3.12). Frequency response functions (FRF) are used to find natural frequencies corresponding to first three bending modes shapes using DEWE Soft software. A typical FRF response associated with E20T syntactic foam is presented in Figure 3.6.

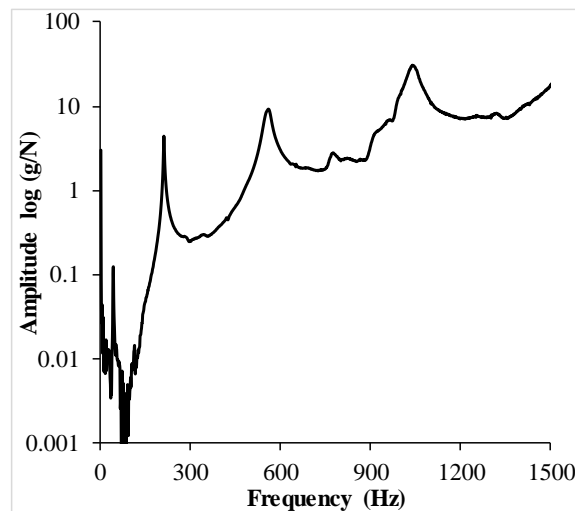
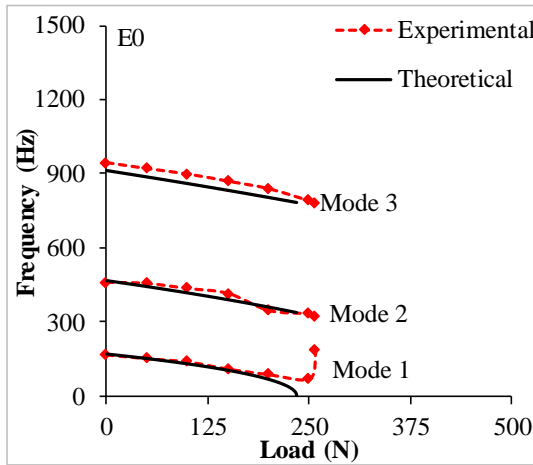


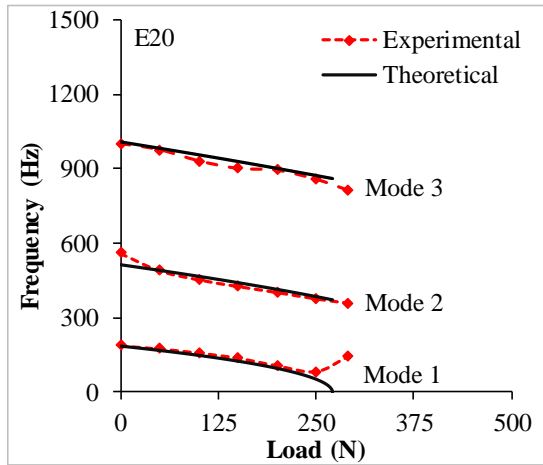
Figure 3.6 Frequency response functions for E20T sample.

Natural frequencies of syntactic foams show an increasing trend with increase in filler content. The increase in natural frequency of syntactic foams can be attributed to increase in overall stiffness of the composite due addition of stiffer cenospheres and enhancement of stiffness due to proper interfacial bonding of particles and matrix, as a result of silane treatment of cenospheres. Further, increase in mean particle diameter also augments the stiffness values. With increase in compressive load decrease in natural frequency is observed for all samples tested. Experimentally the fundamental frequency reaches minimum value at onsite of buckling and increases rapidly in post buckling region due to geometric stiffness gain resulting from beams deflection. Similar trend is observed in previous studies (Rajesh and Pitchaimani 2017) on isotropic/composites beam and columns. Theoretically fundamental frequency becomes zero when the beam is subjected to axial compressive load which is equivalent to critical buckling load (Figure 3.7). The fundamental frequency decreases steadily till the compressive load approaches critical buckling load. Fundamental

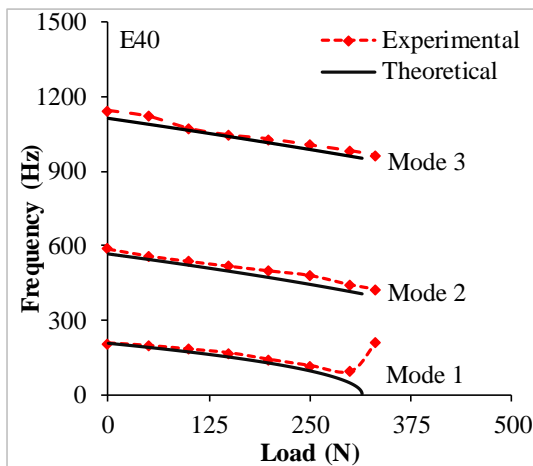
frequency drops suddenly due to loss of structural stiffness when the compressive load is very closer to critical buckling load.



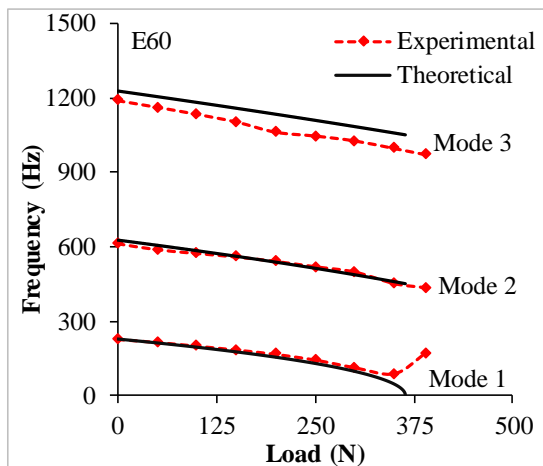
(a)



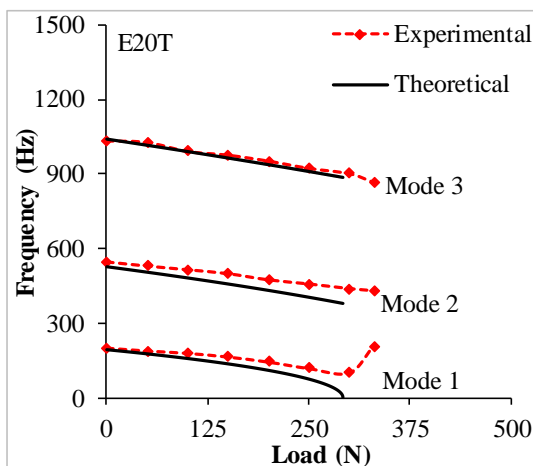
(b)



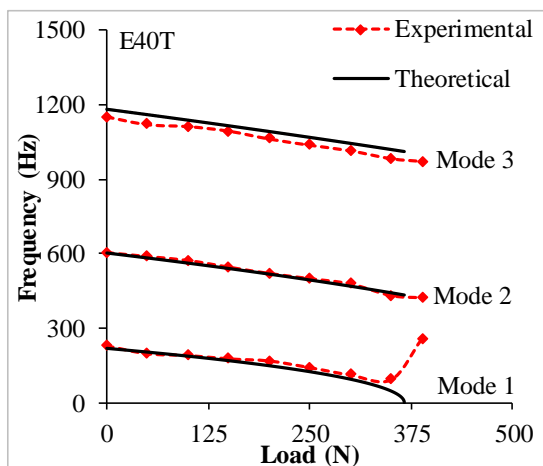
(c)



(d)



(e)



(f)

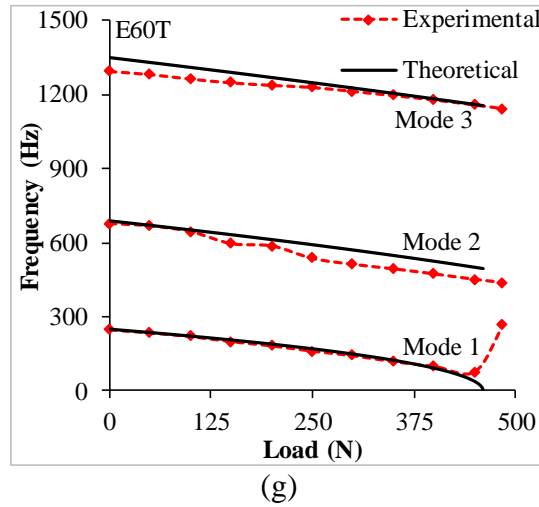


Figure 3.7 Influence of compressive load on natural frequency of (a) E0 (b) E20 (c) E40 (d) E60 (e) E20T (f) E40T (g) E60T samples.

3.10 Comparison with untreated cenosphere/epoxy syntactic foams

Variation of critical buckling load and fundamental natural frequency with respect to cenosphere loading for treated and untreated syntactic foam beams is shown in Figure 3.8. It can be observed that the buckling load and natural frequencies of silane treated cenosphere/epoxy foams are higher than that of the untreated ones. This enhancement in buckling load and natural frequencies can be attributed to strong interfacial bonding between the particles and matrix material, which in turn increases structural stiffness of the samples. The silane treated cenosphere/epoxy syntactic foams shown enhancement of buckling load up to 23.75% and natural frequency up to 11.46% as compared to untreated cenosphere/epoxy syntactic foams.

Lower density of syntactic foams is the most promising feature that enables their application for lightweight structures. Variation of critical buckling load with density of composites available in the literature is analyzed in the present work and is plotted in Figure 3.9. Data is extracted for untreated cenosphere/epoxy syntactic foams and natural fiber reinforced thermosetting composites which find applications in low and medium load structural components. Figure 3.9 shows that, with choice of appropriate constituent materials and concentrations can help in designing structural components subjected to axial compressive loads, where buckling mode failure is predominant. It can be observed that natural fiber composite is more susceptible for buckling failure

than syntactic foam composites. Density of syntactic foams is lower than natural fiber composites implying weight reduction. Thin and lightweight structural components are desired to have higher buckling loads for lower densities, where syntactic foams can provide advantage over their specific properties comparable to several composites having absolute properties.

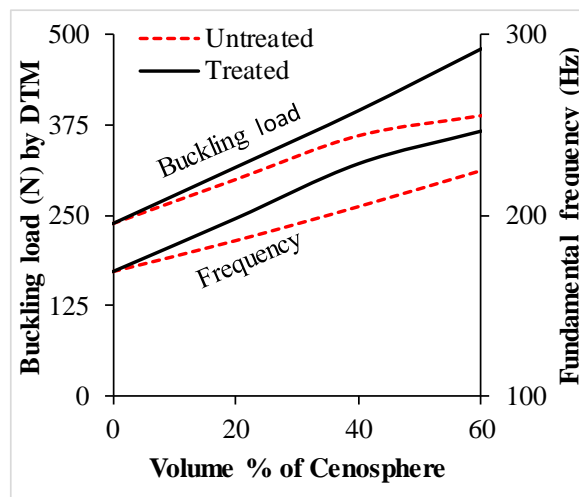


Figure 3.8 Comparison of buckling load and first natural frequency of untreated and treated cenosphere syntactic foams.

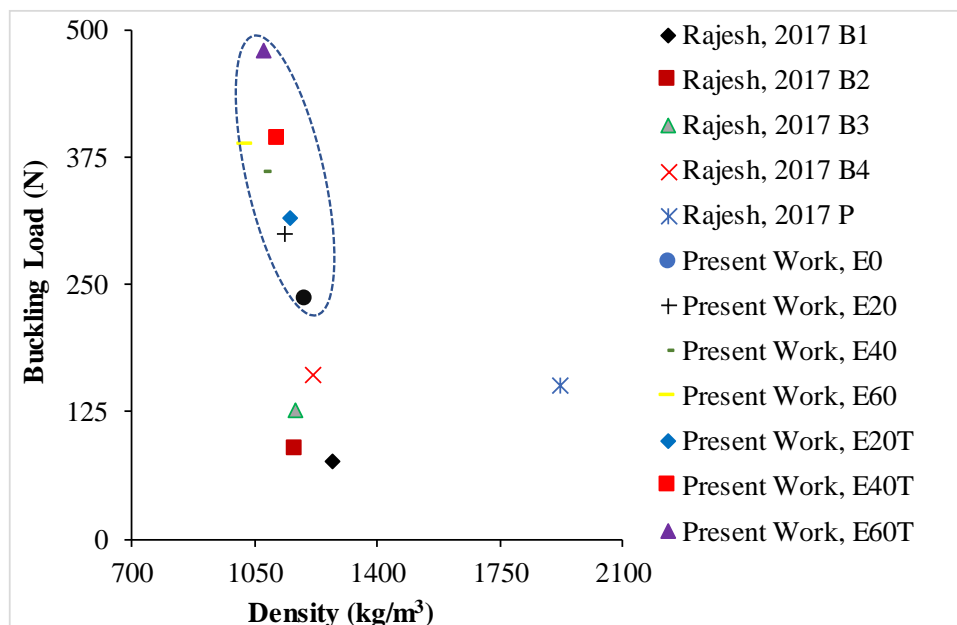


Figure 3.9 Buckling load plotted against density from available studies (Rajesh 2017, Rajesh and Pitchaimani 2017).

3.11 Vibration correlation technique (VCT)

VCT is a non-destructive test used to compute P_{cr} from the vibration data (Abramovich et al. 2015, Arbelo et al. 2014, Arbelo et al. 2015, Plaut and Virgin 1990, Souza and Assaid 1991). The accuracy of the method depends on how well the technique is able to estimate P_{cr} using data which correspond to lower levels of compressive loadings. VCT involves applying compressive load below P_{cr} and evaluating the natural frequency. The procedure is repeated for multiple loading steps. In the present work, squared value of fundamental frequency is plotted against compressive load up to 200 N and is extrapolated to get P_{cr} using a second order polynomial expression obtained based on expression (Jia 2014) and is given by,

$$\left(\frac{f}{f_n}\right)^2 = 1 - \left(\frac{P}{P_{cr}}\right) \quad (3.13)$$

where f_n and f are fundamental frequencies at no load condition and under compressive load P , respectively. Figure 3.10 shows variation of frequency squared values as a function of load. The P_{cr} predicted for each configuration through VCT is marked. VCT predicted buckling load increases with the volume fraction of cenosphere as observed in the buckling experiments. P_{cr} predicted through various techniques for different volume fractions of cenospheres are compared in Figure 3.11. Mixed trends are observed from the comparative results perspective. VCT over-predicted the buckling loads for E0, E60, E20T and E60T samples but underpredicted for E20, E40, and E40T. However, in all cases, the difference is less than 10%.

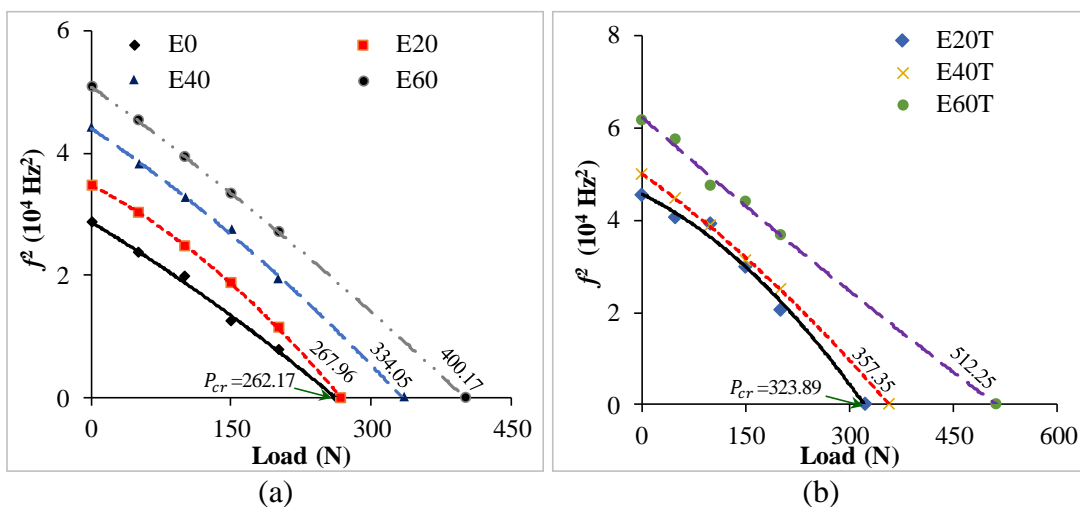


Figure 3.10 P_{cr} using VCT for (a) untreated (b) treated cenosphere/epoxy syntactic foams in Mode 1.

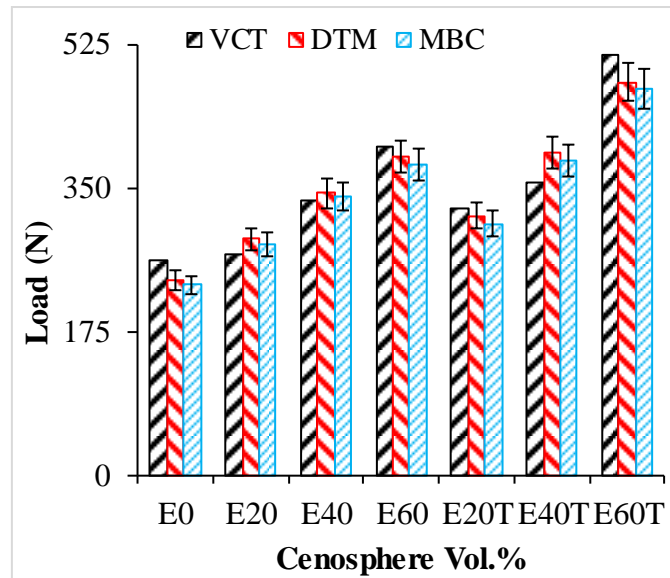


Figure 3.11 Buckling load comparison between VCT and experimental approaches.

3.12 Conclusions

Buckling and free vibrations characteristics of untreated and treated fly ash cenosphere/epoxy syntactic foams are investigated experimentally and compared with analytical results. The buckling load and natural frequencies increase with increase in cenosphere volume fraction. With increase in compressive load, decrease in natural frequency is observed for all samples tested. Experimentally the fundamental frequency reaches minimum value at onsite of buckling and increases rapidly in post buckling region. The buckling load and natural frequencies of silane treated cenosphere/epoxy foams are higher than that of the untreated ones. Property map of buckling load as a function of density is presented by extracting values from the available literature. Density of syntactic foams is lower than other composites considered resulting in weight reduction leading to higher specific properties.

4 BUCKLING BEHAVIOUR OF SYNTACTIC FOAMS UNDER THERMAL LOAD

4.1 Introduction

Literature review indicates that the nature of temperature variation across the structure influences critical buckling temperature of the structures under thermal environment. Similarly, thermal buckling studies on structures made of materials having viscoelastic effect indicate that they are subjected to snap-through buckling. Prepared foam samples are subjected to temperature variations in the range of 27-45°C with three different heating conditions namely *increase-decrease*, *decrease* and *decrease-increase* along the length of the samples. Effect of filler content, surface modification of the filler and heating conditions on snap-through buckling is presented in this chapter. Critical buckling temperature is estimated through temperature-deflection plots which are recorded using a LabVIEW program. Deflection plots of thermal and mechanical loading conditions are compared to discuss the snap-through phenomena. DMA tests are also conducted to understand viscoelastic behaviour of the developed syntactic foams in thermal environment and further to critically analyse snap-through buckling behaviour of syntactic foam beam.

4.2 Buckling under mechanical load

Static transverse deflection of untreated and treated cenosphere/epoxy syntactic foam beam under axial mechanical compressive load is investigated initially. Sample is mounted with clamped-clamped boundary condition in universal testing machine and the axial compressive load is applied as mentioned earlier in section 2.7. For all the tested samples the maximum deflection is seen to be occurring at the beam mid-point (length wise). Test is terminated when beam deflection is seen to be increasing at constant load (region *b-c* in Figure 4.1). Slope change in the curves of the samples presented in Figure 4.1 indicate critical buckling load. Except for E60, slope change can be located easily. In case of E60, non-linearity creeps in during the slope change. This might be due to constrained matrix flow around higher content of cenospheres present at higher filler loading. Buckling load increases with increasing filler content. With higher cenosphere content, load-deflection plot shifts towards right side implying higher load bearing capabilities of these cenosphere/epoxy syntactic foams

under buckling mode. This can be attributed to addition of stiff hollow cenospheres in epoxy matrix which enhances overall stiffness of the composite.

Treated cenosphere/epoxy syntactic foams show enhanced buckling loads which can be attributed to proper adhesion between the constituents which increase overall stiffness of the foam. All the samples are seen to be regaining the original shape in post-test (Figure 4.2c) scenarios as like in pre-test (Figure 4.2a) without any significant indication of plastic/permanent deformation. Figure 4.2b shows buckled shape of syntactic foam specimen during the test. Under thermal environment it would be interesting to see the influence of heating conditions on deflection behaviour of cenosphere/epoxy syntactic foams and if they can retain their original shape post-test. Coefficient of thermal expansion of all the samples needs to be looked into carefully in analysing thermal environment effect on these foams.

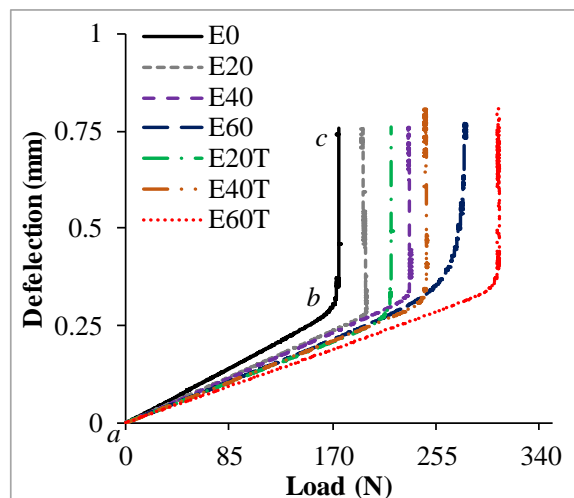


Figure 4.1 Deflection of neat epoxy and their syntactic foams under mechanical loads.

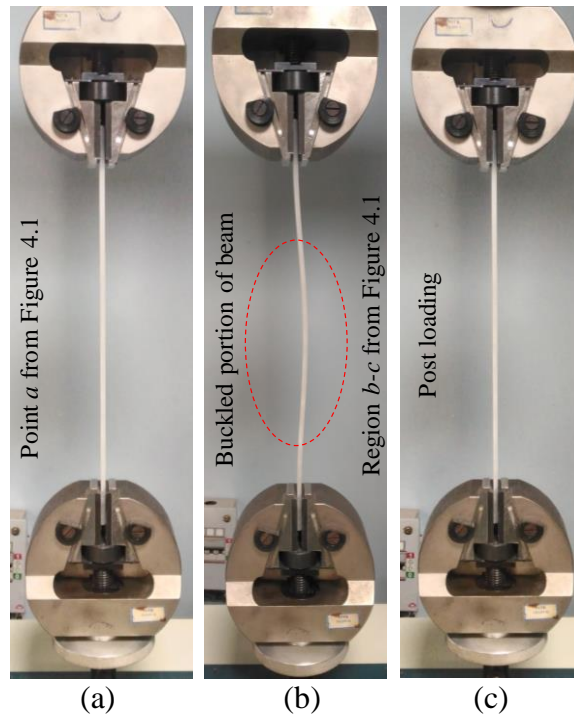


Figure 4.2 Test in-progress for representative foam sample (a) pre (b) during and (c) post loading conditions.

4.3 Coefficient of thermal expansion (CTE)

CTE of neat epoxy and their syntactic foams is presented in Table 4.1. It is observed that CTE of foams reduces significantly with increase in cenosphere content. Such an observation can be attributed to difference in thermal conduction between epoxy resin, cenosphere shell and the gas present within the cenosphere (Labella et al. 2014). CTE of cenosphere/epoxy syntactic foams decreases in the range of 13.92-48.95% with increasing filler content as compared to neat epoxy. Figure 4.3 shows the mechanism in which heat transfer takes place in neat epoxy and syntactic foams. The heat transfer in neat epoxy samples is mainly influenced by thermal conduction (Figure 4.3a), whereas in syntactic foam samples it is influenced by thermal conduction (red color arrows) between epoxy matrix and exterior surface of the cenospheres and vice-versa and thermal convection (blue color arrows) between gas molecules present within the cenospheres (Figure 4.3b). With increasing cenospheres content, heat transmission through the syntactic foam becomes increasingly tough and poses higher resistance for heat flow reducing thermal expansion to a greater extent. Further, presence of low CTE elements like Al_2O_3 and SiO_2 as primary constituents in

fly ash cenospheres (Labella et al. 2014), lowers CTE values for foams at highest filler loading.

Treated cenospheres show increase in mean diameter as seen in Figure 3.1b, thereby rate of heat conduction in treated cenosphere/epoxy syntactic foams might be little slower than the untreated ones. Hence, CTE of treated cenospheres/epoxy syntactic foams are found to less than the untreated ones. Treated cenospheres/epoxy syntactic foams registered lower CTE values in the range of 24.29-52.03% with increasing filler content as compared to neat epoxy. Surface treated cenosphere/epoxy syntactic foams show reduced CTE by 12.05, 8.353 and 6.04% for 20, 40 and 60 volume % respectively as compared untreated cenosphere/epoxy syntactic foams.

Table 4.1 CTE of neat epoxy and their syntactic foams.

Sample Coding	CTE (10^{-6} ($^{\circ}\text{C}$))	% Reduction w.r.t E0
E0	82.03±1.76	-----
E20	70.61±1.54	13.92
E40	48.84±1.19	40.46
E60	41.88±0.83	48.95
E20T	62.10±0.13	24.29
E40T	44.76±0.09	45.41
E60T	39.35±0.80	52.03

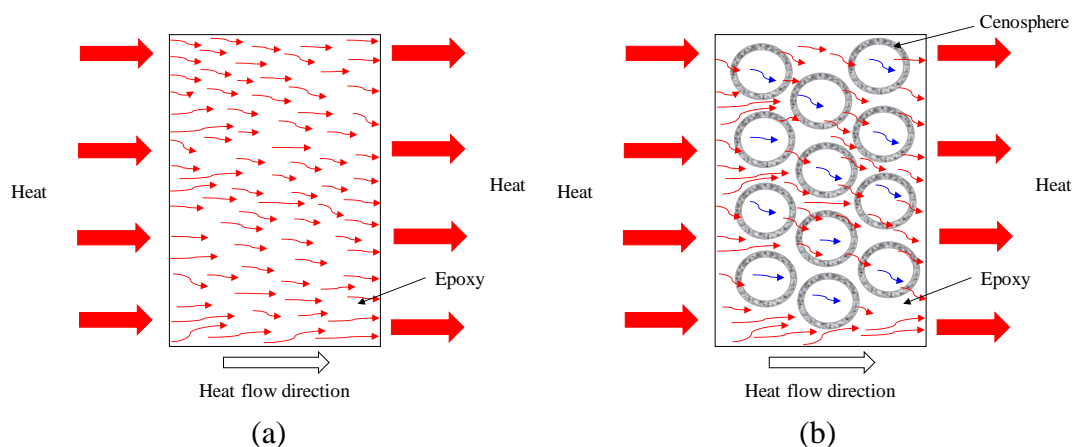


Figure 4.3 Heat flow mechanism in (a) neat epoxy and (b) syntactic foam (red arrows indicate conduction and blue arrows indicate convection mode of heat transfer).

4.4 Comparison of deflection behaviour under mechanical and thermal loading

Deflection behaviour of E0 and E20 samples under room temperature and at different heating conditions are carried out initially. Deflection of E0 and E20 samples under mechanical load is shown in Figure 4.4a. Similarly, deflection of E0 and E20 samples under *increase-decrease* heating condition is shown in is Figure 4.4b. It is observed from the experiments that the beams undergo typical deflection behaviour when subjected to mechanical axial compressive load (Figure 4.4a). However, typical deflection behaviour is not observed for the specimen under thermal load (Figure 4.4b). From Figure 4.4b, it is also that deflection behaviour of neat epoxy (E0) sample is different from syntactic foam (E20) sample under thermal loading. This clearly indicate that reinforcement of fly ash cenosphere in epoxy matrix changes the deflection behaviour significantly under thermal loading. However, there is no significant change in deflection behaviour of E0 and E20 samples under mechanical loading (Figure 4.4a).

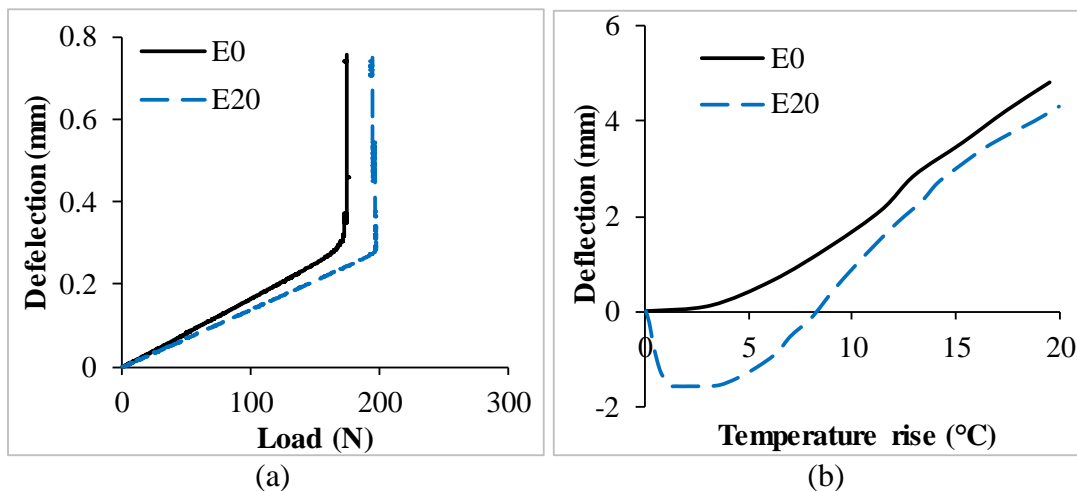


Figure 4.4 Behavior of E20 syntactic foams under (a) mechanical and (b) thermal load.

In order to understand this behaviour temperature-deflection plot associated with E20 under *increase-decrease* heating condition is presented in Figure 4.5. Cenosphere/epoxy syntactic foam samples undergo four changes in the trend.

(I) Initial rapid deflections in negative direction (negative values in Y axis) for the small amount of temperature rise (*a-b*).

(II) No significant change in deflection behaviour for further rise in temperature (*b-c*), i.e. the beam stays with a particular geometrical shape (buckled shape) occurred at the end of step I. This can be attributed to the energy gain i.e., storage of energy till the beam gets snap initiation.

(III) With further increase in temperature, syntactic foam beam starts to deflect in opposite direction (towards zero deflection - positive Y axis) and passes through the initial position (*c-d*).

(IV) Sample continues to undergo deflection exponentially (*d-e*) with temperature rise and experiences same kind of geometrical shape change as exhibited in step II but in opposite direction.

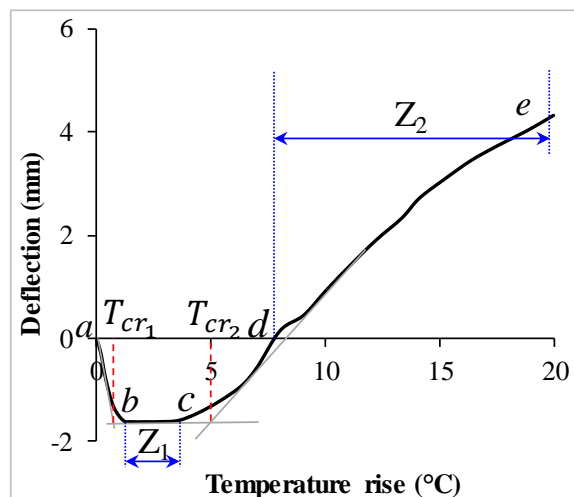


Figure 4.5 Estimation of buckling temperature from the temperature-deflection plot for representative E20 sample.

This clearly indicates that the syntactic foam beam undergoes “snap-through” type of buckling under thermal environment. However, the same beam when subjected to mechanical (room temperature) compression, snaps-through behaviour is absent. This clearly indicates that viscoelastic behaviour creeps in due to temperature rise leads to different temperature-deflection response of syntactic foam composite. The intersection of the tangents drawn at regions *a-b* and *b-c* is considered as first bifurcation point and is represented as T_{cr_1} where as T_{cr_2} is the second bifurcation point at the intersection of tangents drawn to *b-c* and *c-e* regions (George et al. 2016, Shariyat and Asgari 2013). These are two critical buckling temperatures representing

first buckling mode and snap-through buckling initiation point respectively. E20 shows presence of both T_{cr_1} and T_{cr_2} as against T_{cr_1} in E0. The entirely different deflection behaviour of the beam under thermal load is due to the temperature dependent viscoelastic effect of the syntactic foam. This observation clearly indicated influence of cenospheres contributing towards snap-through phenomena. Influence of filler loading, surface treatment of cenospheres and heating conditions on extent of T_{cr} values needs to be explored further.

4.5 Buckling under non-uniform heating

All the samples are subjected to three different non-uniform heating conditions as shown in Figure 2.6. Maximum temperature associated with each heating condition for all the samples are recorded to plot temperature-deflection response. Deflection is measured at the mid-point (length wise) since the samples are expected to deflect in the first bending mode. Deflection variation of neat resin and their syntactic foam composites as a function of temperature under different heating conditions is depicted by Figure 4.6. Figure 4.5 presents all the terminologies used pertaining to four trend changes as discussed in section 4.4. Deflection of syntactic foam composites reduces with increase in filler content in regions *a-b*, *b-c* and *c-d*. This can be attributed to increase in storage modulus of the syntactic foam with increase in volume fraction of fly ash cenospheres (Poveda and Gupta 2014, Zeltmann et al. 2017). Temperature range for which the syntactic foam remains in buckled shape (*b-c* region) increases with increase in cenosphere content (Figure 4.6). With increase in temperature, significant amount of viscoelastic forces develops in foams. This time-dependent phenomenon keeps the beam in the same buckled shape (*b-c* region) for a particular period of time with temperature rise. With further increase in temperature, the buckled beam (Z_1 as seen in Figure 4.5) deforms in opposite direction until it attains buckled geometry Z_2 . This trend is observed for all the syntactic foams subjected to all the three different heating conditions.

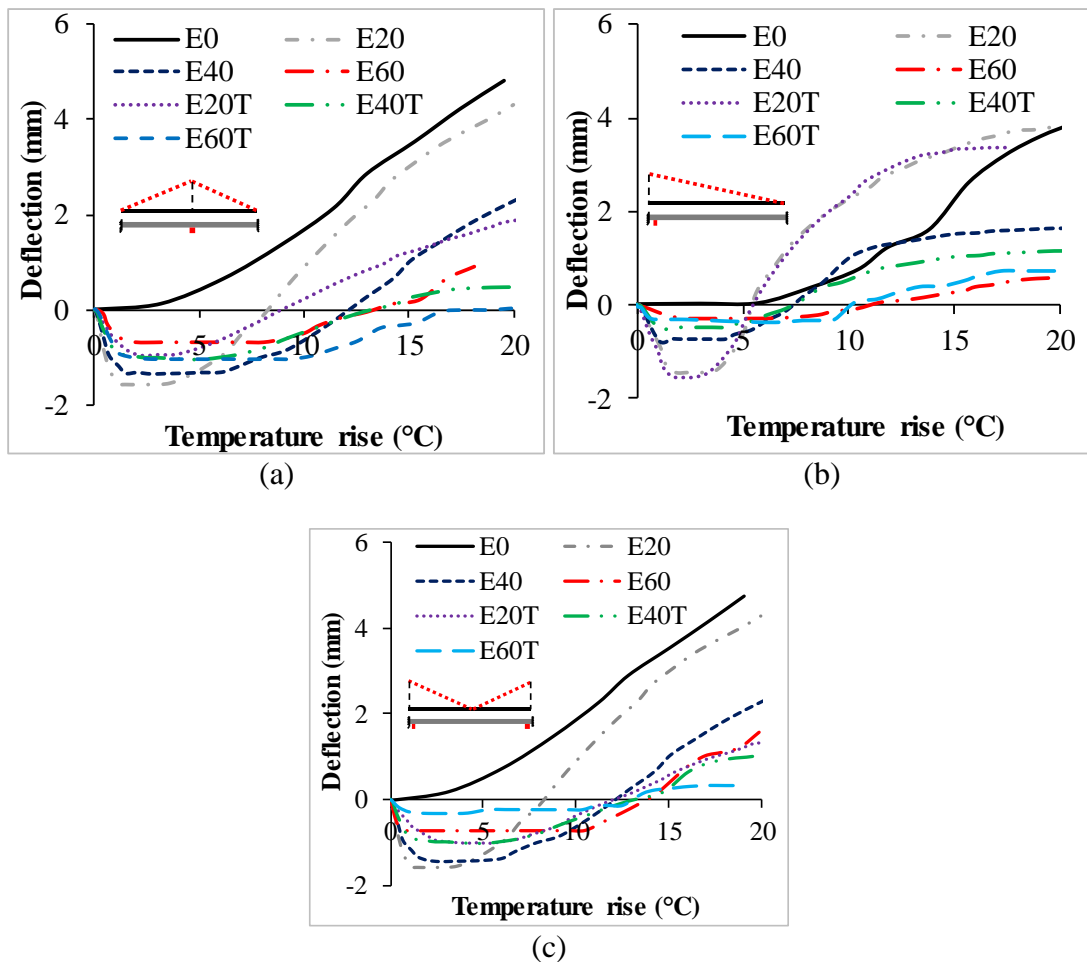
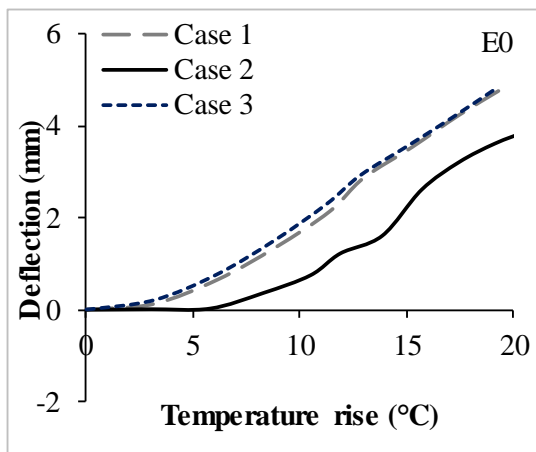


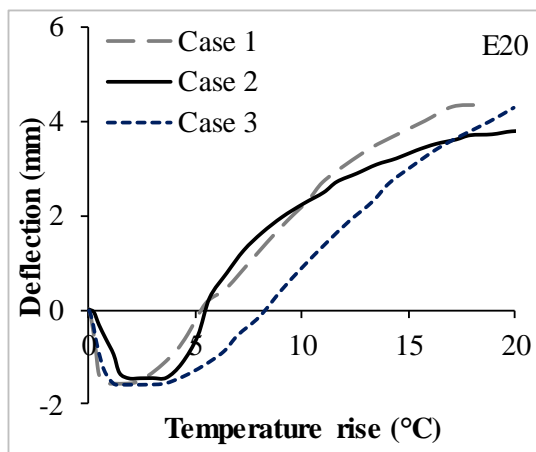
Figure 4.6 Influence of cenosphere loading on (a) Case 1: *Increase-decrease* (b) Case 2: *Decrease* and (c) Case 3: *Decrease-increase* heating conditions.

Figure 4.7 represent temperature-deflection curves for neat resin and their syntactic foam beams subjected to various thermal loading conditions (Figure 2.6). From Figure 4.7, it is observed that the deflection behaviour under *increase-decrease* (Case 1) and *decrease-increase* (Case 3) heating conditions are similar. It is also observed that deflection under *increase-decrease* (Case 1) heating is higher than *decrease-increase* (Case 3) heating which can be attributed to the location of heating source. In the case of *increase-decrease* heating the source is located at the center of the beam where the stiffness of the beam is very less, hence the deflection is more. However, deflection behaviour under *decrease* (Case 2) heating is different from other two cases due to unsymmetrical temperature distribution. In non-uniform heating of structures, the deflection and critical buckling temperature is pronounced by amount of beam portion exposed to highest temperature of a particular temperature profile and location

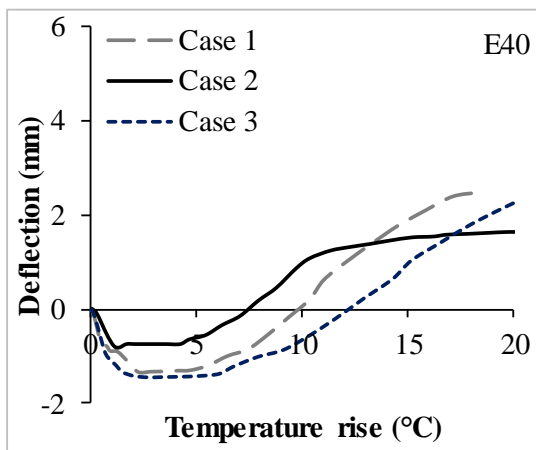
of heat source. During *decrease* heating (Figure 2.6b), the beam is exposed to higher temperature at one of its constrained end and the rate of reduction in structural stiffness is less as compared other heating conditions thereby resulting in lower deflection values. In the case of *increase-decrease* heating (Figure 2.6a), the intensity of heat is high at the mid-point of the beam hence the beam experiences higher deflection.



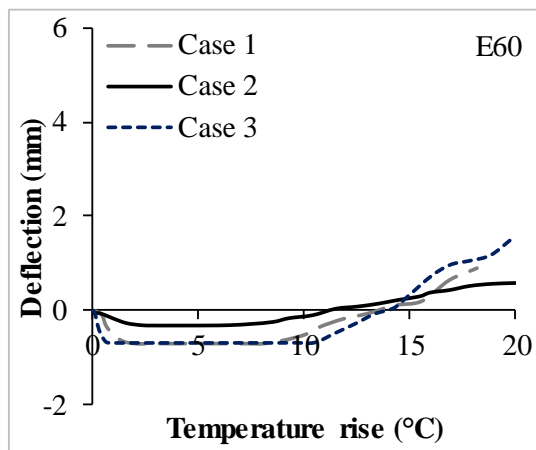
(a)



(b)



(c)



(d)

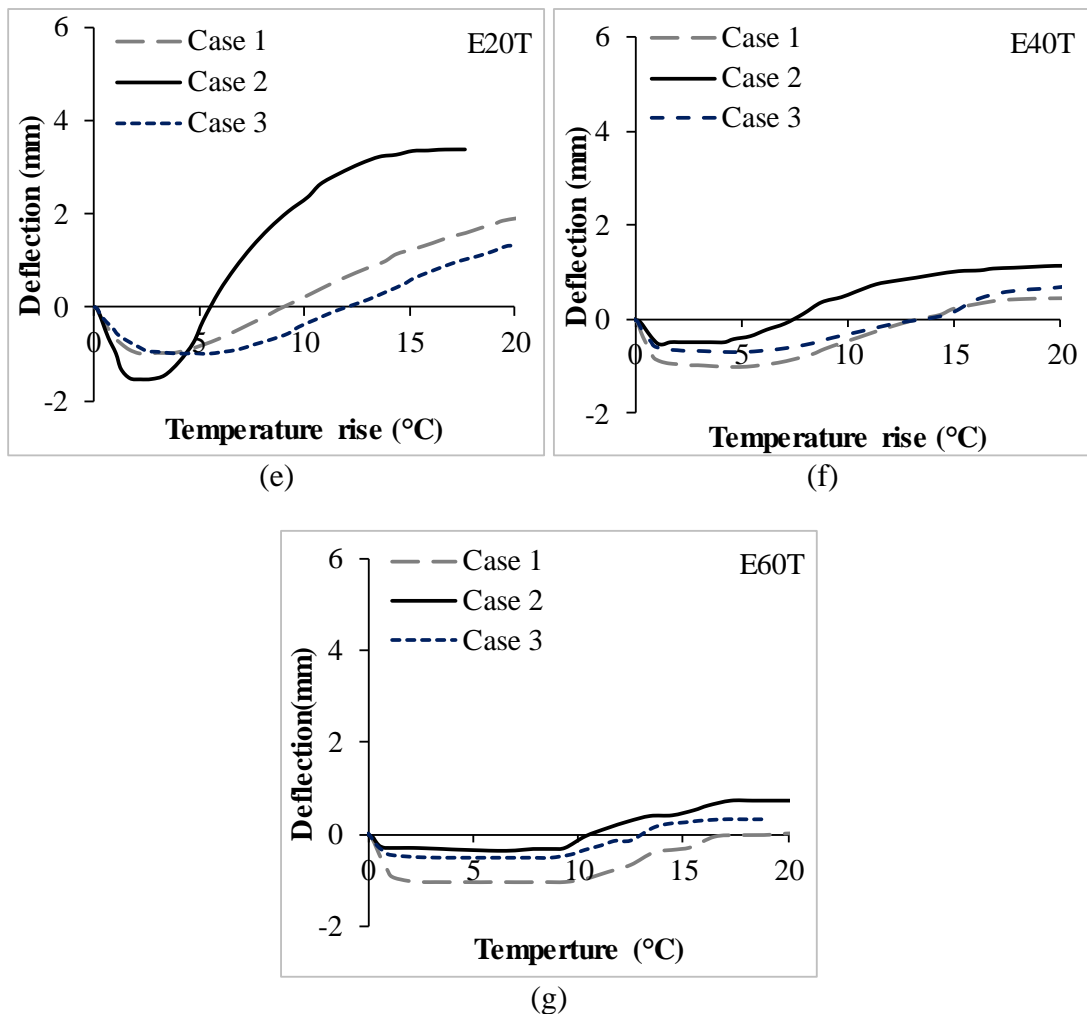


Figure 4.7 Influence of temperature variation on (a) E0 (b) E20 (c) E40 (d) E60 (e) E20T (f) E40T (g) E60T samples.

In *decrease-increase* heating (Figure 2.6c), the intensity of heat is more at both the ends and rate of reduction in structural stiffness is not higher as compared to *increase-decrease* heating case and thereby deflections are lower than the *increase-decrease* case. The temperatures at which neat epoxy and their syntactic foams showed buckled geometrics (due to snap-through action) are presented in Table 4.2. The buckling temperature is maximum for *decrease* heating condition and minimum for *increase-decrease* heating condition. The *decrease-increase* heating condition has intermediate temperature than the other two heating conditions. Treated and untreated cenosphere/epoxy syntactic foams show similar trend of deflection with increase in filler content. However, treated cenosphere/epoxy syntactic foams show slightly enhanced critical buckling temperatures. Enhanced critical buckling temperatures and

decreased deflection behavior can be attributed to good adhesion between the constituents. Figure 4.8 show progressive images of syntactic foam beam undergoing snap through deflection with increase in temperature. Initially the beam undergoes sudden deflection without much increase in temperature ($\leq 2^{\circ}\text{C}$) from the reference temperature (27°C). Figure 4.9a show test specimen before application of thermal load and Figure 4.9b shows buckled shape of syntactic foam specimen after the test indication plastic/permanent deflection. In order to understand the reason behind the sudden deflection with temperature rise, viscoelastic characteristics of the syntactic foams are presented next.

Table 4.2 Buckling temperatures (above ambient) for neat epoxy and syntactic foams at various non-uniform heating conditions.

Sample coding	Case 1:		Case 2:		Case 3:	
	<i>Increase-Decrease</i>		<i>Decrease</i>		<i>Decrease-Increase</i>	
	$T_{cr_1} (^{\circ}\text{C})$	$T_{cr_2} (^{\circ}\text{C})$	$T_{cr_1} (^{\circ}\text{C})$	$T_{cr_2} (^{\circ}\text{C})$	$T_{cr_1} (^{\circ}\text{C})$	$T_{cr_2} (^{\circ}\text{C})$
E0	4.43 ± 0.25	-----	6.45 ± 0.35	-----	4.45 ± 0.07	-----
E20	0.60 ± 0.14	4.50 ± 1.41	1.38 ± 0.18	7.57 ± 0.04	0.80 ± 0.14	4.45 ± 0.78
E40	0.88 ± 0.04	7.60 ± 1.13	0.90 ± 0.14	10.10 ± 0.42	0.95 ± 0.21	6.23 ± 1.03
E60	0.90 ± 0.42	9.15 ± 0.49	1.30 ± 0.57	12.50 ± 1.41	0.55 ± 0.07	11.25 ± 0.07
E20T	1.74 ± 0.37	5.55 ± 1.77	1.50 ± 0.21	8.15 ± 0.49	1.62 ± 0.19	5.13 ± 1.24
E40T	1.20 ± 0.28	6.90 ± 0.85	1.05 ± 0.07	10.49 ± 1.13	1.25 ± 0.35	6.63 ± 1.18
E60T	1.25 ± 0.07	3.39 ± 0.58	0.70 ± 0.28	12.65 ± 1.21	1.38 ± 0.18	7.15 ± 1.20

With increase in cenosphere content the storage modulus of the syntactic foam increases. As a result of this, the period in which the beam stays in *b-c* region (stage II) increases with filler content. The restoring force is very less for neat resin samples and hence does not undergo deformation stages as observed in syntactic foams. Figure 4.10a and Figure 4.10b represents influence of cenosphere volume fraction on storage modulus of untreated and treated cenosphere/epoxy syntactic foams respectively. Storage modulus of neat epoxy resin decreases continuously from room temperature indicating reduction in energy storing capability with temperature rise.

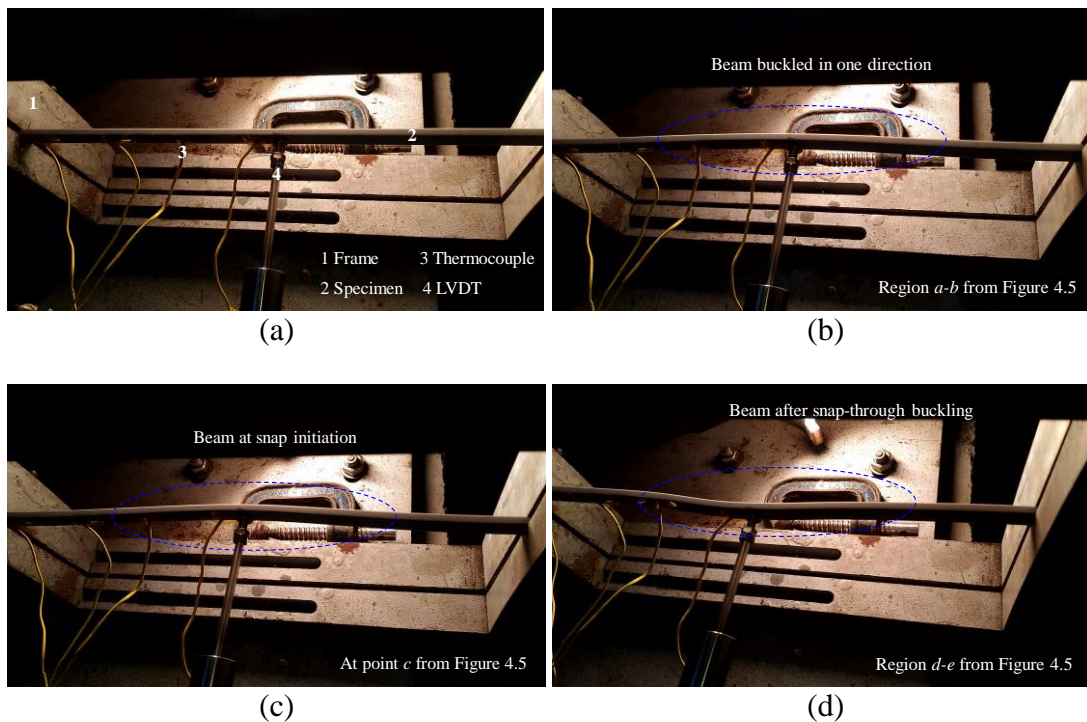


Figure 4.8 Progressive images of syntactic foam beam deflecting under *increase-decrease* heating condition.

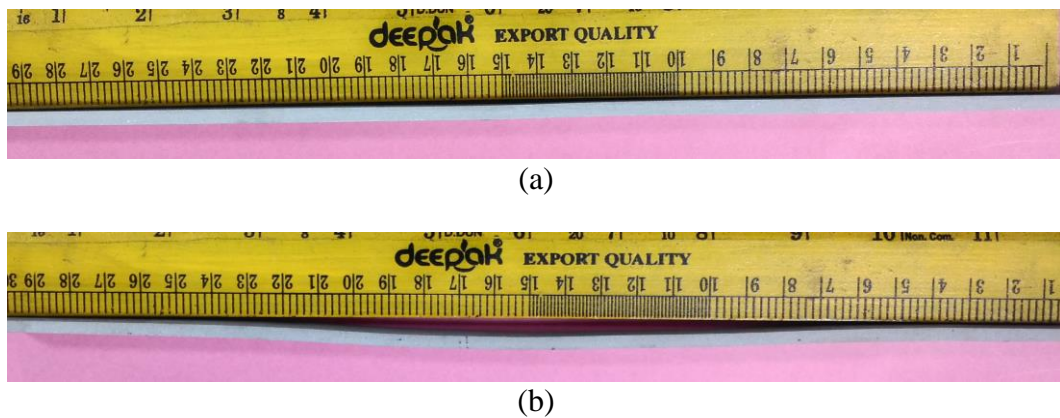


Figure 4.9 Representative foam sample (a) pre-buckling (b) post thermal buckling.

Enhancement of storage modulus (with a conceptual correspondence to stiffness) is seen with increasing filler content. Storage modulus of the syntactic foams when compared with room temperature values, slight increase in storage modulus values is noted from 27 to 32°C followed by decrease thereafter (Figure 4.10a and Figure 4.10b). This observation clearly indicates syntactic foams have better energy storing capability at the initial rise in temperature (until 32°C) as compared to neat resin. This energy storing ability increases with fly ash cenosphere content. This can be attributed

to less molecular motions of epoxy molecules owing to cenosphere addition (Wu et al. 2007) making foam samples to stays in region *b-c* for longer duration.

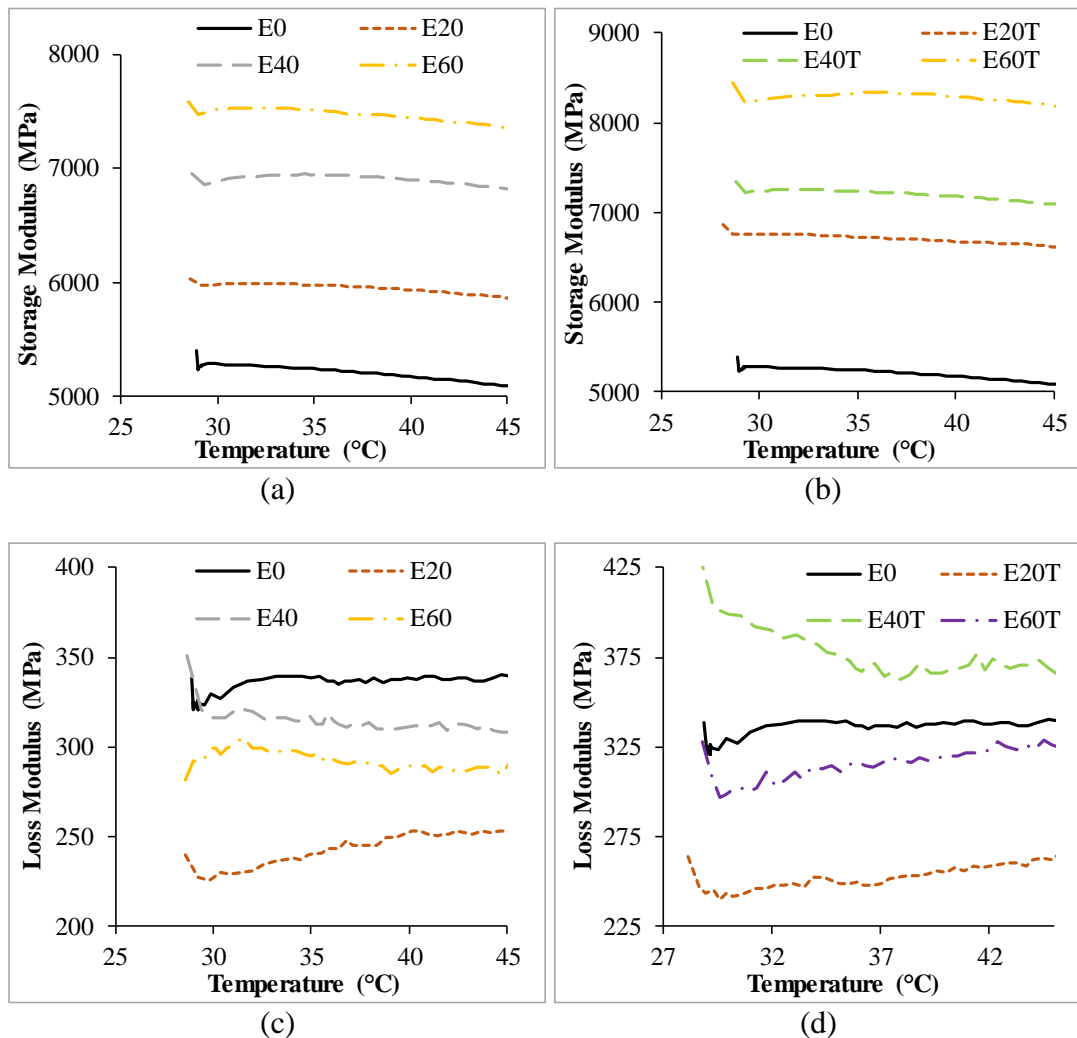


Figure 4.10 Influence of cenosphere volume fraction on storage modulus (a) untreated (b) treated and loss modulus of (c) untreated (d) treated syntactic foams.

Loss modulus represents dissipation of energy. It is observed from Figure 4.10c and Figure 4.10d that the loss modulus of epoxy resin is higher than that of syntactic foams in temperature range of 27-45°C. It can be attributed to less internal sliding between the molecules of epoxy and between the particles and matrix. The effect of matrix viscoelasticity is more and the frictional energy dissipation is relatively low at lower filler loadings. At the higher filler contents, the contribution of matrix viscoelasticity reduces due to intense dilution of cenosphere particles in the epoxy resin. At the same time the intra molecular motion of the matrix becomes difficult that

hinders the frictional energy dissipation of chain segments and thereby reduces the heating loss (Wu et al. 2007). Syntactic foams exhibited higher storage modulus and lower loss modulus as compared to neat resin.

4.6 Conclusions

Deflection behavior of untreated and treated cenosphere/epoxy syntactic foams at room temperature (mechanical load) and under thermal environment (three different heating conditions) is presented in this study and following conclusions are drawn:

- Samples subjected to mechanical axial compression at room temperature show increase in buckling load in range of 14.42-59.01% for increase in cenosphere content from 20-60 vol.% as compared to neat epoxy resin.
- All samples subjected to mechanical axial compressive loads, regained to its original shape after the test, without any indication of plastic/permanent deformation.
- CTE of cenosphere/epoxy syntactic foams decreases in the range of 13.92-48.95% with increasing filler content as compared to neat epoxy resin.
- Treated cenosphere/epoxy syntactic foam show reduced CTE as compared with untreated ones.
- All the samples are subjected to three different non-uniform heating conditions and the temperature-deflection curves reveal that the syntactic foams undergo snap-through buckling behaviour.
- The deflection of syntactic foams reduces with increase in cenosphere content. Temperature range for which the syntactic foam remains in initial buckled shape increases with increase in cenosphere content.
- The treated cenosphere/epoxy syntactic foams do not show much significant variation in deflection behaviour and buckling temperatures as compared to untreated ones.
- *Decrease* heating condition show higher buckling temperatures as compared to other two heating cases.

- Dynamic mechanical analysis of untreated and treated cenosphere/epoxy syntactic foams show that the foams have better energy absorbing capability than neat epoxy resin.

5 BUCKLING AND FREE VIBRATION BEHAVIOUR OF SYNTACTIC FOAM SANDWICH COMPOSITES UNDER MECHANICAL LOAD

5.1 Introduction

Literature review indicates that the sisal fiber reinforced skins with fly ash cenospheres reinforced in polymer matrix core should be explored for sandwich construction owing to its higher specific properties finding applications in marine and aerospace industries. Buckling and dynamic behavior of sandwich beam with fly ash cenosphere/epoxy as core and sisal fibre fabric composite laminate as facing layer under compressive load is discussed in this chapter. Effect of fly ash cenospheres loading and its surface modification on critical buckling load and free vibration frequencies of the sandwich beam under compressive load is studied in detail. Elastic properties of sisal fabric reinforced epoxy laminate are computed experimentally. These values are further used to predict the critical buckling load and free vibration frequencies numerically. Finally, the numerical and experimental results are compared.

5.2 Material characterization

Experimentally density of sisal fibres are found according to ASTM D3800-16 . Sisal yarn specimens of length 1 m are tested. Ten replicates are tested and average values with standard deviations are reported. The density of sisal fibers is found to be $1262.80 \pm 46.23 \text{ kg/m}^3$.

Sandwich composites with sisal fabric/epoxy as skin and fly ash syntactic foam as cores are prepared by hand lay-up process as described in section 2.5. Figure 5.1a shows schematic representation of the sandwich beam and prepared sandwich sample (Figure 5.1b). Figure 5.2 represent micrograph of sandwich composites post freeze fracture. Distinct region of skin indicating firm bonding and core materials is observed from Figure 5.2. Further, both top and bottom skin thickness is uniformly maintained with a thickness of around 0.75 mm (Figure 5.2b). Small variation of $\pm 0.1\text{mm}$ is observed in skin thickness is attributed to undulation of the woven fabric. Absence of voids indicate sound quality of sandwich samples without skin delamination from the core.

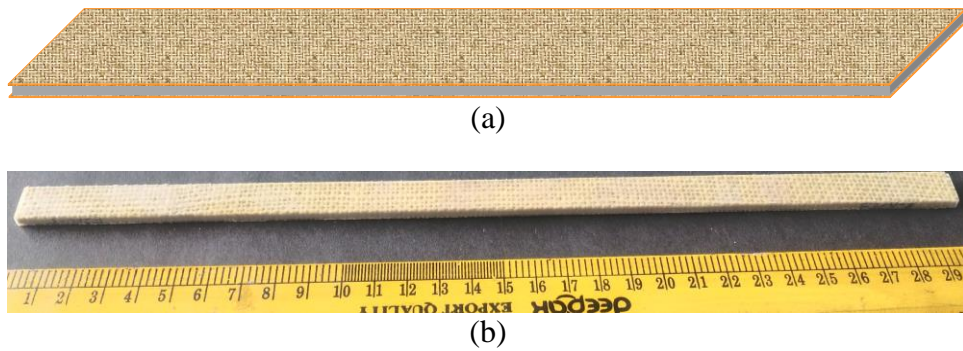


Figure 5.1 (a) Schematic representation of sandwich and (b) prepared sandwich composite.

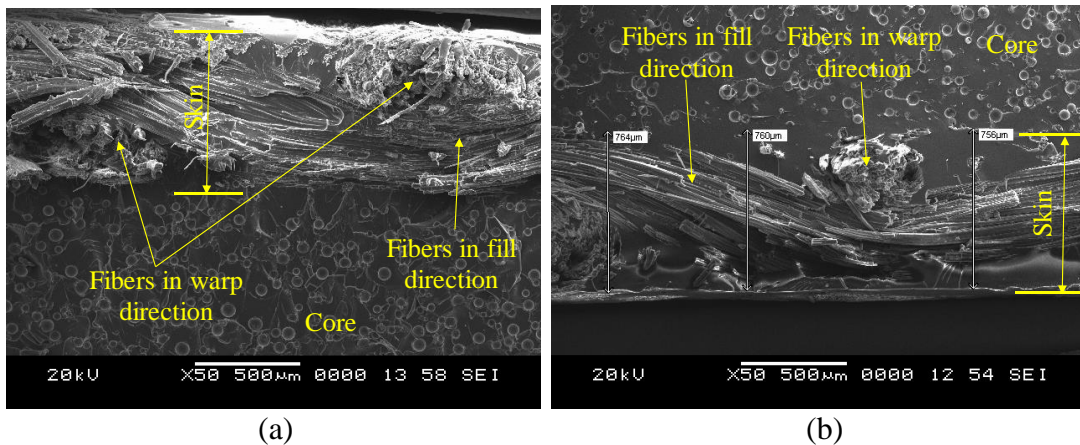


Figure 5.2 SEM images of sandwich composites indicating (a) top and (b) bottom facing thickness and bonding interfaces.

5.3 Density of syntactic foams and their sandwich composites

Quality and properties of syntactic foams and their sandwich composites are dependent on the amount of intact hollow particles in the core and void content. Presence of air entrapment during mechanical mixing of cenospheres in epoxy resin and hand lay-up process during sandwich preparation is accounted for void content. Table 3.1 and Table 5.1 represent density and void content results of syntactic foams and their sandwiches respectively. Theoretical densities are calculated using Equation 2.1 which is noted to be higher as compared to experimental values (Table 5.1). Lower experimental densities compared to theoretical ones are attributed to air entrapment due to mechanical mixing of cenospheres in the epoxy resin in syntactic foam cores and in sandwich facings. Theoretical and experimental densities of cenosphere/epoxy syntactic foam sandwich with sisal/epoxy skin are presented in Table 5.1. From Table 5.1, it is observed that the density of sandwich composites

decrease with increase in cenosphere content in the core material and the void content is in the narrow range of 0.91-4.54%.

Table 5.1 Density and void content of cenosphere/epoxy syntactic foam sandwich composites.

Material type	Theoretical density (kg/m ³)	Experimental density (kg/m ³)	Matrix void content (%)
SE0	1236.93	1225.80±1.09	0.91
SE20	1203.24	1177.97±2.99	2.10
SE40	1169.54	1142.64±5.68	2.30
SE60	1135.86	1105.19±8.24	2.71
SE20T	1213.24	1181.69±3.88	2.61
SE40T	1188.92	1148.73±4.28	3.38
SE60T	1165.86	1112.89±7.17	4.54

5.4 Evaluation of elastic properties of skin

Elastic properties associated with cenosphere/epoxy syntactic foam cores and sisal fabric/epoxy facing are estimated experimentally. These properties are further used to calculate the critical buckling load and free vibration frequencies of the sandwich beam using finite element based numerical approach. Elastic properties of the cenosphere/epoxy syntactic foam core are estimated based on Bardella-Genna model and is presented in section 3.6 of Chapter 3. In order to estimate the skin properties, fiber properties such as tensile strength and Young's modulus of sisal yarn are found by performing tensile test as per ASTM D3822 / D3822M-14 on six samples. Cross head movement is maintained constant at 5 mm/min. Yarn specimens with diameter 0.5 mm and gauge length of 50 mm (Figure 5.3) are used. Elastic properties of sisal fabric/epoxy composite skin materials are estimated according to the procedure as outlined by Barbero (2018). The tensile (Type I), compressive and flexural properties of epoxy matrix are estimated using ASTM D638-14 , ASTM D695-15 , and ASTM D790-17 respectively. Tensile, compression and flexural tests are carried out with the cross-head displacement speed at 5, 1.4 and 1.3 mm/min respectively. Specimens dimension of 127×12.7×3.2 mm and 12.7× 12.7×25.4 mm are used for estimating flexural and compressive properties respectively. Five specimens for each case are tested and average values with standard deviations are reported.

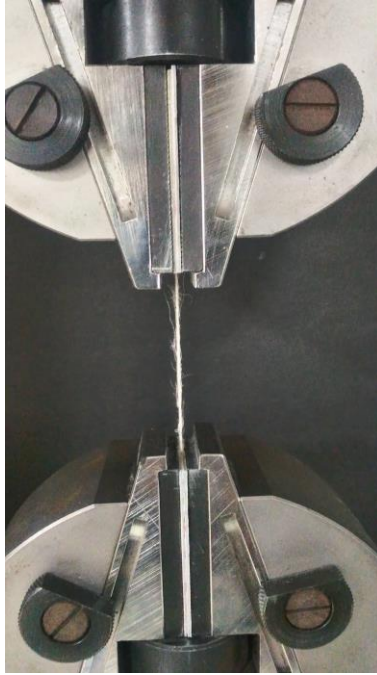


Figure 5.3 Sisal yarn tensile test in-progress.

The microstructural geometry of a plain woven fabric is presented in Figure 5.4. The geometrical parameters of fabric are given as, Fill width $a_f = \frac{1}{N_f}$, warp width $a_w = \frac{1}{N_w}$, where, N_f and N_w are number of yarns per unit width in fill and warp directions respectively. If number of yarns along warp and fill directions are the same then $N_f = N_w$ condition prevails. In this case fill thickness (h_f) and warp thickness (h_w) are equal to half of lamina thickness (h). Harness (n_g) is the number of yarns along one direction of the representative unit cell. Shift (n_s) is the number of yarns between consecutive interlacing regions. Interlacing (n_i) is the number of yarns in the interlacing region. All these parameters define the representative volume element of the fabric reinforced laminate. Based on these values, further moduli of the laminate are computed.

The sisal fabric used in the present work is woven with plain weaving architecture. Fabric being square in symmetry, number of yarns per unit length in fill and warp direction is constant. Hence the transverse modulus is equal to longitudinal modulus (i.e. $E_x = E_y$). The longitudinal modulus (E_x) of a sisal /epoxy tow is calculated using rule of mixtures and is given by,

$$E_x = E_m v_m + E_f v_f \quad (5.1)$$

where, E is Young's modulus, v is volume fraction and suffices m and f represents matrix and fiber respectively.

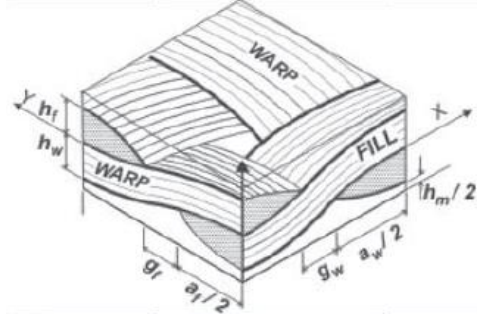


Figure 5.4 Macrostructural geometry of the fabric (Barbero 2018).

Longitudinal and transverse Poisson's ratios are calculated using the relation,

$$\vartheta_{12} = \vartheta_{23} = \vartheta_m v_m + \vartheta_f v_f \quad (5.2)$$

In-plane shear modulus, is computed using periodic microstructure micromechanics (PMM) (Barbero 2018) and is given by,

$$G_{12} = G_m \left[1 + \frac{V_f \left(1 - \frac{G_m}{G_f} \right)}{\frac{G_m}{G_f} + S_3 \left(1 - \left(\frac{G_m}{G_f} \right) \right)} \right] \quad (5.3)$$

where, G represents shear modulus and

$$S_3 = 0.49247 - 0.47603V_f - 0.02748V_f^2 \quad (5.4)$$

Interlaminar shear modulus is calculated using PMM (Barbero 2018) formula and is given by,

$$G_{23} = G_m - \frac{V_f}{D} \quad (5.5)$$

where, D is constant and is given by,

$$D = \frac{(2G_m + C'_{23} - C'_{22})(4S_7 - 2(2 - 2\vartheta_m)S_3) + 2G_m(2 - 2\vartheta_m)}{G_m(2G_m + C'_{23} - C'_{22})(2 - 2\vartheta_m)} \quad (5.6)$$

$$C'_{22} = (1 - \vartheta_f^2) \frac{E_f}{\Delta} \quad (5.7)$$

$$C'_{23} = (\vartheta_f + \vartheta_f^2) \frac{E_f}{\Delta} \quad (5.8)$$

$$\text{where, } \Delta = 1 - \vartheta_f^2 - 2\vartheta_f^3 \quad (5.9)$$

$$S_7 = 0.12346 - 0.32035V_f - 0.23517V_f^2 \quad (5.10)$$

Computer aided design environment for composites (CADEC) (Barbero 2011) is used to find the properties of sisal fabric/epoxy skin which are then used to model the skin. Figure 5.5 shows the methodology followed to compare experimental and numerical results. The Bardella-Genna model (BGM) is used to estimate the properties of the core. BGM uses homogenisation approach and calculates the elastic properties of foams based on volume fraction and radius ratio as explained in section 3.6.

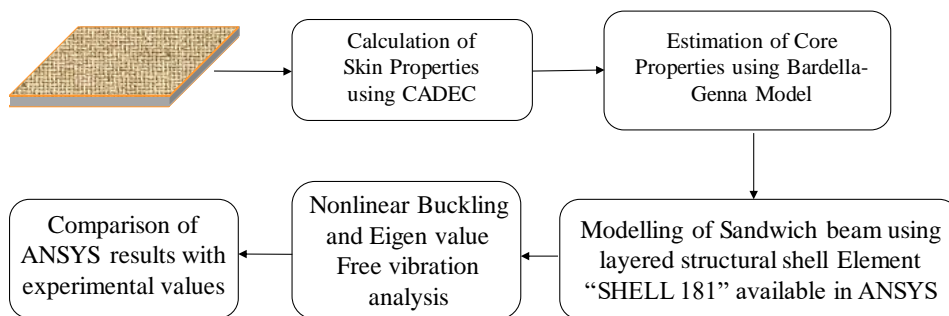


Figure 5.5 Flow chart showing steps of numerical analysis.

5.5 Finite element analysis

The fundamental buckling mode of the sandwich beam is obtained from the linear Eigen value analysis. Further, non-linear static structural analysis (Newton-Rapson

method) is conducted by incorporating geometric imperfections in the model (Tang et al. 2015). The geometrical imperfection shape and amplitude is chosen based on trial and error method such that there is a close match between the experimental and numerical results. Structural stiffness matrix ($[K]$) is given by (Reddy 2014),

$$[K] = \int [B]^T [D][B] dV \quad (5.11)$$

where, $[B]$ and $[D]$ are linear strain-displacement and constitutive matrices respectively. The effect of axial compression in the numerical analysis and pre-stress effect on the structure are considered by the stress stiffness matrix

$$[K_\sigma] = \int_V [B_d]^T [S][B_d] dV \quad (5.12)$$

where $[K_\sigma]$ and $[B_d]$ represents stress stiffness and strain-displacement matrix respectively, $[S]$ represents pre-stress matrix due to the axial compression.

$$[S] = \begin{bmatrix} \sigma_x & \sigma_{xy} \\ \sigma_{xy} & \sigma_y \end{bmatrix} \quad (5.13)$$

where, $\sigma_x, \sigma_{xy}, \sigma_y$ are membrane forces developed in the structure due to the axial compression. Further, linear eigenvalue buckling analysis is performed using the structural and stress stiffness matrices and as follows,

$$([K] + \lambda_i [K_\sigma])\{\psi_i\} = 0 \quad (5.14)$$

where, λ is buckling load, ψ represent mode shape and i is the mode number. Equation 5.14 estimates buckling load and fundamental mode shape, which is used in non-linear static analysis as follows,

$$[K(u)]\{u\} = \{F\} \quad (5.15)$$

where, $[K(u)]$ represents tangent stiffness matrix and ‘F’ is the load in each sub-step in Newton-Raphson method. The total load is subdivided into a series of increments and is applied over several sub-steps. The maximum load considered for nonlinear analysis is P_{cr} obtained from linear buckling analysis. The outcome of Equation 5.15 is a load-deflection curve based on numerical simulations which then is compared with experimental results.

The experimentally obtained first three bending natural frequencies of the sandwich beam in absence of axial compressive load is compared with numerical results. Modal analysis is carried out to extract the first three natural frequencies. The natural frequencies are calculated by solving the following Eigen value problem (Reddy 2014),

$$([K] - \omega_i^2[M])\{\phi_i\} = 0 \quad (5.16)$$

where, $[K]$ is the stiffness matrix, $[M]$ structural mass matrix, $\{\phi_i\}$ is free vibration mode shape and ω represents the circular natural frequency.

The sandwich beam is modelled in a layered configuration using four noded layered structural shell element SHELL 181. SHELL 181 is capable of analysing layered structures which has six degrees of freedom (three translation and three rotation) and formulated based first order shear deformation. A rectangle of size 210×12.5 mm is created to represent the geometry of the sandwich beam. Sandwich skin and core are modelled as orthotropic and isotropic materials respectively. Material properties of core and skin materials are specified for the respective layers. Geometry is meshed with 50 number of “SHELL181” elements. Displacement boundary conditions and loads are applied. ANSYS is used to perform buckling and vibration analysis.

5.6 Buckling behaviour

Sandwich beams are subjected to axial compressive load using universal testing machine with clamped-clamped condition (Figure 2.4). The axial compressive load applied and deflection along the beam axis is recorded using data acquisition system.

The P_{cr} of sandwich composites show increasing trend as a function of cenosphere content (Figure 5.6 and Table 5.2). This is attributed to addition of stiffer cenospheres increase the overall stiffness of the syntactic foam core. Further, presence of woven sisal fiber fabric skin renders additional stiffness to the beam. During the test the sandwich beams exhibit global buckling mode and maximum deflection is observed at the mid portion of the beam as depicted by Figure 5.7b. There are no signs of skin wrinkling and skin microbuckling as evident from Figure 5.7b. This can be attributed to the lesser amount of axial compressive stresses developed in the skins as compared to skin plastic microbuckling and wrinkling strength (Fleck and Sridhar 2002).

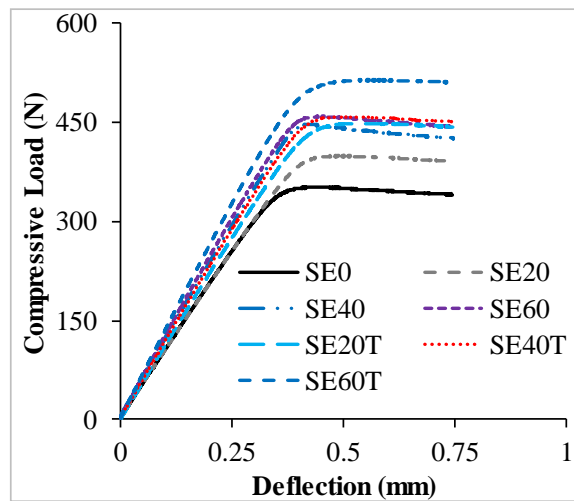


Figure 5.6 Representative set of compressive load-deflection behavior for sandwich beams with syntactic foam core.

Table 5.2 Critical buckling loads for sandwich composites.

Sandwich type	P_{cr} (N)		% Increase w.r.t SE0 (DTM)
	DTM	MBC	
SE0	370.10±17.42	364.28±5.89	----
SE20	399.17±4.87	392.71±9.18	7.86
SE40	444.00±3.56	438.10±5.91	19.96
SE60	464.27±18.82	459.92±8.08	25.44
SE20T	443.83±3.30	437.86±5.64	19.92
SE40T	448.17±7.41	442.52±4.62	21.09
SE60T	514.43±4.05	509.85±5.29	38.99

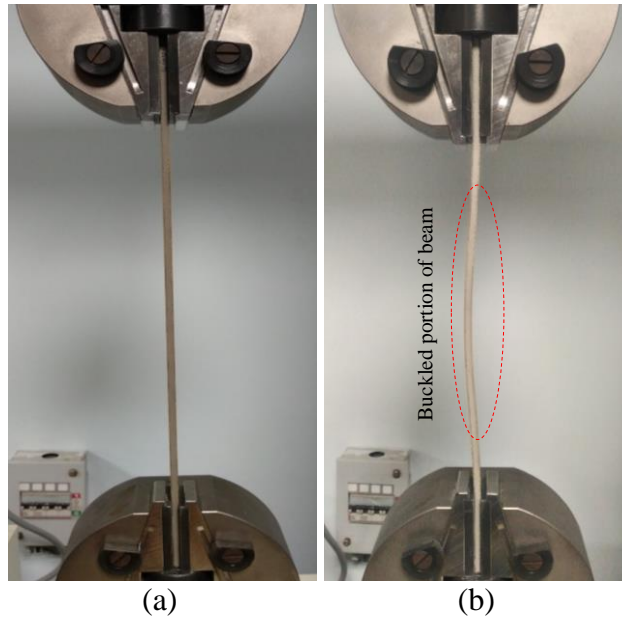


Figure 5.7 Representative images of syntactic foam sandwich beams (a) before and (b) during buckling test.

The most common mode of failure associated with sandwich structures is skin delamination which is seen to be absent for all the samples analysed in the present case (Figure 5.8). This also indicates good adhesive strength between the skin and core. In Table 5.2, sandwich beams having treated cenosphere/epoxy foam as cores have higher buckling loads than the untreated ones. Silane treated cenospheres in epoxy resin enhances the elastic modulus due enhanced interfacial bonding between the constituents increasing overall stiffness of the foams. Increase in mean particle size due to silane treatment also augments for increase in overall stiffness of the foams enabling them for structural applications. The buckling load increase in the range of 7.86-25.44% and 19.92-38.99% respectively for untreated and treated syntactic foam sandwich composites as compared to neat epoxy core sandwich. P_{cr} estimates by DTM and MBC techniques match very closely (within 2%) as seen from Table 5.2.

Table 5.3 presents comparison of buckling loads of cenosphere/epoxy syntactic foams and their sandwich beams tested in present study. It can be observed from Table 5.3 that the buckling loads of the sandwich beams are higher (7.32- 55.72%) than the syntactic foam for the same specimen dimensions subjected to similar testing

conditions. Such an increment can be attributed to enhanced stiffness due to sisal/epoxy skins in sandwich beams. Change in stiffness due to axial compressive loads influences dynamic properties, particularly natural frequency necessitating their estimates.

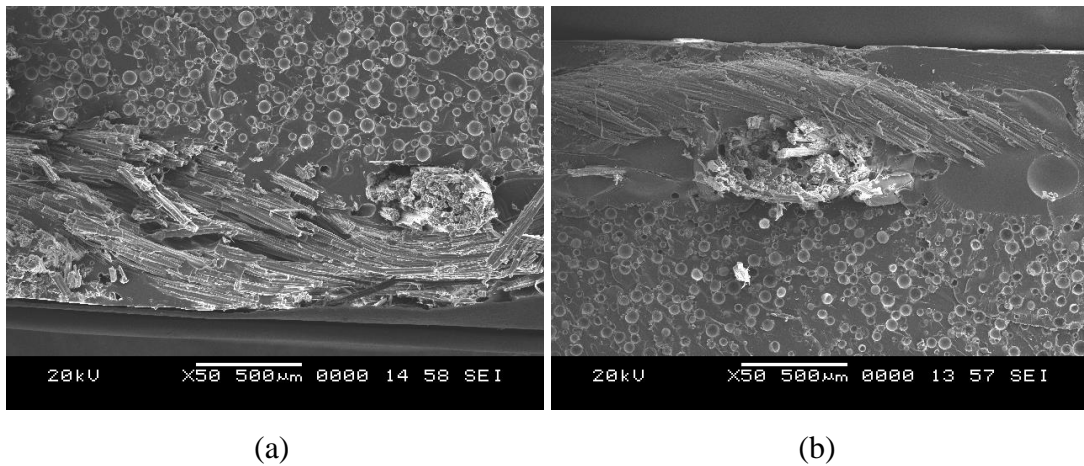


Figure 5.8 Representative micrographs of SE40 sample (a) lower skin (b) upper skin showing no delamination.

Table 5.3 Comparison of buckling loads of cenosphere/epoxy syntactic foams and their sandwiches.

Syntactic foam	P_{cr} (N)		Sandwich type	P_{cr} (N)		% Increase w.r.t syntactic foam (DTM)
	DTM	MBC		DTM	MBC	
E0	237.67 ± 11.02	231.83 ± 12.51	SE0	370.10 ± 17.42	364.28 ± 5.89	55.72
E20	287.58 ± 12.35	281.83 ± 12.85	SE20	399.17 ± 4.87	392.71 ± 9.18	38.81
E40	343.45 ± 14.29	339.33 ± 14.36	SE40	444.00 ± 3.56	438.10 ± 5.91	29.28
E60	387.33 ± 15.04	379.17 ± 17.03	SE60	464.27 ± 18.82	459.92 ± 8.08	19.87
E20T	315.50 ± 12.78	306.67 ± 12.52	SE20T	443.83 ± 3.30	437.86 ± 5.64	39.79
E40T	393.85 ± 16.37	383.83 ± 17.29	SE40T	448.17 ± 7.41	442.52 ± 4.62	13.79
E60T	479.33 ± 17.76	470.67 ± 16.16	SE60T	514.43 ± 4.05	509.85 ± 5.29	7.32

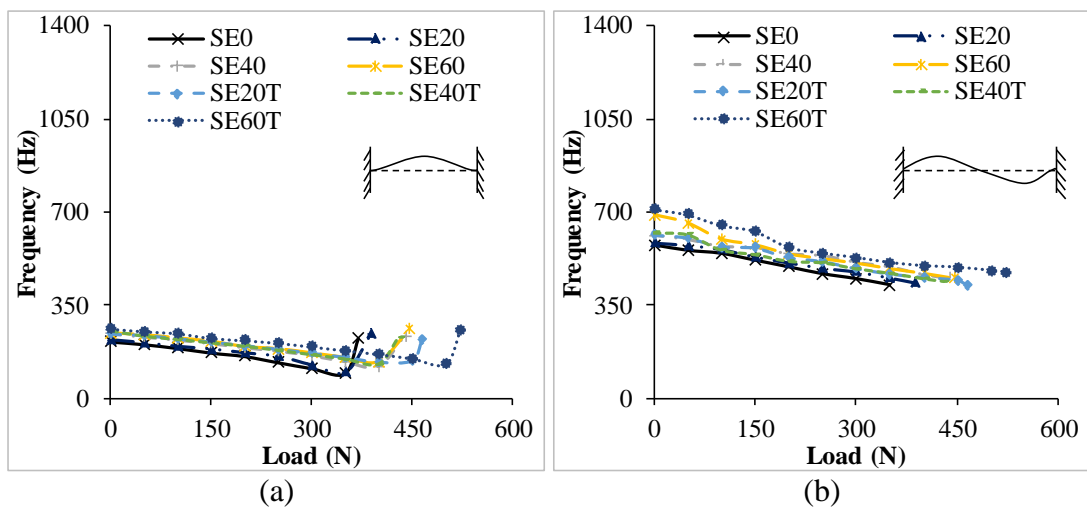
5.7 Free vibration behaviour at no load and axial compression

Experimental modal analysis is carried out to compute natural frequencies corresponding to first three transverse bending mode shapes of the sandwich beam. DEWE Soft software is used for converting time domain signals into frequency domain (Frequency response functions) using Fast Fourier transform algorithm. Further, experimental natural frequencies are validated with numerical results obtained through finite element method. Table 5.4 depicts first three natural frequencies of the sandwich beams in clamped-clamped condition at no load condition. Natural frequencies of syntactic foams show an increasing trend with filler content. The increase in natural frequency of sandwich can be attributed to increase in overall stiffness of the composite due to surface modified intact cenospheres. Thereby the natural frequencies of the sandwich composites with treated syntactic foam cores are higher as compared to untreated syntactic foam core sandwiches for all the filler loadings (Table 5.4).

Table 5.4 Experimental natural frequencies of sandwich beams at no load condition.

Sample Coding	Mode	Natural Frequency (Hz)
SE0	1	212.72±4.25
	2	576.26±13.25
	3	1123.90±23.60
SE20	1	221.47±5.09
	2	583.54±12.25
	3	1181.90±23.64
SE40	1	242.38±5.57
	2	611.02±12.83
	3	1254.30±28.84
SE60	1	246.80±5.18
	2	689.94±13.79
	3	1285.50±29.56
SE20T	1	241.98±5.56
	2	615.59±12.31
	3	1125.00±23.63
SE40T	1	251.41±5.28
	2	620.09±14.26
	3	1240.00±24.91
SE60T	1	261.49±5.23
	2	711.71±14.94
	3	1323.30±30.43

Increasing compressive load decreases natural frequency (Figure 5.9). Fundamental natural frequency reaches minimum value at the onsite of buckling and increases rapidly in post buckling region due to geometric stiffness gain resulting from beams deflection. Similar trend is observed for syntactic foams (Chapter 3) and in previous studies (Mirzabeigy and Madoliat 2016, Rajesh and Pitchaimani 2017, Wu et al. 2015) of isotropic/composites beam and columns. Fundamental natural frequency declines steadily till the compressive load approaches critical buckling load (Figure 5.9a). First natural frequency drops suddenly due to loss of structural stiffness when the compressive load is very closer to critical buckling load (Figure 5.9a). The syntactic foam modulus increases with increase in filler content. Further, stiffness of the sandwich composite increases owing to the woven natural fiber reinforced epoxy skin. Volume fraction of the natural fiber used as skin in sandwiches is approximately the same for the tested samples. Thereby, natural frequencies enhancement is solely attributed to the filler loading.



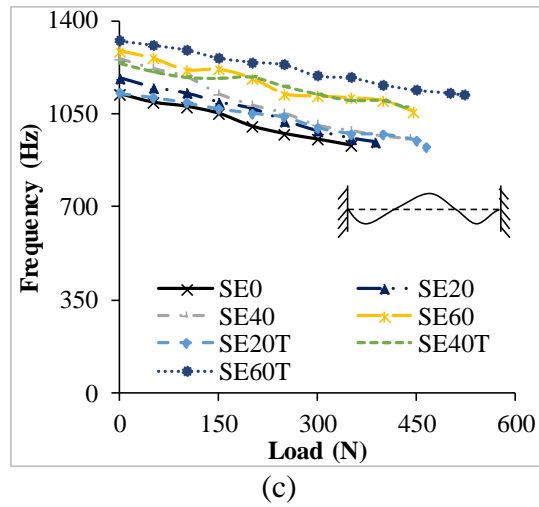


Figure 5.9 Effect of axial compressive load on natural frequencies of (a) 1st (b) 2nd and (c) 3rd mode.

5.8 Comparison of experimental and numerical buckling and free vibration results

Figure 5.10 represents images of sisal fiber, yarn and plain-woven fabric samples used in the present study. The tensile test (Figure 5.3) of yarn is carried out and the stress-strain response is plotted in Figure 5.11. The properties of sisal fiber is listed in Table 5.5. The tensile strength and modulus of yarn is found to be 255 and 8861.11 MPa respectively. Tensile, compressive and flexural properties of neat epoxy samples are deduced by conducting the tests as outlined in section 5.4. The properties of Epoxy matrix are presented in Table 5.6.

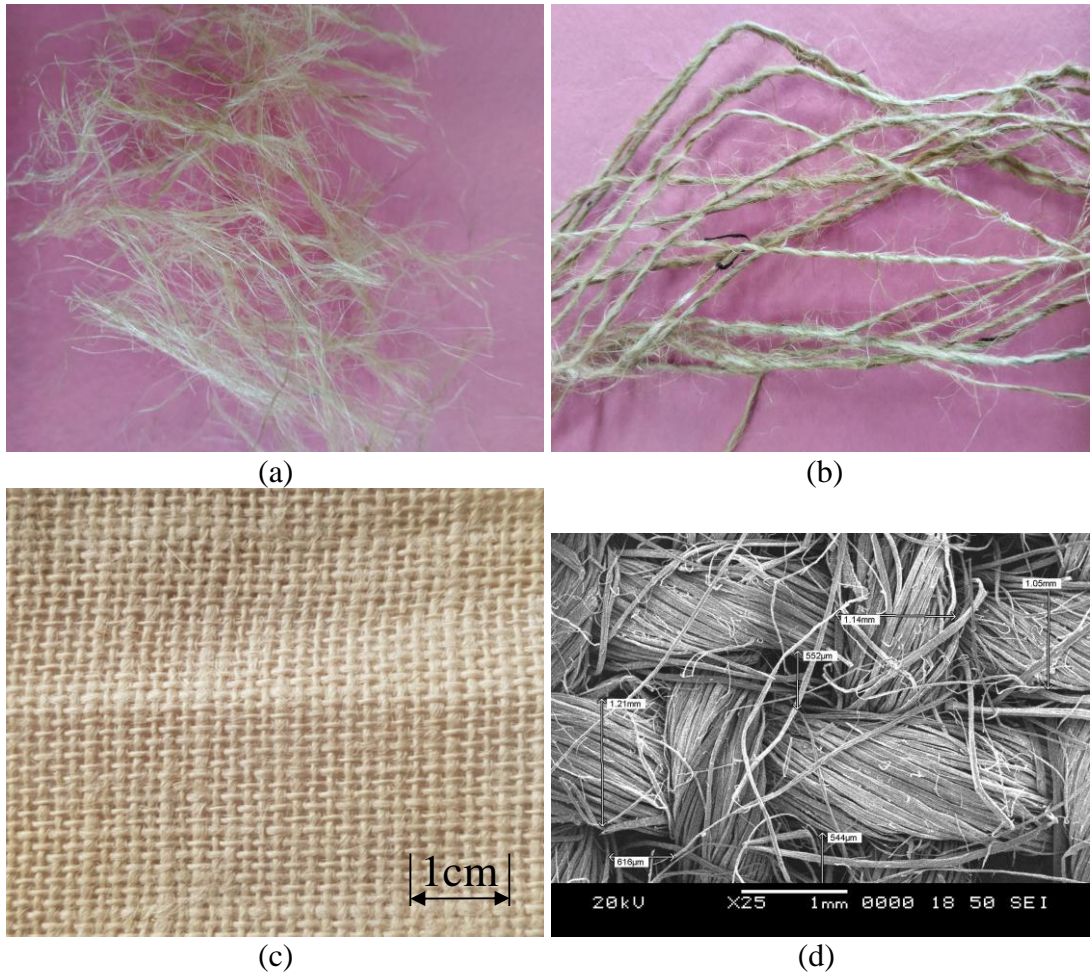


Figure 5.10 (a) Sisal fibers (b) yarns (c) plain woven fabric and (d) SEM image of dry fabric.

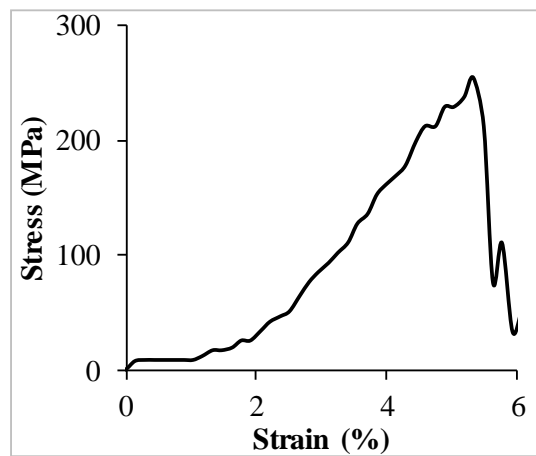


Figure 5.11 Representative stress-strain response for tested yarn.

Table 5.5 Properties of sisal fibres.

Parameter	Value
Young's modulus of Natural fiber (Yarn) (MPa)	8861.11±138.90
Strength of the natural fiber (Yarn) (MPa)	255±8.35
Density of fibre (kg/m ³)	1262.86±46.21
Poisson's ratio	0.2

Table 5.6 Properties of Epoxy matrix.

Property	Value
Density (kg/m ³)	1189.54
Young's Modulus of matrix (MPa)	3917.80
Poisson's ratio of matrix	0.35
Tensile strength (MPa)	36.62
Compressive strength (MPa)	70.74
Flexural Strength (MPa)	70.06
Coefficient of thermal expansion (1/°C)	82×10 ⁻⁶

The fabric geometry is measured to obtain the necessary geometric parameters (Figure 5.4). Different intrinsic fabric lamina properties and geometric parameters obtained for sisal fabric are listed in Table 5.7. Using the data associated with fiber, epoxy and geometry of fabric, the elastic properties of the skin material are estimated with the help of CADEC. The methodology used by CADEC is explained by Barbero (2018). Predicted skin properties (CADEC results) are reported in Table 5.8. Tensile properties of single layer sisal fabric/epoxy are also compared with CADEC values (Table 5.8). Tensile specimens of dimension 250×25×0.75 mm are prepared and tested. The cross head displacement rate is maintained at 2mm/min, as per ASTM D3039/D3039M-17 . Good agreement between CADEC and experimental values are obtained. These properties are further used for numerical analysis to find the natural frequencies of the sandwich beams.

Table 5.7 Lamina intrinsic properties and reinforcement geometry.

Property	Value
Volume fraction of fiber	0.4852
Thickness of lamina (mm)	0.75
Number of fibers in wrap and fill direction(1/cm)	6
Average thickness of dry lamina (mm)	0.723
Fill width (mm)	1.667
Fill thickness (mm)	0.32
Gap between tows in fill direction (mm)	0.5
Warp width (mm)	1.667
Warp thickness (mm)	0.32
Gap between tows in warp direction (mm)	0.5
Neat matrix thickness (mm)	0.11
Harness	2
Shift	1
Interlacing	1

Table 5.8 Comparison of sisal fabric/epoxy laminate properties obtained from CADEC and experimental.

Property	CADEC	Experimental	% difference w.r.t CADEC
Young's Moduli, E_x (MPa)	6331	6950.01±139	-8.91
Young's Moduli, E_y (MPa)	6331	5783.33±115	9.47
Poisson's Ratio, ν_{12}	0.252	----	
Poisson's Ratio, ν_{23}	0.252	----	
Shear Moduli, G_{12} (MPa)	2522	----	
Shear Moduli, G_{23} (MPa)	2522	----	

Elastic properties associated with cenosphere/epoxy syntactic foam are obtained using BGM and are used as input to finite element analysis. Estimated elastic properties of fly ash cenosphere/epoxy syntactic foams that are listed in Table 3.2 of Chapter 3. Young's modulus increases with filler content, and such effect is more prominent when treated cenospheres are used. Improved interfacial bonding between the constituents plays a crucial role for such an observation.

Elastic properties of the skin material (sisal fabric/epoxy) (Table 5.8) estimated with CADEC and elastic properties of the (cenosphere/epoxy) core material estimated using BGM (Table 3.2 of Chapter 3) are used as an input to numerical analysis using ANSYS. Linear eigen-value buckling analysis is carried out to understand the fundamental buckling mode which is considered to represent the geometric imperfection. Subsequently non-linear static structural analysis is carried out. Load-deflection responses are graphed to compare experimental values with numerical results. Figure 5.12 presents comparative plots for SE40 and SE40T sandwich samples. Numerical and experimental buckling loads are presented in Table 5.9. Maximum deviation is noted to be 18.41% between numerical and experimental buckling results. Numerical simulations predict the load-deflection behavior and buckling load reasonably yet lower than experimental results. Modulus variation is clearly evident from these plots. Numerous surface defects on cenospheres like non-sphericity, wall thickness variations and built-in porosity in the walls are thought to be responsible for that responsible for the deviations of numerically predicted values from that of experimental results. Accuracy in obtaining skin properties can be improved with more accurate measurements of microstructural properties of fabric as input to CADEC.

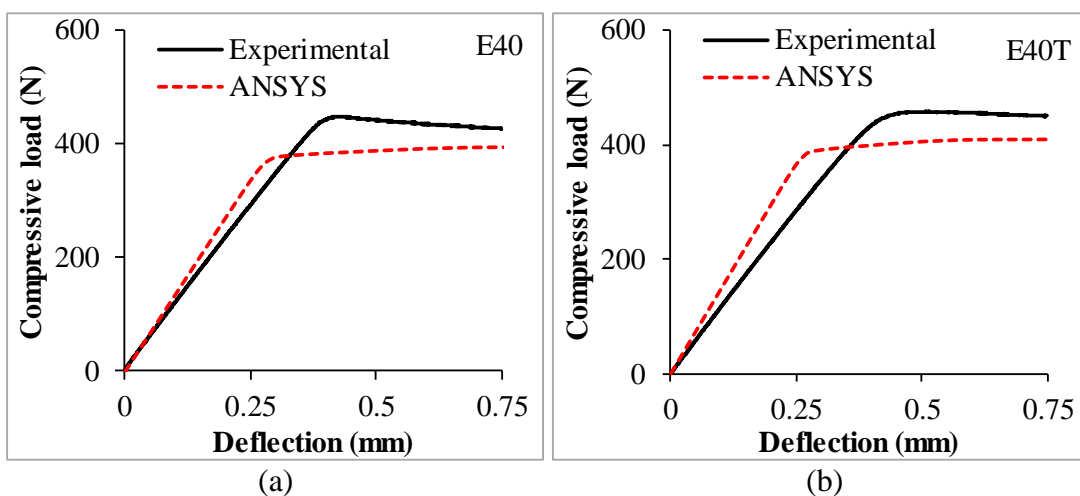


Figure 5.12 Comparison of load-deflection curves obtained experimentally and numerically for (a) SE40 and (b) SE40T sandwich composites.

Table 5.9 Comparison of experimental and numerically obtained buckling loads of sandwich composites.

Sample Type	Experimental P_{cr} (N)		Numerical P_{cr} (N)		% Difference w.r.t Experimental (DTM)	% Difference w.r.t Experimental (MBC)
	DTM	MBC	DTM	MBC		
SE0	370.10 ± 17.42	364.28 ± 5.89	360	355	2.73	2.55
SE20	399.17 ± 4.87	392.71 ± 9.18	368	365	7.81	7.06
SE40	444.00 ± 3.56	438.10 ± 5.91	385	377	13.29	13.95
SE60	464.27 ± 18.82	459.92 ± 8.08	419	410	9.75	10.85
SE20T	443.83 ± 3.30	437.86 ± 5.64	383	380	13.7	13.21
SE40T	448.17 ± 7.41	442.52 ± 4.62	395	385	11.86	12.99
SE60T	514.43 ± 4.05	509.85 ± 5.29	425	416	17.39	18.41

Modal analysis is carried out to extract first three natural frequencies for sandwiches. Comparison of numerical results with experimental values is presented in Table 5.10. Experimental and numerical results are in good agreement (within 12.9%). Sandwich composites with sisal/epoxy skin and cenosphere/epoxy cores show better buckling and free vibrations characteristics than sandwiches with neat epoxy core.

5.9 Conclusions

Buckling and free vibration characteristics of sisal fabric/epoxy skin and syntactic foam core is investigated experimentally and numerically. The sandwich beams show global buckling mode shape without skin delamination or skin wrinkling. The buckling load and natural frequencies increase with cenosphere content. The buckling load and natural frequencies of sandwich composites with treated cenosphere/epoxy foam core are higher than untreated cenosphere/epoxy foam sandwich samples because enhanced stiffness of core due to proper adhesion between the constituents. Further, the natural frequencies decrease with increase of the axial compressive load. The first natural frequency represents minimum value at critical buckling load and later increases exponentially post critical buckling load due to gain in geometrical

stiffness of the material. The skin properties are found using CADEC and are found in good agreement with the experimental values. Further properties obtained from CADEC and Bardella-Genna model are used for numerical analysis. Experimental results are compared with numerically predicted values and are found to be in good agreement.

Table 5.10 Comparison of natural frequency values obtained through experimental and numerical approaches.

Sample Coding	Mode	Natural Frequency (Hz)		% deviation
		Experimental	Numerical	
SE0	1	212.72	205.12	3.57
	2	576.26	581.86	-0.97
	3	1123.90	1187.30	-5.64
SE20	1	221.47	210.75	4.84
	2	583.54	597.48	-2.39
	3	1181.90	1221.40	-3.34
SE40	1	242.38	216.97	10.48
	2	611.02	615.35	-0.71
	3	1254.30	1258.70	-0.35
SE60	1	246.80	223.92	9.27
	2	689.94	644.51	9.44
	3	1285.50	1300.20	-1.14
SE20T	1	241.98	211.48	12.6
	2	615.59	599.66	2.59
	3	1125.00	1226.20	-9
SE40T	1	251.41	218.99	12.90
	2	620.09	630.73	-1.72
	3	1240.00	1271.40	-2.53
SE60T	1	261.49	227.95	12.83
	2	711.71	686.11	3.60
	3	1323.30	1324.80	-0.11

6 BUCKLING BEHAVIOUR OF SANDWICH COMPOSITES UNDER THERMAL LOAD

6.1 Introduction

Experimental investigation carried out on buckling behaviour of syntactic foam sandwich beam with sisal fabric/epoxy skin under non-uniform heating is presented. Temperature is varied in range of 26-60°C for three different heating conditions Case 1 (*Increase-decrease*), Case 2 (*Decrease*) and Case 3 (*Decrease-increase*) and its effect on thermal buckling behaviour of sandwich composites is analysed.

6.2 Buckling under non-uniform thermal load

Sandwich beam with length 310 mm, width 12.5 mm, core thickness 2.5 mm and facing layer thickness of 0.75 mm is considered. Each facing is made of single layer of sisal fabric. The sandwich beams are subjected three different heating conditions as shown in Figure 2.5 and Figure 2.6. The highest temperature associated with a particular temperature case and transverse deflection of the beam are recorded using a thermocouple and a LVDT respectively. Further these values are used to plot temperature-deflection response. As the beams were expected to deflect in the first bending mode, transverse deflection is measured at the mid-point of the beam.

In order to understand the deflection trend of syntactic foam sandwich beam, temperature-deflection plot associated with SE40 subjected to case 1 (*increase-decrease*) heating condition is presented in Figure 6.1a. With increase in temperature the undergoes the following four trends in general.

Region I: When the beam is exposed to heat, the beam is not experiencing any significant deflection even though there is a significant increase in the elevated temperature. Portion of the deflection curve *a-b* (Figure 6.1a) indicates this clearly. This also indicates that the temperature rise till the point *b*, is not able to develop sufficient amount of compressive stress to cause any significant amount of out-of-plane deflection. However, the behaviour of syntactic foam is different as seen in Figure 6.1b. So, this indicates that sandwiching of syntactic foam between the natural fiber/epoxy laminate facings controls the out-of-plane deflection of the syntactic

foam. This can be also attributed to structural stiffness enhancement due to the sandwich effect.

Region II: With further increase in temperature rise beyond point b , the out of plane deflection increases drastically even with a small increase in temperature rise. Portion of deflection curve from point b to point c indicates this region. It is observed that the deflection behaviour between the points b and c is linear. And beam deflects away from the heating source. The reason for drastic increase in deflection in this region is generated compressive stresses and thermal moments (Liu et al. 2006). The portion of curve from a - c shows typical load-deflection behaviour of a beam under a compressive load and the first bifurcation point is b . The temperature rise corresponding to point b is considered as first critical buckling temperature (T_{cr_1}).

Region III: The linear deflection behaviour vanishes at point c . With further increase in temperature rise beyond point c , the beam continues to deflect in same direction till point d . However, the rate of increase in deflection with respect to temperature rise is not as rapid as observed in Region II. This is change in rate of deflection may be due energy storage of the sandwich beam.

Region IV: With further increase in the temperature beyond point d , the beam starts moving towards the heating source. So, the temperature rise corresponding to point d is considered as snap-initiation temperature and is denoted as T_{cr_2} .

Figure 6.1a represents the method used to predict initial critical buckling temperature (T_{cr_1}) and snap-initiation temperature (T_{cr_2}). For all the tested samples, it is observed that deflections take place away from the heating source initially and towards the heating source at higher temperatures. The trend observed for cenosphere/epoxy syntactic foams and their sandwiches with sisal/epoxy skins are entirely different as evident from Figure 6.1b and Figure 6.1a respectively. The syntactic foams undergone deflection at initial small increase in temperature ($<2^\circ\text{C}$) and remained in first buckled shape for longer duration and snap-through phenomena took place when viscoelastic forces were developed into the syntactic foam beam. But in sandwiches the beam

remained in its positions at initial rise in temperature and then undergone deflection. The sandwich beams with syntactic foam core exhibited snap-through phenomena at very high temperature as compared to that of syntactic foams.

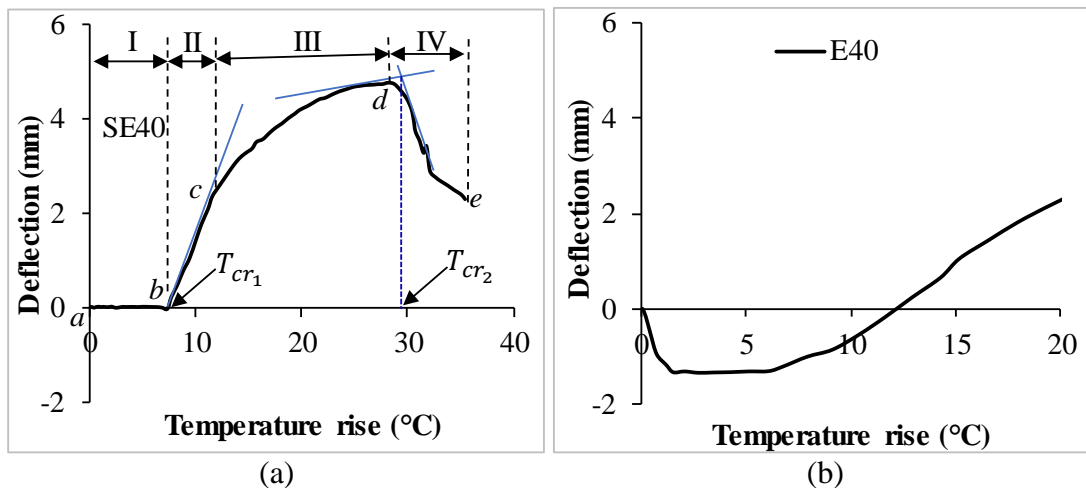


Figure 6.1 (a) Determination of critical buckling temperatures from temperature-deflection curve of sandwich beam (b) deflection behaviour of syntactic foam.

Buckling behaviour of sandwich composites with neat epoxy core and syntactic foam core under different heating conditions is presented in Figure 6.2. It is observed that with increase in cenosphere content the first critical buckling temperature increases and deflection of the beams also reduces. This can be attributed to enhanced stiffness of the composite due to addition of stiff cenospheres into the epoxy matrix. The time duration of the beam remained in the first buckling mode shape increase with increase in filler content. With increase in temperature, significant amount of viscoelastic forces develops in the sandwich beams. This time-dependent phenomenon keeps the beam in the same buckled shape for a particular period of time with temperature rise. With further increase in temperature, compressive stresses and viscoelastic forces gets developed simultaneously and buckled beam deforms back towards the original position. This trend is observed for all the sandwich composites subjected to the three different heating conditions analysed.

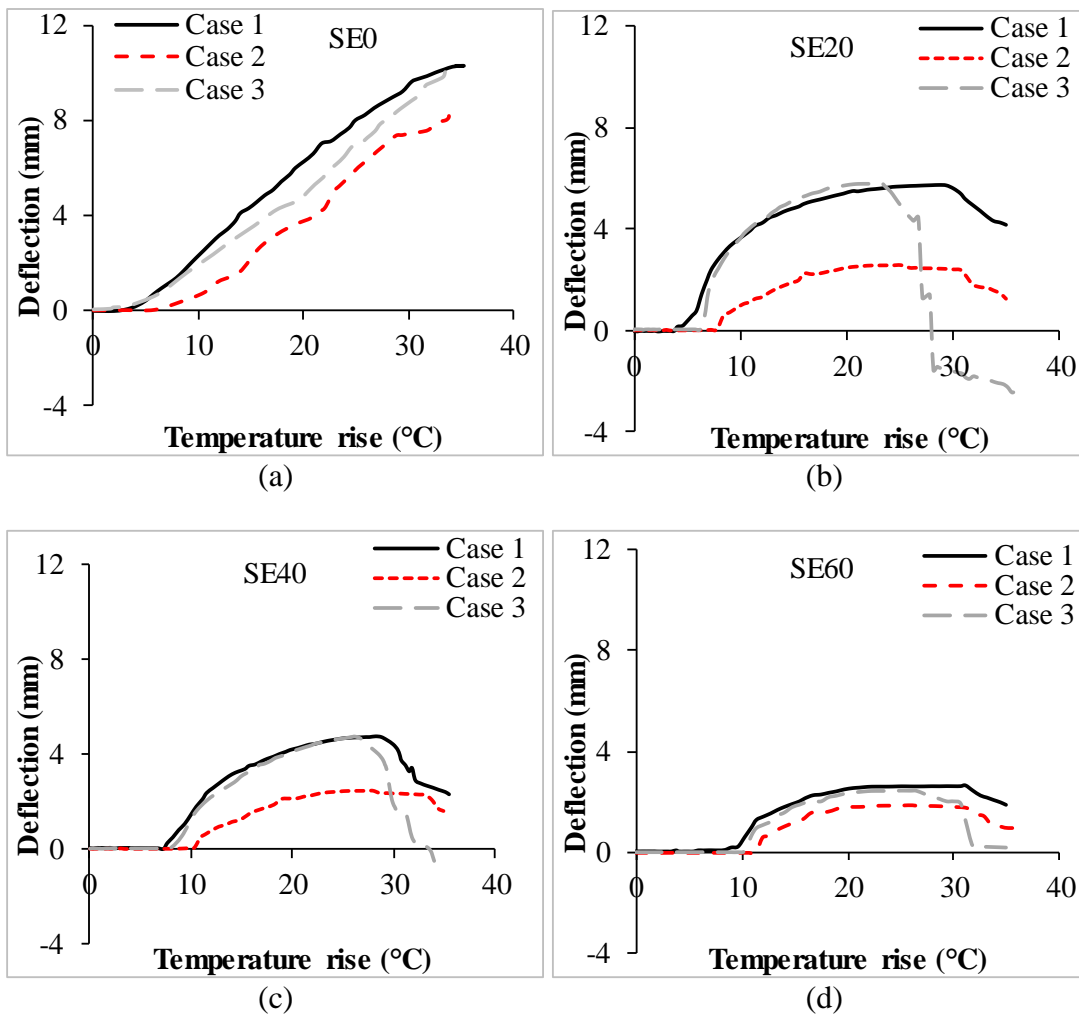


Figure 6.2 Effect of non-uniform heating of (a) SE0 (b) SE20 (c) SE40 (d) SE60 sandwich composites.

Figure 6.3 represent temperature-deflection curves for sandwich beams with neat resin and syntactic foam cores subjected to three different thermal loading conditions. The critical buckling temperatures and deflection behaviour of non-uniformly heated structures are prominently depend on the location of the heating source and amount of portion of the structural member exposed to highest temperature of the particular temperature profile. From Figure 6.3, the deflection trend observed for all the heating conditions is similar till the snap initiation position of the beams. In *Decrease-increase* (Figure 2.6c) heating case snap-through phenomena is quicker than the other two heating conditions. This may be due to more viscoelastic forces developed due to higher intensity of heating. *Increase-decrease* (Figure 2.6a), heating reported lower critical buckling temperatures and snap-through initiation temperature (Table 6.1)

which can be attributed to the location of heating source. In the case of *increase-decrease* heating the source is located at the center of the beam where the sandwich beam offers less stiffness, hence the critical buckling temperatures are less compared to other heating cases.

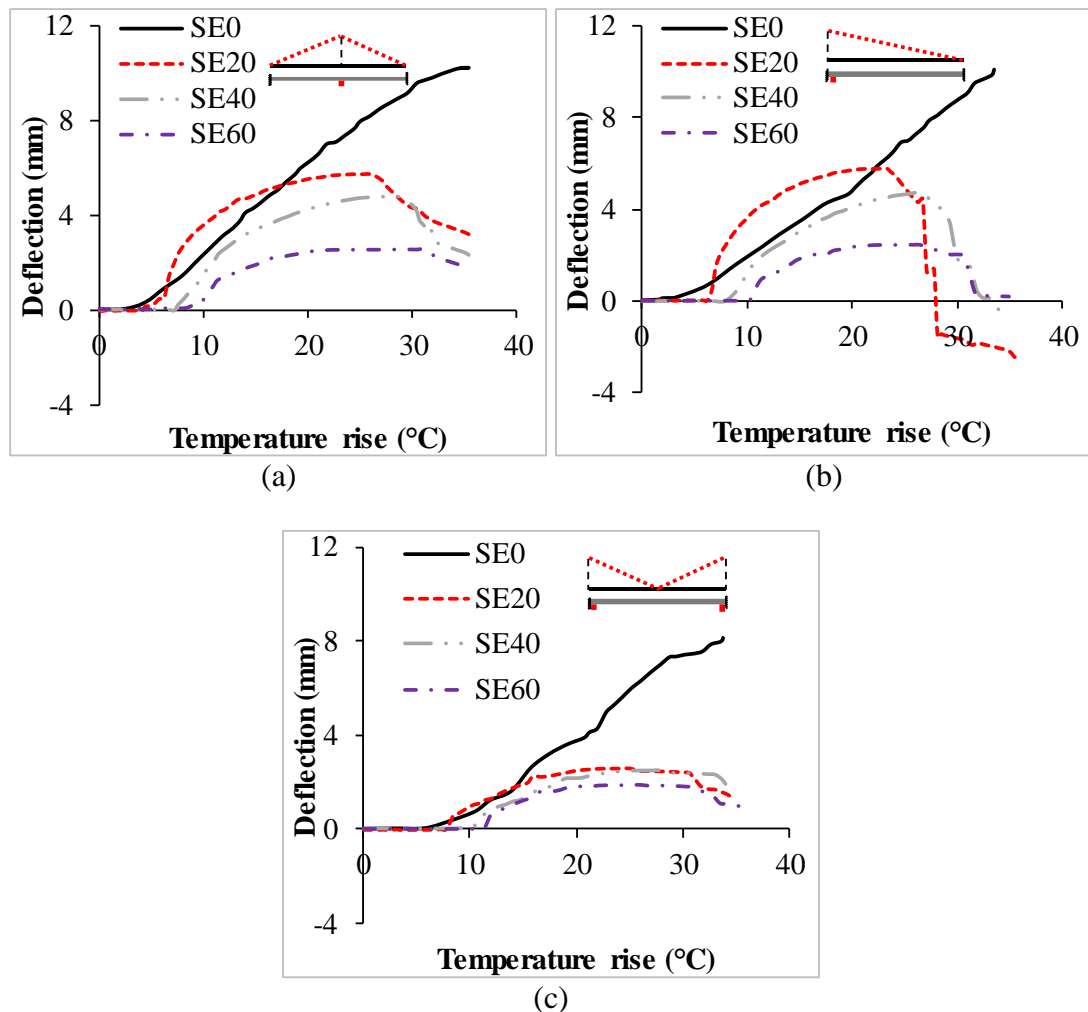


Figure 6.3 Effect of filler content on (a) *Increase-decrease* (b) *Decrease* and (c) *decrease-increase* heating conditions.

During *decrease* (Figure 2.6b) heating condition, the sandwich beam is exposed to higher temperature at one of its constrained end and the rate of reduction in structural stiffness is less as compared other heating conditions thereby results in higher critical buckling temperature and higher snap-initiation temperatures. In *decrease-increase* heating (Figure 2.6c), the intensity of heat is more at both the ends and rate of reduction in structural stiffness is not higher as compared to *increase-decrease*

heating case and thereby deflections are lower than the *increase-decrease* case. represents critical buckling temperature and snap-initiation temperature of sandwich beams. *Decrease* heating condition resulted in higher critical buckling temperatures of the beams than other two heating conditions.

The surface modified cenosphere/epoxy syntactic foam sandwich composites show slight enhancement in the critical buckling temperatures and snap-initiation temperatures (Figure 6.4 and Table 6.1). The temperatures values are found to be within the standard deviation values of the untreated cenosphere/epoxy syntactic foam sandwich composites. Surface modification of the cenospheres enhances proper interfacial bonding between the constituents and thereby enhances the stiffness of the sandwich core material. This effect of enhancement of the stiffness of core due to surface modification is not replicated in the enhancement of critical buckling temperatures significantly, when subjected to three different heating conditions.

Table 6.1 Thermal buckling temperatures of the sandwich composites subjected to non-uniform thermal loads.

Sample coding	Case 1 <i>Increase-Decrease</i>		Case 2 <i>Decrease</i>		Case 3 <i>Decrease-Increase</i>	
	T_{cr_1} (°C)	T_{cr_2} (°C)	T_{cr_1} (°C)	T_{cr_2} (°C)	T_{cr_1} (°C)	T_{cr_2} (°C)
SE0	3.82 ±0.46	-----	6.25 ±0.69	-----	4.28 ±0.82	-----
SE20	4.18 ±0.58	29.15 ±1.53	6.28 ±0.76	30.5 ±1.89	7.80 ±0.29	23.25 ±1.95
SE40	7.25 ±1.02	30.50 ±1.68	10.25 ±0.98	33.56 ±1.28	8.16 ±0.50	28.15 ±1.30
SE60	8.75 ±1.09	30.25 ±1.59	11.30 ±1.08	32.60 ±2.41	10.12 ±1.21	29.15 ±2.05
SE20T	4.85 ±0.41	28.15 ±1.41	8.2 ±0.64	31.25 ±1.54	7.05 ±0.62	25.75 ±2.01
SE40T	8.15 ±0.40	31.78 ±1.13	11.08 ±0.84	34.68 ±1.22	9.17 ±1.21	29.15 ±2.03
SE60T	9.58 ±0.69	32.05 ±2.49	12.86 ±2.67	33.66 ±2.41	11.06 ±1.20	29.98 ±2.92

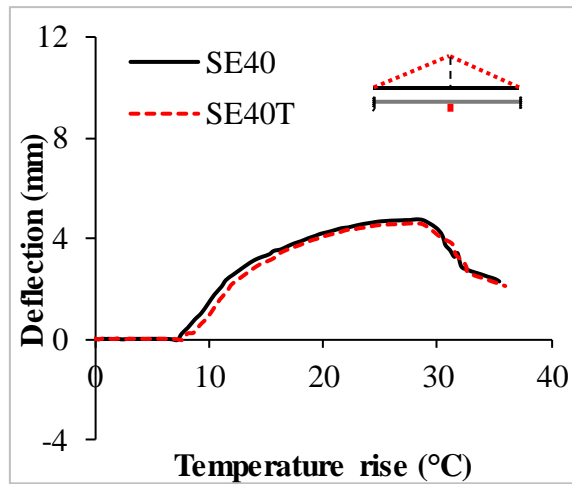


Figure 6.4 Effect of surface modification on thermal buckling behaviour of representative sandwich sample under *increase-decrease* heating.

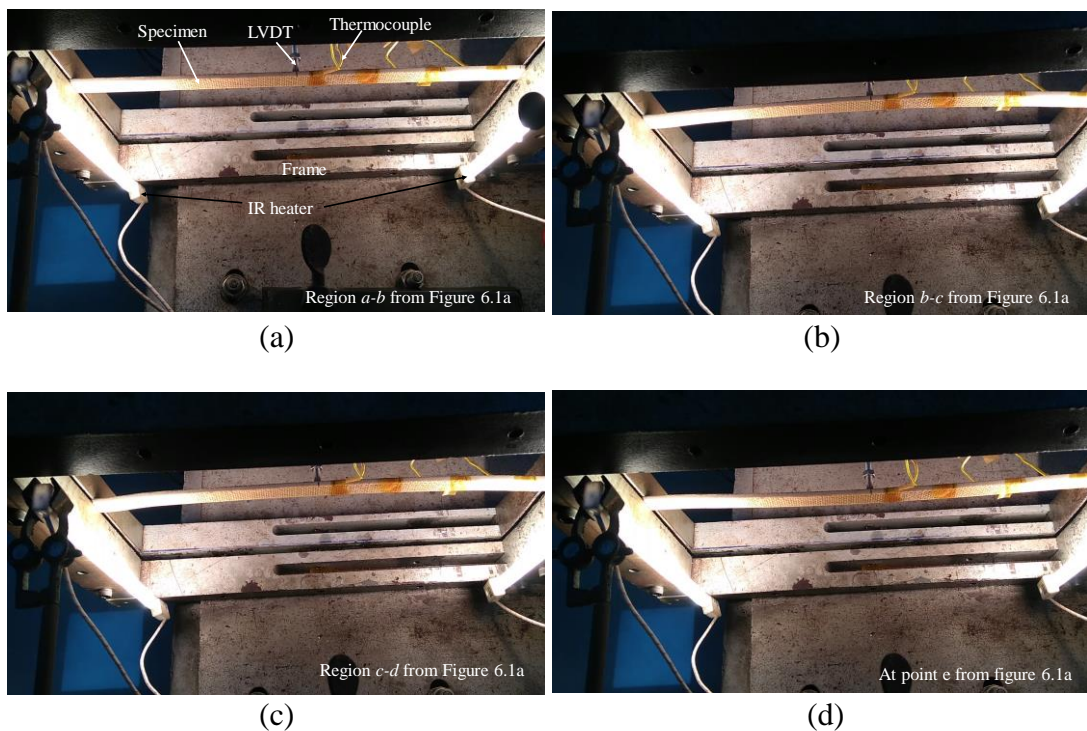


Figure 6.5 Test in progress images of the representative sample under *decrease-increase* heating condition.

6.3 Conclusions

Sandwich composites with untreated and treated cenosphere/epoxy syntactic foam cores and sisal woven fabric/epoxy skins are prepared and tested under non-uniform heating conditions for its deflection behaviour. It is observed that the deflection

behaviour of the sandwich beams with syntactic foam core are experiencing snap-through deflection behaviour with increase in temperature rise, due to release of temperature dependent viscoelastic forces. However, the sandwich beam with epoxy core is not experiencing this snap-through deflection behaviour. The critical buckling temperature show increasing trend with filler content. Surface modified cenosphere/epoxy sandwich composites do not show significant increase in buckling temperatures but lower deflections are observed due to increased stiffness of the foams as compared with untreated ones.

7 SUMMARY AND CONCLUSIONS

7.1 Summary

A comprehensive investigation is conducted on buckling and dynamic behaviour of fly ash cenosphere/epoxy syntactic foams and its sandwich composites under mechanical and thermal loads. Use of cenospheres in structural applications can reduce the landfill burden and help in effectively addressing the environmental concern of fly ash disposal. In the present study, manual stir casting method is used to develop the cenosphere/epoxy syntactic foam specimens and buckling and free vibration behaviour is carried out. Syntactic foams are fabricated with 20, 40 and 60 vol.% of cenospheres in epoxy matrix. The effect of filler volume fraction and surface treatment of cenospheres are investigated. Sandwich composites with natural fiber woven fabric reinforced in epoxy is used as skin material and syntactic foam core is also investigated for buckling and free vibration behaviour subjected to mechanical and thermal loads.

Experiments are conducted on cenospheres/epoxy syntactic foams and sandwiches to evaluate the effectiveness of reinforcing cenospheres in epoxy matrix. Properties of cenosphere/epoxy syntactic foams obtained using free vibration testes are compared with available theoretical models. Influence of axial compressive loads on buckling free vibration characteristics of cenosphere/epoxy syntactic foams and their sandwiches are carried under mechanical loads. Thermal buckling behaviour of syntactic foams and sandwiches are also carried out at different non-uniform heating conditions. In order to understand heat flow mechanism in syntactic foams coefficient of thermal expansions is found experimentally. Viscoelastic behaviour of syntactic foams is understood by carrying dynamic mechanical analysis. The properties of skins used in making sandwiches are found experimentally by performing tensile tests on laminate and also compared analytically using CADEC. Finally, non-linear buckling analysis of sandwich composites is carried out and compared with experimental load-deflection data.

7.2 Conclusions

The main conclusions are summarized as:

Density of syntactic foams

- Reduction in the density of composites is observed as compared to the theoretical ones and is attributed to the air entrapment in matrix during the process of mechanical mixing of cenospheres in the resin.
- Syntactic foams with untreated cenospheres are noted to have better weight saving potential as compared to treated cenospheres. Silane coating on as received cenospheres increases the effective mean diameter, thereby increasing their density.
- The void content increases with increase in filler content and is found to be less than 5.58%.
- Highest weight saving potential of 15.81% and 14.61% is observed for E60 for E60T respectively.

Buckling and free vibration behaviour of syntactic foams under mechanical load

- The buckling load and natural frequencies increase with increase in cenosphere volume fraction.
- With increase in compressive load, decrease in natural frequency is observed for all samples tested.
- Experimentally the first natural frequency reaches minimum value at onsite of buckling and increases rapidly in post buckling region.
- The buckling load and natural frequencies of silane treated cenosphere/epoxy foams are higher than that of the untreated ones.
- Good agreement between analytical and experimental results are observed.
- Buckling loads found using different approaches are in close agreement.
- Property map of buckling load as a function of density is presented by extracting values from the available literature.

Buckling behaviour of syntactic foams under thermal load

- Samples subjected to mechanical axial compression at room temperature show increase in buckling load in range of 14.42-59.01% for increase in cenosphere content from 20-60 volume % as compared to neat epoxy resin.
- All samples subjected to mechanical axial compressive loads, regained to its original shape after the test, without any indication of plastic/permanent deformation.
- CTE of cenosphere/epoxy syntactic foams decreases in the range of 13.92-48.95% with increasing filler content as compared to neat epoxy resin.
- Treated cenosphere/epoxy syntactic foam show reduced CTE as compared with untreated ones.
- All the samples are subjected to three different non-uniform heating conditions and the temperature-deflection curves reveal that the syntactic foams undergo snap-through buckling behaviour.
- The deflection of syntactic foams reduces with increase in cenosphere content. Temperature range for which the syntactic foam remains in initial buckled shape increases with increase in cenosphere content.
- The treated cenosphere/epoxy syntactic foams do not show much significant variation in deflection behaviour and buckling temperatures as compared to untreated ones.
- Decrease heating condition show higher buckling temperatures as compared to other two heating cases.
- Dynamic mechanical analysis of untreated and treated cenosphere/epoxy syntactic foams show that the foams have better energy absorbing capability than neat epoxy resin.

Buckling and free vibration behaviour of syntactic foam sandwich composites under mechanical load

- The sandwich beams show global buckling mode shape without skin delamination or skin wrinkling.
- The buckling load and natural frequencies increase with cenosphere content.

- The buckling load and natural frequencies of sandwich composites with treated cenosphere/epoxy foam core are higher than untreated cenosphere/epoxy foam sandwich samples because enhanced stiffness of core due to proper adhesion between the constituents.
- Further, the natural frequencies decrease with increase of the axial compressive load.
- The first natural frequency represents minimum value at critical buckling load and later increases exponentially post critical buckling load due to gain in geometrical stiffness of the material.
- The skin properties are found using CADEC and are found in good agreement with the experimental values. Further properties obtained from CADEC and Bardella-Genna model are used for numerical analysis.
- Experimental results are compared with numerically predicted values and are found to be in good agreement.

Buckling behaviour of sandwich composites under thermal load

- All samples subjected to thermal load undergo deflection far from heating source at lower temperatures and towards the heating source at the higher temperatures.
- The critical buckling temperature show increasing trend with filler content.
- Surface modified cenosphere/epoxy sandwich composites do not show significant increase in buckling temperatures but lower deflections are observed due to increased stiffness of the foams as compared with untreated ones.
- The buckling of sandwich temperatures is significantly higher than syntactic foams.

Present work successfully demonstrates feasibility of manual stirring method for developing thermosetting syntactic foam composites based on fly ash cenospheres and hand lay-up process for developing sandwich composites with natural fiber reinforced skin. Composites are eco-friendly, lightweight and more importantly provides 15.81% weight savings potential. Further, usage of fly ash cenospheres and natural fibers reduce environmental linked issues. Experiments are conducted to evaluate the effect of filler content and surface modification of cenospheres on buckling and free

vibration behaviour of cenosphere/epoxy syntactic foams and their sandwiches, subjected to mechanical load and thermal loads. The experimental results presented as part of this work can be used by industry professionals for development of syntactic foams and sandwich composites with natural fiber skin for specific applications. E60T and SE60T is the best choice based on the work presented here.

SCOPE OF FUTURE WORK

In the present research work, buckling and free vibration of syntactic foams and their sandwiches subjected to mechanical and thermal loads are studied. The analytical and numerical formulations for viscoelastic behaviour syntactic foams and their sandwich subjected to temperature variation can be addressed. The effect of particle size, surface modification on viscoelastic behaviour of syntactic foams due temperature variation can be studied. Coefficient of thermal expansion behaviour of the sisal/epoxy facing can be addressed to understand the expansion behaviour of sisal fiber fabric reinforced in epoxy matrix, when used in sandwich composites in structural applications subjected to thermal loads. More experimental work can be carried by varying thickness of syntactic foam core and by using skins of different materials.

REFERENCES

- Abramovich, H., Govich, D. and Grunwald, A. (2015). "Buckling prediction of panels using the vibration correlation technique." *Progress in Aerospace Sciences*, 78, 62-73.
- Aiello, M. A. and Ombres, L. (2007). "Buckling load design of sandwich panels made with hybrid laminated faces and transversely flexible core." *Journal of Sandwich Structures & Materials*, 9(5), 467-485.
- Alkadasi, N. A., Hundiwale, D. and Kapadi, U. (2004). "Effect of coupling agent on the mechanical properties of fly ash-filled polybutadiene rubber." *Journal of applied polymer science*, 91(2), 1322-1328.
- Amba-Rao, C. L. (1967). "Effect of end conditions on the lateral frequencies of uniform straight columns." *The Journal of the Acoustical Society of America*, 42(4), 900-901.
- Arbelo, M. A., de Almeida, S. F., Donadon, M. V., Rett, S. R., Degenhardt, R., Castro, S. G., Kalnins, K. and Ozolins, O. (2014). "Vibration correlation technique for the estimation of real boundary conditions and buckling load of unstiffened plates and cylindrical shells." *Thin-Walled Structures*, 79, 119-128.
- Arbelo, M. A., Kalnins, K., Ozolins, O., Skukis, E., Castro, S. G. and Degenhardt, R. (2015). "Experimental and numerical estimation of buckling load on unstiffened cylindrical shells using a vibration correlation technique." *Thin-Walled Structures*, 94, 273-279.
- ASTM D638-14, *Standard Test Method for Tensile Properties of Plastics*, ASTM International, West Conshohocken, PA, USA.
- ASTM D695-15, *Standard Test Method for Compressive Properties of Rigid Plastics*, ASTM International, West Conshohocken, PA, USA.
- ASTM D696-13, *Standard Test Method for Coefficient of Linear Thermal Expansion of Plastics Between -30°C and 30°C with a Vitreous Silica Dilatometer*, ASTM International, West Conshohocken, PA, USA.
- ASTM D790-17, *Standard Test Methods for Flexural Properties of Unreinforced and Reinforced Plastics and Electrical Insulating Materials*, ASTM International, West Conshohocken, PA, USA.
- ASTM D792-13, *Standard Test Methods for Density and Specific Gravity (Relative Density) of Plastics by Displacement*, ASTM International, West Conshohocken, PA, USA.
- ASTM D3039/D3039M-17, *Standard Test Method for Tensile Properties of Polymer Matrix Composite Materials*, ASTM International, West Conshohocken, PA, USA.
- ASTM D3800-16, *Standard Test Method for Density of High-Modulus Fibers*, ASTM International, West Conshohocken, PA, USA.

ASTM D3822 / D3822M-14, *Standard Test Method for Tensile Properties of Single Textile Fibers*, ASTM International, West Conshohocken, PA, USA.

ASTM D3878-18, *Standard Terminology for Composite Materials*, ASTM International, West Conshohocken, PA, USA.

Atikler, U., Basalp, D. and Tihminlioglu, F. (2006). "Mechanical and morphological properties of recycled high-density polyethylene, filled with calcium carbonate and fly ash." *Journal of applied polymer science*, 102(5), 4460-4467.

Aureli, M., Porfiri, M. and Gupta, N. (2010). "Effect of polydispersivity and porosity on the elastic properties of hollow particle filled composites." *Mechanics of Materials*, 42(7), 726-739.

Aydogdu, M. (2007). "Thermal buckling analysis of cross-ply laminated composite beams with general boundary conditions." *Composites Science and Technology*, 67(6), 1096-1104.

Bajaj, P., Jha, N. and Kumar, R. A. (1992). "Effect of coupling agents on the mechanical properties of mica/epoxy and glass fiber/mica/epoxy composites." *Journal of applied polymer science*, 44(11), 1921-1930.

Barbero, E. J. (2011). *Computer Aided Design Environment for Composites*. <http://en.cadec-online.com/>

Barbero, E. J. (2018). *Introduction to composite materials design* (3rd ed.): CRC press.

Bardella, L. and Genna, F. (2001). "On the elastic behavior of syntactic foams." *International Journal of Solids and Structures*, 38(40-41), 7235-7260.

Bhagat, V. and Jeyaraj, P. (2018). "Experimental investigation on buckling strength of cylindrical panel: Effect of non-uniform temperature field." *International Journal of Non-Linear Mechanics*, 99, 247-257.

Bharath Kumar, B., Doddamani, M., Zeltmann, S. E., Gupta, N., Gurupadu, S. and Sailaja, R. (2016). "Effect of particle surface treatment and blending method on flexural properties of injection-molded cenosphere/HDPE syntactic foams." *Journal of materials science*, 51(8), 3793-3805.

Bharath Kumar, B., Doddamani, M., Zeltmann, S. E., Gupta, N., Ramesh, M. and Ramakrishna, S. (2016). "Processing of cenosphere/HDPE syntactic foams using an industrial scale polymer injection molding machine." *Materials & Design*, 92, 414-423.

Bharath Kumar, B., Zeltmann, S. E., Doddamani, M., Gupta, N., Gurupadu, S. and Sailaja, R. (2016). "Effect of cenosphere surface treatment and blending method on the tensile properties of thermoplastic matrix syntactic foams." *Journal of applied polymer science*, 133(35).

- Biswas, P. (1976). "Thermal buckling of orthotropic plates." *Journal of Applied Mechanics*, 43, 361.
- Bokaian, A. (1988). "Natural frequencies of beams under compressive axial loads." *Journal of sound and vibration*, 126(1), 49-65.
- Bouazza, M., Benseddiq, N. and Zenkour, A. M. (2018). "Thermal buckling analysis of laminated composite beams using hyperbolic refined shear deformation theory." *Journal of Thermal Stresses*, 1-9.
- Byklum, E., Steen, E. and Amdahl, J. (2004). "A semi-analytical model for global buckling and postbuckling analysis of stiffened panels." *Thin-Walled Structures*, 42(5), 701-717.
- Carpinteri, A., Malvano, R., Manuello, A. and Piana, G. (2014). "Fundamental frequency evolution in slender beams subjected to imposed axial displacements." *Journal of sound and vibration*, 333(11), 2390-2403.
- Chandra, Y., Stanciulescu, I., Eason, T. and Spottswood, M. (2012). "Numerical pathologies in snap-through simulations." *Engineering Structures*, 34, 495-504.
- Chandra, Y., Wiebe, R., Stanciulescu, I., Virgin, L. N., Spottswood, S. M. and Eason, T. G. (2013). "Characterizing dynamic transitions associated with snap-through of clamped shallow arches." *Journal of sound and vibration*, 332(22), 5837-5855.
- Chao, C. and Lin, I. (1990). "Static and dynamic snap-through of orthotropic spherical caps." *Composite Structures*, 14(4), 281-301.
- Chawla, K. K. (2012). *Composite materials: science and engineering*: Springer Science & Business Media.
- Chen, J.-S. and Hung, S.-Y. (2011). "Snapping of an elastica under various loading mechanisms." *European Journal of Mechanics-A/Solids*, 30(4), 525-531.
- Colloca, M., Gupta, N. and Porfiri, M. (2013). "Tensile properties of carbon nanofiber reinforced multiscale syntactic foams." *Composites Part B: Engineering*, 44(1), 584-591.
- Cotterell, B. and Parkes, E. W. (1962). *Thermal buckling of circular plates*: HM Stationery Office.
- Crisfield, M. (1981). A fast incremental/iterative solution procedure that handles "snap-through" *Computational Methods in Nonlinear Structural and Solid Mechanics* (pp. 55-62): Elsevier.
- Dehrouyeh-Semnani, A. M., Mostafaei, H., Dehrouyeh, M. and Nikkhah-Bahrami, M. (2017). "Thermal pre-and post-snap-through buckling of a geometrically imperfect doubly-clamped microbeam made of temperature-dependent functionally graded materials." *Composite Structures*, 170, 122-134.

- Esfahani, M., Ghasemnejad, H. and Barrington, P. (2010). "Experimental and numerical buckling analysis of delaminated hybrid composite beam structures." *Applied Mechanics and Materials*, 24-25, 393-400.
- Farinha, J., Winnik, M. and Hahn, K. (2000). "Characterization of oil droplets under a polymer film by laser scanning confocal fluorescence microscopy." *Langmuir*, 16(7), 3391-3400.
- Fleck, N. A. and Sridhar, I. (2002). "End compression of sandwich columns." *Composites Part A: Applied Science and Manufacturing*, 33(3), 353-359.
- Fu, Y., Wang, J. and Hu, S. (2014). "Analytical solutions of thermal buckling and postbuckling of symmetric laminated composite beams with various boundary conditions." *Acta Mechanica*, 225(1), 13-29.
- Galef, A. (1968). "Bending frequencies of compressed beams." *The Journal of the Acoustical Society of America*, 44(2), 643-643.
- Garcia, C. D., Shahapurkar, K., Doddamani, M., Kumar, G. C. M. and Prabhakar, P. (2018). "Effect of arctic environment on flexural behavior of fly ash cenosphere reinforced epoxy syntactic foams." *Composites Part B: Engineering*, 151, 265-273.
- George, N., Jeyaraj, P. and Murigendrappa, S. (2016). "Buckling of non-uniformly heated isotropic beam: Experimental and theoretical investigations." *Thin-Walled Structures*, 108, 245-255.
- Goncalves, B. R., Karttunen, A., Romanoff, J. and Reddy, J. (2017). "Buckling and free vibration of shear-flexible sandwich beams using a couple-stress-based finite element." *Composite Structures*, 165, 233-241.
- Grygorowicz, M., Magnucki, K. and Malinowski, M. (2015). "Elastic buckling of a sandwich beam with variable mechanical properties of the core." *Thin-Walled Structures*, 87, 127-132.
- Gu, J., Wu, G. and Zhang, Q. (2007). "Preparation and damping properties of fly ash filled epoxy composites." *Materials Science and Engineering: A*, 452, 614-618.
- Gu, J., Wu, G. and Zhao, X. (2009). "Effect of surface-modification on the dynamic behaviors of fly ash cenospheres filled epoxy composites." *Polymer composites*, 30(2), 232-238.
- Guhanathan, S., Devi, M. S. and Murugesan, V. (2001). "Effect of coupling agents on the mechanical properties of fly ash/polyester particulate composites." *Journal of applied polymer science*, 82(7), 1755-1760.
- Gupta, N., Gupta, S. K. and Mueller, B. J. (2008). "Analysis of a functionally graded particulate composite under flexural loading conditions." *Materials Science and Engineering: A*, 485(1-2), 439-447.

- Gupta, N., Karthikeyan, C. and Sankaran, S. (1999). "Correlation of processing methodology to the physical and mechanical properties of syntactic foams with and without fibers." *Materials Characterization*, 43(4), 271-277.
- Gupta, N., Maharsia, R. and Jerro, H. D. (2005). "Enhancement of energy absorption characteristics of hollow glass particle filled composites by rubber addition." *Materials Science and Engineering: A*, 395(1-2), 233-240.
- Gupta, N. and Pinisetty, D. (2013). "A review of thermal conductivity of polymer matrix syntactic foams-effect of hollow particle wall thickness and volume fraction." *JOM*, 65(2), 234-245.
- Gupta, N., Pinisetty, D. and Shunmugasamy, V. C. (2013). *Reinforced polymer matrix syntactic foams: effect of nano and micro-scale reinforcement*: Springer Science & Business Media.
- Gupta, N. and Sankaran, S. (1999). "On the characterisation of syntactic foam core sandwich composites for compressive properties." *Journal of Reinforced Plastics and Composites*, 18(14), 1347-1357.
- Gupta, N. and Woldesenbet, E. (2005). "Characterization of flexural properties of syntactic foam core sandwich composites and effect of density variation." *Journal of Composite Materials*, 39(24), 2197-2212.
- Gupta, N., Woldesenbet, E., hore, K. and Sankaran, S. (2002). "Response of syntactic foam core sandwich structured composites to three-point bending." *Journal of Sandwich Structures & Materials*, 4(3), 249-272.
- Gupta, N., Woldesenbet, E. and Mensah, P. (2004). "Compression properties of syntactic foams: effect of cenosphere radius ratio and specimen aspect ratio." *Composites Part A: Applied Science and Manufacturing*, 35(1), 103-111.
- Gupta, N., Zeltmann, S. E., Luong, D. D. and Doddamani, M. (2018). "Testing of foams." *Handbook of Mechanics of Materials*, 1-40.
- Gupta, N., Zeltmann, S. E., Shunmugasamy, V. C. and Pinisetty, D. (2014). "Applications of Polymer Matrix Syntactic Foams." *JOM*, 66(2), 245-254.
- Gupta, R., Babu, G. J., Janardhan, G. R. and Rao, G. V. (2009). "Comparative study of thermal post-buckling analysis of uniform slender & shear flexible columns using rigorous finite element and intuitive formulations." *International Journal of Mechanical Sciences*, 51(3), 204-212.
- Guru, K., Mishra, S. B. and Shukla, K. K. (2015). "Effect of temperature and functionalization on the interfacial properties of CNT reinforced nanocomposites." *Applied Surface Science*, 349, 59-65.

- Haftka, R. T. and Mallett, R. H. (1971). "Adaption of Koiter's method to finite element analysis of snap-through buckling behavior." *International Journal of Solids and Structures*, 7(10), 1427-1445.
- Hu, G. and Yu, D. (2011). "Tensile, thermal and dynamic mechanical properties of hollow polymer particle-filled epoxy syntactic foam." *Materials Science and Engineering: A*, 528(15), 5177-5183.
- Huang, N. and Vahidi, B. (1971). "Snap-through buckling of two simple structures." *International Journal of Non-Linear Mechanics*, 6(3), 295-310.
- Hull, D. and Clyne, T. W. (1996). *An introduction to composite materials* (2 ed.). Cambridge: Cambridge University Press.
- Islam, M. M. and Kim, H. S. (2012). "Sandwich composites made of syntactic foam core and paper skin: manufacturing and mechanical behavior." *Journal of Sandwich Structures & Materials*, 14(1), 111-127.
- Jasion, P. and Magnucki, K. (2013). "Global buckling of a sandwich column with metal foam core." *Journal of Sandwich Structures & Materials*, 15(6), 718-732.
- Jeyaraj, P. (2013). "Buckling and free vibration behavior of an isotropic plate under nonuniform thermal load." *International Journal of Structural Stability and Dynamics*, 13(03), 1250071.
- Jia, J. (2014). *Essentials of applied dynamic analysis*. Berlin Heidelberg: Springer.
- John, B., Reghunadhan Nair, C., Mathew, D. and Ninan, K. (2008). "Foam sandwich composites with cyanate ester based syntactic foam as core and carbon-cyanate ester as skin: Processing and properties." *Journal of applied polymer science*, 110(3), 1366-1374.
- Kant, T. and Babu, C. (2000). "Thermal buckling analysis of skew fibre-reinforced composite and sandwich plates using shear deformable finite element models." *Composite Structures*, 49(1), 77-85.
- Keleshteri, M., Asadi, H. and Wang, Q. (2018). "On the snap-through instability of post-buckled FG-CNTRC rectangular plates with integrated piezoelectric layers." *Computer Methods in Applied Mechanics and Engineering*, 331, 53-71.
- Kiani, Y. (2016). "Thermal postbuckling of temperature-dependent sandwich beams with carbon nanotube-reinforced face sheets." *Journal of Thermal Stresses*, 39(9), 1098-1110.
- Ku, H., Wang, H., Pattarachaiyakoop, N. and Trada, M. (2011). "A review on the tensile properties of natural fiber reinforced polymer composites." *Composites Part B: Engineering*, 42(4), 856-873.

- Kulkarni, S. and Kishore. (2002). "Effect of contact at the interface on the compressive properties of fly ash-epoxy composites." *The Journal of Adhesion*, 78(2), 155-166.
- Labella, M., Zeltmann, S. E., Shunmugasamy, V. C., Gupta, N. and Rohatgi, P. K. (2014). "Mechanical and thermal properties of fly ash/vinyl ester syntactic foams." *Fuel*, 121, 240-249.
- Lan, T., Lin, P. D. and Chen, L. W. (1993). "Thermal buckling of bimodular sandwich beams." *Composite Structures*, 25(1-4), 345-352.
- Le Grogneq, P. and Saoud, K. S. (2015). "Elastoplastic buckling and post-buckling analysis of sandwich columns." *International Journal of Non-Linear Mechanics*, 72, 67-79.
- Lee, C.-Y. and Kim, J.-H. (2013). "Thermal post-buckling and snap-through instabilities of FGM panels in hypersonic flows." *Aerospace Science and Technology*, 30(1), 175-182.
- Lenci, S. and Rega, G. (2016). "Nonlinear free vibrations of planar elastic beams: A unified treatment of geometrical and mechanical Effects." *Procedia IUTAM*, 19, 35-42.
- Li, J., Narita, Y. and Wang, Z. (2015). "The effects of non-uniform temperature distribution and locally distributed anisotropic properties on thermal buckling of laminated panels." *Composite Structures*, 119, 610-619.
- Li, X., Yu, B., Wang, P., Zhang, X., Fan, T. and Yang, J. (2017). "Unit cells for thermal analyses of syntactic foams with imperfect interfaces." *Composites Communications*, 3, 28-32.
- Li, Z.-M. and Qiao, P. (2015). "Buckling and postbuckling behavior of shear deformable anisotropic laminated beams with initial geometric imperfections subjected to axial compression." *Engineering Structures*, 85, 277-292.
- Lin, T. C., Gupta, N. and Talalayev, A. (2009). "Thermoanalytical characterization of epoxy matrix-glass microballoon syntactic foams." *Journal of materials science*, 44(6), 1520-1527.
- Liu, L., Kardomateas, G. A., Birman, V., Holmes, J. and Simitises, G. J. (2006). "Thermal buckling of a heat-exposed, axially restrained composite column." *Composites Part A: Applied Science and Manufacturing*, 37(7), 972-980.
- Liu, L., Lv, B. and He, T. (2015). "The stochastic dynamic snap-through response of thermally buckled composite panels." *Composite Structures*, 131, 344-355.
- Luu, A.-T. and Lee, J. (2016). "Non-linear buckling of elliptical curved beams." *International Journal of Non-Linear Mechanics*, 82, 132-143.

- Mahfuz, H., Islam, S., Saha, M., Carlsson, L. and Jeelani, S. (2005). "Buckling of sandwich composites; effects of core–skin debonding and core density." *Applied Composite Materials*, 12(2), 73-91.
- Mathew, G., Huh, M. Y., Rhee, J., Lee, M. H. and Nah, C. (2004). "Improvement of properties of silica-filled styrene-butadiene rubber composites through plasma surface modification of silica." *Polymers for Advanced Technologies*, 15(7), 400-408.
- Mathieson, H. and Fam, A. (2014). "Axial loading tests and simplified modeling of sandwich panels with GFRP skins and soft core at various slenderness ratios." *Journal of Composites for Construction*, 19(2), 04014040.
- Matsunaga, H. (1996). "Buckling instabilities of thick elastic beams subjected to axial stresses." *Computers & structures*, 59(5), 859-868.
- Matsunaga, H. (1999). "Vibration and buckling of deep beam-columns on two-parameter elastic foundations." *Journal of sound and vibration*, 228(2), 359-376.
- Mead, D. (2003). "Vibration and buckling of flat free–free plates under non-uniform in-plane thermal stresses." *Journal of sound and vibration*, 260(1), 141-165.
- Mirzabeigy, A. and Madoliat, R. (2016). "Large amplitude free vibration of axially loaded beams resting on variable elastic foundation." *Alexandria Engineering Journal*, 55(2), 1107-1114.
- Mirzaei, M. and Kiani, Y. (2015). "Snap-through phenomenon in a thermally postbuckled temperature dependent sandwich beam with FG-CNTRC face sheets." *Composite Structures*, 134, 1004-1013.
- Mittal, V., Saini, R. and Sinha, S. (2016). "Natural fiber-mediated epoxy composites–a review." *Composites Part B: Engineering*, 99, 425-435.
- Moita, J., Araújo, A., Correia, V. F., Soares, C. M. and Soares, C. M. (2015). "Buckling and geometrically nonlinear analysis of sandwich structures." *International Journal of Mechanical Sciences*, 92, 154-161.
- Mukherjee, P. and Satyanarayana, K. (1984). "Structure and properties of some vegetable fibres." *Journal of materials science*, 19(12), 3925-3934.
- Naik, N. K. and Shembekar, P. S. (1992). "Elastic Behavior of Woven Fabric Composites: I—Lamina Analysis." *Journal of Composite Materials*, 26(15), 2196-2225.
- Narkis, M., Puterman, M. and Kenig, S. (1980). "Syntactic foams II. Preparation and characterization of three-phase systems." *Journal of Cellular Plastics*, 16(6), 326-330.
- Noor, A. K., Burton, W. S. and Bert, C. W. (1996). "Computational models for sandwich panels and shells." *Applied Mechanics Reviews*, 49(3), 155-199.

- Park, Y. K., Kim, J.-G. and Lee, J.-K. (2008). "Prediction of thermal conductivity of composites with spherical microballoons." *Materials transactions*, 49(12), 2781-2785.
- Plaut, R. H. (2015). "Snap-through of arches and buckled beams under unilateral displacement control." *International Journal of Solids and Structures*, 63, 109-113.
- Plaut, R. H. and Virgin, L. N. (1990). "Use of frequency data to predict buckling." *Journal of Engineering Mechanics*, 116(10), 2330-2335.
- Plaut, R. H. and Virgin, L. N. (2017). "Snap-through under unilateral displacement control with constant velocity." *International Journal of Non-Linear Mechanics*, 94, 292-299.
- Plueddemann, E. P. (2016). *Interfaces in Polymer Matrix Composites: Composite Materials* (Vol. 6): Elsevier.
- Poveda, R. L. and Gupta, N. (2014). "Carbon-nanofiber-reinforced syntactic foams: compressive properties and strain rate sensitivity." *JOM*, 66(1), 66-77.
- Pradeep, V., Ganesan, N. and Bhaskar, K. (2007). "Vibration and thermal buckling of composite sandwich beams with viscoelastic core." *Composite Structures*, 81(1), 60-69.
- Puterman, M., Narkis, M. and Kenig, S. (1980). "Syntactic Foams I. Preparation, Structure and Properties." *Journal of Cellular Plastics*, 16(4), 223-229.
- Rahmani, O., Khalili, S., Malekzadeh, K. and Hadavinia, H. (2009). "Free vibration analysis of sandwich structures with a flexible functionally graded syntactic core." *Composite Structures*, 91(2), 229-235.
- Rajesh, M. (2017). *Dynamic mechanical characterization of woven natural fiber polymer composite*. (Doctor of Philosophy), National Institute of Technology Karnataka Surathkal, Mangalore-575025, India.
- Rajesh, M. and Pitchaimani, J. (2017). "Experimental investigation on buckling and free vibration behavior of woven natural fiber fabric composite under axial compression." *Composite Structures*, 163, 302-311.
- Ramakrishna, H., Priya, S. P. and Rai, S. (2006). "Utilization of granite powder as filler in epoxy phenol cashew nut shell liquid-toughened epoxy resin for impact and compression strength." *Journal of Reinforced Plastics and Composites*, 25(3), 227-234.
- Reddy, J. N. (2014). *An Introduction to Nonlinear Finite Element Analysis: with applications to heat transfer, fluid mechanics, and solid mechanics*: OUP Oxford.
- Rugele, K., Lehmus, D., Hussainova, I., Peculevica, J., Lisnanskis, M. and Shishkin, A. (2017). "Effect of Fly-Ash Cenospheres on Properties of Clay-Ceramic Syntactic Foams." *Materials*, 10(7), 828.

- Salleh, Z., Islam, M. M., Epaarachchi, J. A. and Su, H. (2016). "Mechanical properties of sandwich composite made of syntactic foam core and GFRP skins." *AIMS Materials Science*, 3(4), 1704-1727.
- Sankaran, S., Sekhar, K. R., Raju, G. and Kumar, M. J. (2006). "Characterization of epoxy syntactic foams by dynamic mechanical analysis." *Journal of materials science*, 41(13), 4041-4046.
- Shahapurkar, K., Chavan, V. B., Doddamani, M. and Kumar, G. C. M. (2018a). "Influence of surface modification on wear behavior of fly ash cenosphere/epoxy syntactic foam." *Wear*, 414-415, 327-340.
- Shahapurkar, K., Garcia, C. D., Doddamani, M., Kumar, G. M. and Prabhakar, P. (2018b). "Compressive behavior of cenosphere/epoxy syntactic foams in arctic conditions." *Composites Part B: Engineering*, 135, 253-262.
- Shaker, F. J. (1975). "Effect of axial load on mode shapes and frequencies of beams."
- Shams, A., Aureli, M. and Porfiri, M. (2013). "Nonlinear buckling of a spherical shell embedded in an elastic medium with imperfect interface." *International Journal of Solids and Structures*, 50(14-15), 2310-2327.
- Shams, A. and Porfiri, M. (2013). "A generalized Vlasov-Jones foundation model for micromechanics studies of syntactic foams." *Composite Structures*, 103, 168-178.
- Sharifian, R. (2010). "Buckling of isotropic plates with two opposite simply supported edges and the other two edges rotationally restrained unloaded ". *Proc. of the Yerevan State Univ. Phys. and Mathem. Sci*(1), 32-36.
- Shariyat, M. (2007). "Thermal buckling analysis of rectangular composite plates with temperature-dependent properties based on a layerwise theory." *Thin-Walled Structures*, 45(4), 439-452.
- Shariyat, M. and Asgari, D. (2013). "Nonlinear thermal buckling and postbuckling analyses of imperfect variable thickness temperature-dependent bidirectional functionally graded cylindrical shells." *International Journal of Pressure Vessels and Piping*, 111, 310-320.
- Shen, H.-S., Xiang, Y. and Lin, F. (2017). "Thermal buckling and postbuckling of functionally graded graphene-reinforced composite laminated plates resting on elastic foundations." *Thin-Walled Structures*, 118, 229-237.
- Shiau, L.-C. and Kuo, S.-Y. (2004). "Thermal buckling of composite sandwich plates." *Mechanics based design of structures and machines*, 32(1), 57-72.
- Shiau, L.-C. and Kuo, S.-Y. (2004). "Thermal postbuckling behavior of composite sandwich plates." *Journal of Engineering Mechanics*, 130(10), 1160-1167.

- Smyczynski, M. and Magnucka-Blandzi, E. (2015). "Static and dynamic stability of an axially compressed five-layer sandwich beam." *Thin-Walled Structures*, 90, 23-30.
- Sokolinsky, V. S., Von Bremen, H. F., Lavoie, J. A. and Nutt, S. R. (2004). "Analytical and experimental study of free vibration response of soft-core sandwich beams." *Journal of Sandwich Structures & Materials*, 6(3), 239-261.
- Souza, M. and Assaid, L. (1991). "A new technique for the prediction of buckling loads from nondestructive vibration tests." *Experimental mechanics*, 31(2), 93-97.
- Srivastava, V. and Shembekar, P. (1990). "Tensile and fracture properties of epoxy resin filled with flyash particles." *Journal of materials science*, 25(8), 3513-3516.
- Sudhir Sastry, Y., Budarapu, P. R., Madhavi, N. and Krishna, Y. (2015). "Buckling analysis of thin wall stiffened composite panels." *Computational Materials Science*, 96, 459-471.
- Tagliavia, G., Porfiri, M. and Gupta, N. (2010). "Analysis of flexural properties of hollow-particle filled composites." *Composites Part B: Engineering*, 41(1), 86-93.
- Tagliavia, G., Porfiri, M. and Gupta, N. (2010). "Analysis of hollow inclusion–matrix debonding in particulate composites." *International Journal of Solids and Structures*, 47(16), 2164-2177.
- Tang, Z., Zha, X. and Ma, J. (2015). "Buckling of axially loaded sandwich composite panels with reinforced calcium silicate faces and polyurethane cores." *Journal of Reinforced Plastics and Composites*, 34(17), 1378-1391.
- Tariq, M. A., Hamad, Q. A. and Alwan, M. K. (2011). "Tensile and Buckling Analysis of the Polymer Composite Beam Reinforced by Natural Jute Fiber." *Engineering and Technology Journal*, 29(1), 129-140.
- Thomson, W. T., Dahleh, M. D. and Padmanabhan, C. (2008). *Theory of vibrations with applications*, (5th ed.). India: Pearson Education.
- Thongsang, S. and Sombatsompop, N. (2006). "Effect of NaOH and Si69 treatments on the properties of fly ash/natural rubber composites." *Polymer composites*, 27(1), 30-40.
- Tuttle, M., Singhatanadgid, P. and Hinds, G. (1999). "Buckling of composite panels subjected to biaxial loading." *Experimental mechanics*, 39(3), 191-201.
- van Belle, B. (2002). *Advances in High-Temperature Syntactic Foam Technology for Offshore Systems*. Offshore Technology Conference, Houston, Texas. <https://doi.org/10.4043/14120-MS>
- Van Vuure, A., Ivens, J. and Verpoest, I. (2000). "Mechanical properties of composite panels based on woven sandwich-fabric preforms." *Composites Part A: Applied Science and Manufacturing*, 31(7), 671-680.

- Wang, B. and Fancey, K. S. (2015). "A bistable morphing composite using viscoelastically generated prestress." *Materials Letters*, 158, 108-110.
- Watts, G., Singha, M. and Pradyumna, S. (2018). "Nonlinear bending and snap-through instability analyses of conical shell panels using element free Galerkin method." *Thin-Walled Structures*, 122, 452-462.
- Wouterson, E. M., Boey, F. Y. C., Hu, X. and Wong, S.-C. (2005). "Specific properties and fracture toughness of syntactic foam: Effect of foam microstructures." *Composites Science and Technology*, 65(11), 1840-1850.
- Wu, G., Gu, J. and Zhao, X. (2007). "Preparation and dynamic mechanical properties of polyurethane-modified epoxy composites filled with functionalized fly ash particulates." *Journal of applied polymer science*, 105(3), 1118-1126.
- Wu, H., Kitipornchai, S. and Yang, J. (2015). "Free vibration and buckling analysis of sandwich beams with functionally graded carbon nanotube-reinforced composite face sheets." *International Journal of Structural Stability and Dynamics*, 15(07), 1540011.
- Yang, J., Wu, H. and Kitipornchai, S. (2017). "Buckling and postbuckling of functionally graded multilayer graphene platelet-reinforced composite beams." *Composite Structures*, 161, 111-118.
- Yuan, W., Song, H., Wang, X. and Huang, C. (2014). "Experimental investigation on thermal buckling behavior of truss-core sandwich panels." *AIAA Journal*, 53(4), 948-957.
- Zeltmann, S. E., Prakash, K. A., Doddamani, M. and Gupta, N. (2017). "Prediction of modulus at various strain rates from dynamic mechanical analysis data for polymer matrix composites." *Composites Part B: Engineering*, 120, 27-34.
- Zhu, P., Lei, Z. and Liew, K. M. (2012). "Static and free vibration analyses of carbon nanotube-reinforced composite plates using finite element method with first order shear deformation plate theory." *Composite Structures*, 94(4), 1450-1460.

LIST OF PUBLICATIONS

INTERNATIONAL JOURNALS

1. Sunil Waddar, P Jeyaraj, Mrityunjay Doddamani (2018). “Influence of axial compressive loads on buckling and free vibration response of surface-modified fly ash cenosphere/epoxy syntactic foams.” *Journal of Composite Materials*, 52(19), 2621-2630. (**Sage, SCI, IF=1.613**)
2. Sunil Waddar, Jeyaraj Pitchaimani, Mrityunjay Doddamani (2018). “Snap-through buckling of fly ash cenosphere/epoxy syntactic foams under thermal environment.” *Thin-Walled Structures*, 131, 417-427. (**Elsevier, SCI, IF=2.883**)
3. Sunil Waddar, Jeyaraj Pitchaimani, Mrityunjay Doddamani, Nikhil Gupta (2018). “Buckling and free vibration behavior of cenosphere/epoxy syntactic foams under axial compressive loading.” *Materials Performance and Characterization*, 7(1),532-546. (**ASTM, Scopus**)
4. Sunil Waddar, Jeyaraj Pitchaimani, Mrityunjay Doddamani, Ever Barbero (2019). “Buckling and free vibration behavior of cenosphere/epoxy syntactic foam sandwich beam with natural fibre fabric composite facings under mechanical load.” *Composites Part B: Engineering*, (Major Revision) (**Elsevier, SCI, IF=4.92**).
5. Sunil Waddar, Jeyaraj Pitchaimani, Mrityunjay Doddamani (2019). “Effect of thermal loading on the syntactic foam sandwich composites with natural fiber skin.” *Composite Structures*, (With Editor) (**Elsevier, SCI, IF=4.101**).

INTERNATIONAL CONFERENCE

1. S. Waddar, J. Pitchaimani, M. Doddamani (2017). “Free vibration characteristics of fly ash cenosphere/epoxy syntactic foam composites.” ICOVP, 13th International Conference on Vibration Problems, 29th November – 2nd December, 2017, Indian Institute of Technology Guwahati, INDIA.

BIO-DATA

1. Name : Sunil Shankar Waddar
2. Father's Name : Shankar Govind Waddar
3. Date of Birth : 2nd July 1990
4. Nationality : Indian
5. Marital Status : Married
6. Address : Department of Mechanical Engineering
National Institute of Technology Karnataka
Surathkal, PO Srinivasnagar-575 025
Karnataka, India.
7. Mobile Number : +91 8123376890
8. E-mail id. : *sunilwaddar98@gmail.com*
9. Educational Qualification :

Qualification	University/Board	Year of Passing
Ph.D. (Mechanical Engineering)	National Institute of Technology Karnataka, Surathkal, Mangalore	Pursuing
M.Tech (Mechanical Machine Design)	Visvesvaraya Technological University, Belgaum	2014
B.E. (Mechanical Engineering)	Visvesvaraya Technological University, Belgaum	2012